Université d'Ottawa · University of Ottawa

INFORMATION TRANSFER IN P-TYPE ELECTRORECEPTORS

By

Martin St-Hilaire

A thesis submitted to
the School of Graduate Studies and Research
in partial fulfillment of the requirements
for the degree of Master of Science in Physics

Department of Physics

University of Ottawa
Ottawa, Ontario
18 January 2002

Summary

Weakly electric fish continuously emit a quasi-sinusoidal electric organ discharge (EOD) to probe their near environment (electrolocation). P-type tuberous receptors located on their skin respond to the periodic EOD by triggering action potentials in a phase locked manner. It is observed that the intervals between firing times are random multiples of the EOD period. This is known as skipping. Weak carrier amplitude modulations caused by relevant stimuli are encoded by P-type receptors through modulation of their output firing rate.

We investigate the effect of P — the baseline firing probability per EOD cycle of a receptor — as well as of other parameters on the quality of information transfer in four biophysically plausible numerical receptor models. In particular, we study how internal noise affects the transduction of random EOD modulations, since noise is perhaps essential for good neural computation. Information is quantified using the stimulus reconstruction technique. We discuss the firing characteristics of the four considered models and discuss their relevance as models of P-afferents. Our information measurements indicate that the presence of noise may enhance information transfer in these receptors. And the coding quality is found to not depend on P alone, but also on the actual combination of biophysical parameters that determine P.

Sommaire

Le poisson électrique émet continuellement une décharge électrique quasi sinusoïdale afin de sonder son environnement rapproché (électrolocation). Des afferents de type P situés à la surface de sa peau répondent à la décharge périodique en émettant des potentiels d'action (impulsions électriques) en phase avec le forçage. On observe que les intervalles de temps entre ces impulsions sont des multiples aléatoires de la période de forçage. Ce phénomène est appelé "skipping". Les faibles modulations d'amplitude du champ électrique local se traduisent en une modulation de la fréquence à laquelle les potentiels d'action sont émis par le récepteur.

Nous étudions l'effet de P — la probilité de tirer par cycle de la décharge sinusoïdale pour un récepteur — ainsi que d'autres variables de dynamique neuronale sur la qualité de la transmission d'information par quatre modèles numériques de ces récepteurs. En particulier, notre étude porte sur l'effet du bruit interne dans le processus d'encodage de modulations d'amplitude aléatoires, sachant que le bruit est considéré comme étant possiblement essentiel à une bonne transmission d'information par les neurones. Notre mesure d'information est effectuée à l'aide de la méthode de reconstruction de stimulus. Nous présentons les caractéristiques de décharge des quatres modèles considérés et discutons de leur pertinence en tant que modèles d'afférents de type P. Entre autres résultats, nous montrons que le transfert d'information dans ces récepteurs peut être amélioré par la présence de bruit. Aussi, la qualité du codage ne dépend pas seulement de P, mais bien de la combinaison des paramètres biophysiques déterminant la valeur de P.

Acknowledgements

I wish to express my deepest gratitude to my thesis director Dr. André Longtin for his advice and guidance throughout my Master's Degree. His patience was truly appreciated. Also, I could not have completed this research without the financial support he granted me. Its been a pleasure being part of his research team.

I would also like to thank Maurice Chacron and Brent Doiron for the invaluable discussions and pleasant company. I am grateful to M. Chacron for contributing to a few figures in this thesis. Thanks also to Dr. Len Maler for very helpful discussions.

In the last moments of completing this document, the generous help of Michel Gauthier and Jean-François Mercier got me through many technical difficulties. It was deeply appreciated.

Finally, a special thought for those of my friends who spent some time with me in Ottawa for the time of my Master's Degree. They never doubted I would succeed and I felt it.

Contents

Summary ii

Sommaire iii

Acknowledgements iv

Contents v

List of Figures viii

List of Tables x

1 Introduction 1

1.1 Electrolocation and the role of P-afferents 3

1.2 P-Afferents 4

1.2.1 Physiology 4

1.2.2 Basic Dynamics 5

1.2.3 Measurements on P-units 6

1.3 Introduction to Neuron Models 10

1.4 Understanding the neural code 13

1.4.1 Encoding: the neuron as a transfer function 14

1.4.2 Decoding: linear reconstruction 15

1.5 Tools 16

1.5.1 Interspike Interval Histograms 16

1.5.2 Tuning Curves 17

1.5.3 Devil's Staircase 18

1.6 Recent Work on Information Transfer in P-Afferents 19

1.7 Scope and organization of thesis 19

2 Method 21

2.1 Simulations 21

2.1.1 Random Deviate Generation 23

2.1.2 Correlated noise generator 23

2.1.3 Bandlimited Gaussian Random Signal 24

2.2 Quantifying Information Transfer 25

2.2.1 Stimulus Reconstruction Technique 25

2.2.2 Coding Fraction and Information Rate 26

3 LIFDT 28

3.1 Spiking Mechanism 28

3.2 Numerical Implementation 29

3.3 Firing Characteristics 32

3.4 Results 34

3.5 Discussion 38

4 FitzHugh-Nagumo 40

4.1 Spiking Mechanism 40

4.2 Numerical Implementation 41

4.3 Firing Characteristics 42

4.4 Results 50

4.5 Discussion 53

5 Morris-Lecar 56

5.1 Spiking Mechanism 56

5.2 Numerical Implementation 61

5.3 Firing Characteristics 62

5.4 Results 66

5.5 Discussion 72

6 Nelson 75

6.1 Spiking Mechanism 75

6.2 Numerical Implementation 77

6.3 Firing Characteristics 80

6.4 Results 84
6.5 Discussion 87

7 Conclusions **90**

A Fourth order filter **94**

List of Figures

1.1 Basic parts of a neuron. 2
1.2 Active electrolocation. 3
1.3 Illustration of P-unit. 5
1.4 Baseline firing characteristics of P-units. 7
1.5 The role of noise in skipping. 9
1.6 The encoding/decoding process. 16
1.7 Tuning curve of a cell in the cat auditory nerve. 18

3.1 Time series of various variables in the LIFDT model. 30
3.2 Effect of noise on LIFDT dynamics. 33
3.3 P value in LIFDT. 34
3.4 Multimodal interval histograms in LIFDT. 35
3.5 Tuning curve of LIFDT. 35
3.6 Coding fraction vs multiplicative noise variance σ_m^2. 36
3.7 Coding fraction vs r_0 in LIFDT. 37
3.8 Coding fraction vs P in LIFDT. 38

4.1 Devil's staircase of the FHN model. 43
4.2 Voltage response and ISIH in FHN at rest. 44
4.3 Encoding an amplitude modulation in the FHN model, in the subthreshold regime. 46
4.4 Encoding an amplitude modulation in the FHN model, in the suprathreshold regime. 47
4.5 Interspike intervals histograms in the FHN model, in the subthreshold regime. 48
4.6 Interspike intervals histograms in the FHN model, in the suprathreshold regime. 49
4.7 Tuning curve in the FHN model. 50

4.8 Coding fraction vs synaptic noise amplitude in the FHN model. 51
4.9 Coding fraction vs mean EOD amplitude in the FHN model. 52
4.10 Coding fraction vs P in the FHN model. 53
4.11 Coding fraction vs carrier frequency in the FHN model. 54

5.1 Dynamics of type II Morris-Lecar. 58
5.2 Dynamics of type I Morris-Lecar. 60
5.3 Devil's staircase of type II Morris-Lecar. 63
5.4 Interspike Interval Histogram of type II Morris-Lecar with constant amplitude periodic forcing. 64
5.5 Tuning curve of type II Morris-Lecar. 65
5.6 Devil's staircase of type I Morris-Lecar. 66
5.7 Interspike Interval Histogram of type I Morris-Lecar with constant amplitude periodic forcing. 67
5.8 Tuning curve of type I Morris-Lecar. 67
5.9 P vs D for different input current values in TYPE II Morris-Lecar. 68
5.10 P vs D for different input current values in TYPE I Morris-Lecar. 69
5.11 Comparative P-D curves for both subthreshold and suprathreshold cases. . . 70
5.12 Coding fraction vs noise amplitude in the subthreshold ML model. 71
5.13 Coding fraction vs noise amplitude in the suprathreshold ML model. 72
5.14 Coding fraction vs distance to bifurcation. 73
5.15 Mean firing rate vs noise amplitude. 74

6.1 P-units response characteristics to sinusoidal AM's 76
6.2 P vs baserate in Nelson's model with constant contrast stimulation. 81
6.3 P vs baserate in Nelson's model with fixed stimulus amplitude. 81
6.4 Effect of m over interspike interval histogram in Nelson's model 83
6.5 Coding fraction and information rate vs baserate in Nelson's model. 85
6.6 Information per spike vs baserate in Nelson's model. 87
6.7 Coding fraction, information rate and information per spike vs m in Nelson's model. 88

List of Tables

3.1 Leaky Integrate-and-Fire with dynamic threshold model parameters 32

4.1 FitzHugh-Nagumo model parameters 42

5.1 Morris-Lecar parameters for type II and type I spiking mechanisms. 62

6.1 NELSON model parameters 78

Chapter 1 Introduction

Neuroscience or the science of neurons is the study of the basic principles and dynamics of information transmission via propagating electric signals in single or multiple neuron systems. Scientists from such diverse disciplines as physics, mathematics and biology and from more precise areas such as dynamical systems, statistics, electromagnetism and physiology are investigating neural dynamics by trying to explain its complex biological phenomena in terms of basic physical concepts.

Most neurons transmit information by generating and propagating action potentials — sudden changes or "spikes" in membrane voltage — to and from the nervous centers of living bodies. The dynamic of action potentials generation is very complex due to the diversity of the neuron membrane constituents and to the multitude of ions and chemicals involved in the process. A most celebrated neuron model was proposed by Hodgkin and Huxley in 1952 [1]. It describes the dynamics of the local membrane potential of a giant squid axon using 4 differential equations based on observations made of the non-linear voltage dependent kinetics of ion channels. Although it was a very simplified vision of the actual process, Hodgkin-Huxley's model captured the basics of spike generation. Nowadays powerful computers can handle and solve more complex models or very large networks of them, a key element in the investigation of dynamics of biological neural networks.

It has been observed that the information carried by action potentials is not encoded in their particular shape or magnitude but in their position in time — or at least in their instantaneous occurrence rate (see references therein [16] section 9.1). On the other hand, neuroscientists are aware that any neuronal transmission process is in part a stochastic process and that it is not entirely reproducible; one neuron stimulated twice with the same exact stimulus won't trigger spikes at the exact same times! In an attempt to unify these two contrasting concepts, nonlinear dynamics, stochastic processes, statistics and signal processing are used along with numerical neuron models to clarify the importance of the exact timing

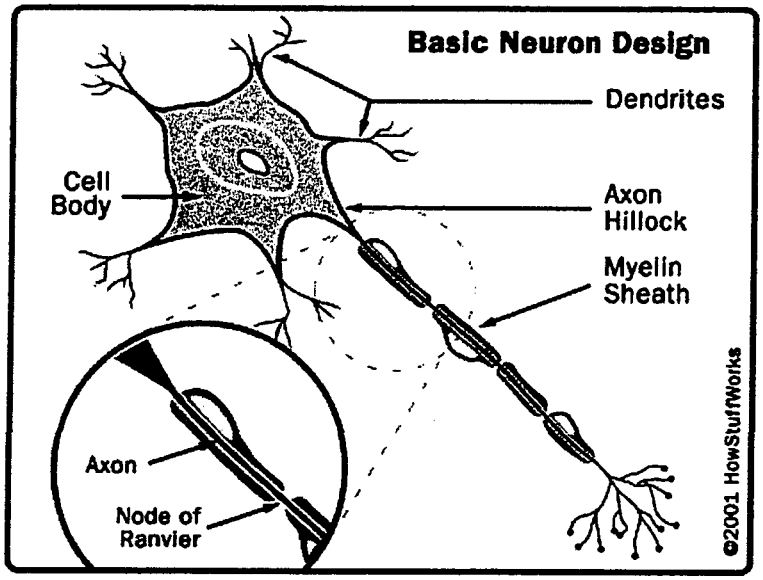

Figure 1.1: Basic parts of a neuron. Excitatory and inhibitory inputs from the outside world or neighboring neurons stimulate the neuron at the dendrites and are combined at the soma (cell body). When the potential at the soma reaches a certain threshold, an action potential (voltage impulse) is sent along the axon (from left to right) to the basal dendrites to be transmitted to other neurons.

of action potentials.

Although most neurons communicate through action potentials, each type of nervous receptor is specialized in detecting certain forms of exterior stimuli. Temperature, light, chemicals and electric fields are a few of the stimuli detected by neurons involved in sensory transduction. In particular, the spatio-temporal characteristics of the stimulus is also an important factor for transduction (see e.g. [35]). As an example, the response of certain receptors to periodical stimuli such as the sound receptors in the cochlea and other mechanoreceptors is now an important part of the research in neuroscience (see e.g. [33, 22, 23]). Often this response depends on the frequency of the stimulus; resonant and phase locked behaviors are very commonly observed in such specialized neurons.

A process called active electrolocation and electrocommunication observed in the weakly electric fish also involves the periodic stimulation of a neuron. Using receptors sensitive to time-varying electric fields, some fish can communicate and learn about their immediate environment.

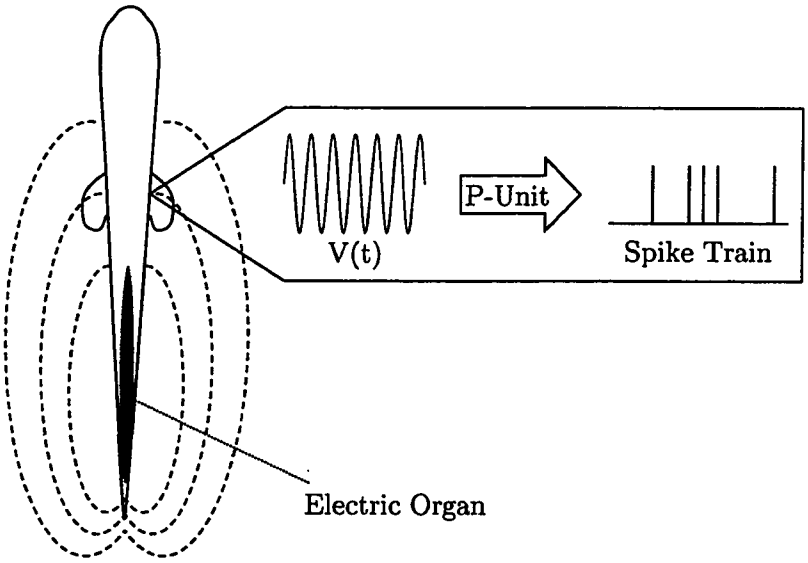

Figure 1.2: Active electrolocation. The electric field resulting from the electric organ discharges induces a periodic transdermal potential that is sensed by electrosensory afferents located at the surface of the fish's skin and transmitted to the higher levels of the nervous center via trains of action potentials.

1.1 Electrolocation and the role of P-afferents

The weakly electric fish probes its environment via active electrolocation (see e.g. [3]). For this purpose, the fish possesses an electric organ located in its tail. This organ emits a periodic electric discharge resulting in a time-varying pattern of electric field lines around the body of the fish. The resulting periodic electric field is usually referred to as the Electric Organ Discharge or EOD and is characterized by a frequency and shape — continuous functions such as sinusoids or intermittent pulsed discharges — proper to each species.

Along the surface of the fish's skin, the EOD induces a varying transdermal potential (see figure 1.2) that is detected by receptors sensible to electrical potentials. These "electroreceptors" sense changes in local transdermal potential and respond by sending action potentials (AP) to higher levels of the nervous system via afferent nerves.

Spiking activity in the electroreceptors tends to be phase locked to the frequency of the EOD [37, 40, 41]. Indeed, a close look at spike occurrence times reveals that firings always occur within a certain EOD phase interval and at most once per cycle. Consequently, consecutive action potentials are separated in time by roughly a random number of EOD cycles. This behavior is called "skipping". Accordingly, we associate to each of those receptors a probability P that it triggers a spike at each EOD cycle. It is observed that the P value is

a smoothly increasing function of the EOD amplitude [40]. It turns out that this particular response has a very important role in signal detection and processing.

The periodic electric field generated by the fish can be perturbed by the presence of nearby objects or other fish with an impedance different from the surrounding water[3]. This results in a modulation of the otherwise constant amplitude of the EOD carrier signal. Since the spike rate of the receptors depends on the carrier amplitude, their instantaneous firing rate gets modulated. Thus information about the fish's environment is carried to higher centers of the brain through timing of firing events. Also, as in most neuronal detection processes, the input signal has very little influence on the shape and magnitude of individual action potentials, which, as we said earlier, points to an even greater importance of the timing of spikes.

The transduction process through which the modulated EOD is translated in a train of action potentials by P-type electrosensory afferent is addressed in the present work. Earlier work has revealed that a certain population of these receptors show a wide range of values of P — even within the same specimen for which the EOD frequency is constant for all receptors [41]. In the light of this observation we ask ourselves if this distribution is an essential feature for modulation detection. If so, we would like to understand and quantify the effect of P on the encoding process going on in the receptors.

The phenomenon of electrolocation and electrocommunication is observed for instance among some species of gymnotiform electric fish for which the periodic EOD is a continuous quasi-sinusoidal signal [3]. The frequency of this signal is not only distinct from one species to another but also within the same species, as gender usually has an influence. The *Apteronotus Leptorynchus* is one on these species and exhibits EOD frequencies ranging from 600 Hz to as much as 1 kHz. Another species called *Eigenmannia* is characterized by a lower frequency with values around 400 Hz. It is not known why this frequency varies across species.

1.2 P-Afferents

1.2.1 Physiology

A single P-type electrosensory unit consists in tens of individual receptor cells grouped at the base of an epidermal pit [3]. Each of the receptor cells releases neurotransmitter from its "basal" portion located under the skin (see figure 1.3) when submitted to an electric field. The neurotransmitter diffuses to an afferent nerve that innervates the whole unit and triggers

an action potential when the stimulation from the receptor cells reaches a given threshold.

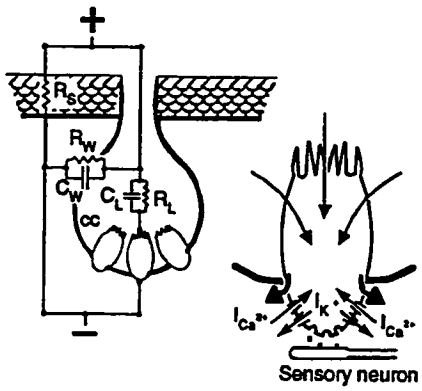

Figure 1.3: Illustration of a P-unit. Multiple receptor cells are located in an epidermal pit. On the right is the detail of a receptor cell releasing neurotransmitter to the afferent nerve. (From [3])

Neurotransmitter release rate and conductance are known to be unreliable during the synaptic transmission process (unreliable here is used in the sense of "noisy"). Although no recording of the intracellular dynamics are yet possible, it is strongly believed that the synaptic transmission process at the release sites, given their large number and their associated unreliability, is responsible for most of the stochastic part of the encoding process in P-units [5, 31, 42]. For instance, the threshold value of the electric field capable of causing the emission of neurotransmitter at different release sites is not well defined and seems to be highly influenced by the instantaneous state of the ressources (transmitter vesicles, etc.) of the synaptic process. [39].

1.2.2 Basic Dynamics

In the species *Apteronotus Leptorynchus*, changes in transdermal potential are encoded by electrosensory afferents that are commonly divided in two types based on their anatomy and their sensitivity to electric signals: tuberous and ampullary receptors. Tuberous receptors respond to changes in the amplitude of the EOD carrier, whereas ampullary receptors respond to much lower frequency signals whose origin is also extrinsic to the fish. Tuberous high frequency afferents also divide into two subtypes that can be easily distinguished by their response to the unmodulated EOD [37].

P is defined as the probability of a tuberous receptor to trigger a spike at each cycle. Time coders or T-type afferents fire one spike at each EOD cycle within a very narrow phase

of the periodic carrier without regards to fluctuations in the instantaneous amplitude of the carrier. This translates in a P value of 1. The information transmitted by such receptors, if there is, can only be contained in the phase, thus in the very precise timing of the spikes.

The other type of tuberous receptors, *which is the one of interest in the present work*, encodes carrier amplitude modulations (AM) rather than exact timing of the input discharges (cycles). A P-unit or "probability coder" fires irregularly and at most once per EOD cycle; hence its firing rate cannot exceed the fish's own EOD frequency. Like T-units, its firings are also restricted within a certain phase interval although this interval is broader.

The probability P of firing per cycle associated with a P-unit is given by its baseline firing or "firing rate" at rest. It is usually estimated by dividing the total number of spikes observed during a given time interval by the number of carrier cycles over that period. When the fish is in a calm environment, free of nearby objects, the driving force of the fish's own electric field on its P-units is unperturbed and a constant (i.e. unmodulated) amplitude EOD is sensed at the receptor locations. In these conditions, the mean number of spikes per EOD cycle defines the baseline firing rate. It is observed that P, a quantity between 0 and 1, actually depends smoothly on the carrier amplitude and thus, the instantaneous firing rate of a P-unit conveys some amplitude information [31].

1.2.3 Measurements on P-units

The dependence of the firing rate on stimulus amplitude in P-units was measured for instance by Wessel [40] on afferents from specimens of the Eigenmannia species. The firing rate of P-units forced with an artificial periodic electric discharge with constant amplitude was measured at the afferent nerve that innervates the whole unit. The rate increased monotonically with the driving amplitude with saturation effects observed at high firing rates as the firing probability is never greater than one.

Numerous aspects of the baseline firing statistics of P-units is presented in [31]. The baseline firing activity of more than a hundred receptors selected from 9 Apteronotus Leptorynchus specimens (EOD frequency around 800 Hz) was measured. Values of P ranging from 0.2 to 0.6 spikes per cycle were found and baseline firing rates ranged from 100 to 600 Hz. Similar firing statistics were also measured by Bastian (unpublished data) and analyzed by Longtin [29].

A closer look at higher orders of the firing statistics revealed two classes of firing patterns:

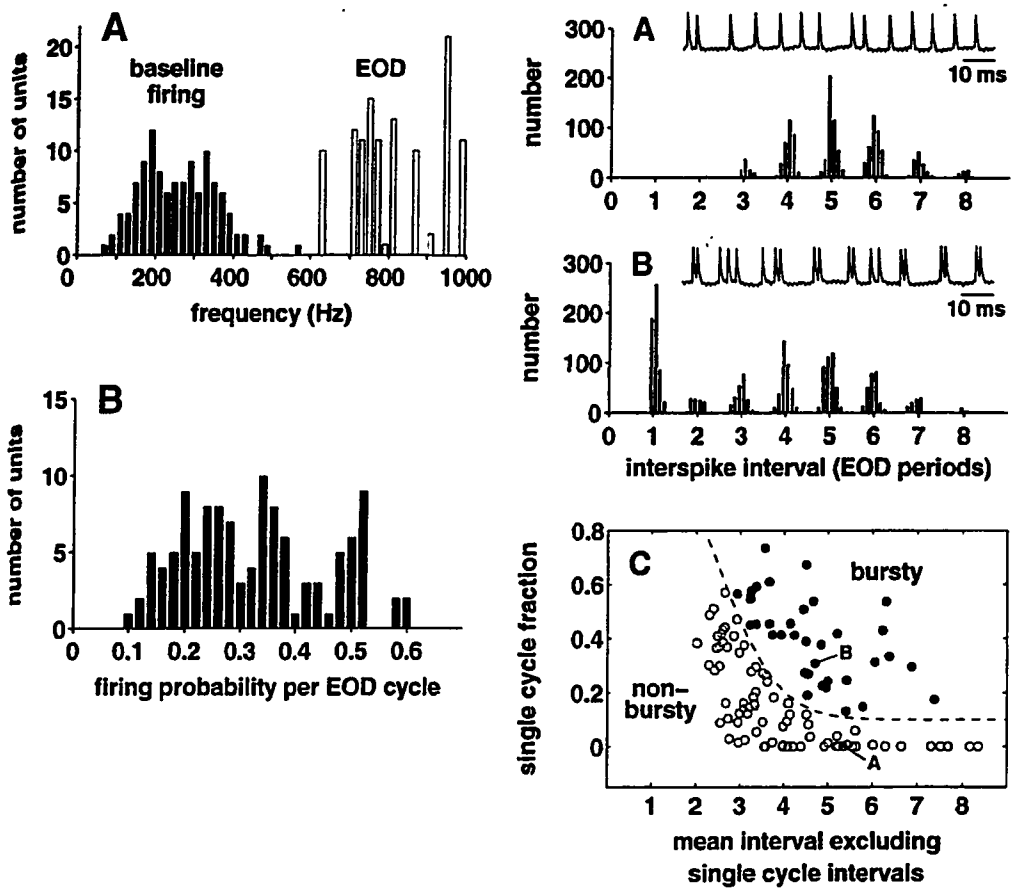

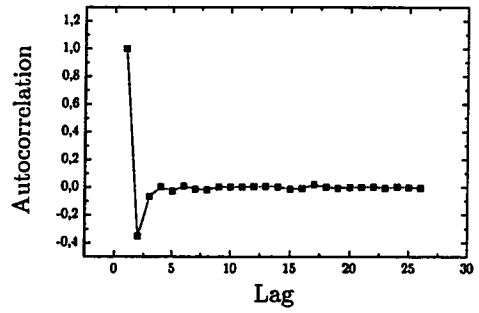

Figure 1.4: Baseline firing characteristics of P-units of A. Leptorynchus in the presence of the EOD alone (no amplitude modulations). (A, left) Histogram of EOD and firing frequencies from a population of afferents. (B, left) Histogram of P values across a population. Top right illustrations show two classes of firing patterns in P-units. Typical spike trains and histograms of spike intervals expressed in terms of EOD periods reveal a non-bursty (A) and a bursty unit (B). The latter type often triggers spikes in pairs or triplets with longer pauses in between those pairs or triplets. (From Nelson [31]) (BOTTOM) Autocorrelation of interspike intervals in Apteronotus Leptorynchus P-units. (From [5]).

bursty and non-bursty units. Non-bursty units fire in phase locked manner with the driving frequency and skip a random integer number of EOD cycles between successive firing events. The distribution of times between spikes revealed a bell-shaped histogram centered at around 5 EOD cycles (figure 1.4 A,right). Within this distribution, interspike times appear gathered at entire multiples of the driving period because of the tendency of P-units to fire within a certain EOD phase interval. Bursty units, as opposed to non-bursty ones, tend to trigger spikes in pairs and triplets of consecutive EOD cycles (figure 1.4 B,right).

An even closer look at the firing statistics reveals an important feature of the spiking activity. As random as they may look, the skipping intervals observed in the spike train of P-units are not exactly independent. By computing the autocorrelation (figure 1.4,bottom) from the time-series of interspike intervals, a negative correlation between consecutive intervals reveals the following pattern: when the time between two firing events is long, it is likely that the next interval will be short. Similarly, a short interval will more likely be followed by a long one as though the receptor needs to "rest" from sustained spiking activity. Apart from immediately consecutive intervals, those separated by one or more intervals show no significant correlations with one another.

All of the measurements that were performed on P-units were made at the output of whole units, directly outside the afferent nerve. These are known as "extracellular" voltage measurements. As no measurements of the spiking mechanism inside the receptors can yet be made, the exact mechanism of synaptic transmission and of firing are not known. Thus we rely on numerical calculations and mathematical neuron models to reproduce the firing statistics of P-units and understand the underlying dynamics.

A Simple Threshold Model of a P-Afferent

We now consider a simple mathematical model of a P-unit to illustrate the role of noise in the skipping dynamics of these receptors. From the point of view of a very general additively driven model ($\dot{v}$ depends linearly on the forcing term), the membrane potential v of a P-unit behaves according to:

$$\frac{dv(t)}{dt} \approx ... + \gamma x(t) \tag{1.1}$$

where "..." is a general v-dependent non-linear term, γ is a constant and $x(t)$ is the periodic forcing term.

In the case of a periodically driven neuron, the potential also fluctuates roughly according to a periodic function. Figure 1.5 proposes a very simplified model of skipping dynamics. The voltage here is represented by a sine wave; such simplification is only for the purpose of illustration and voltage response is much more complex in reality. A fixed threshold is represented by a straight line near the maximum of the voltage function. When the voltage crosses this threshold line, the neuron fires an action potential.

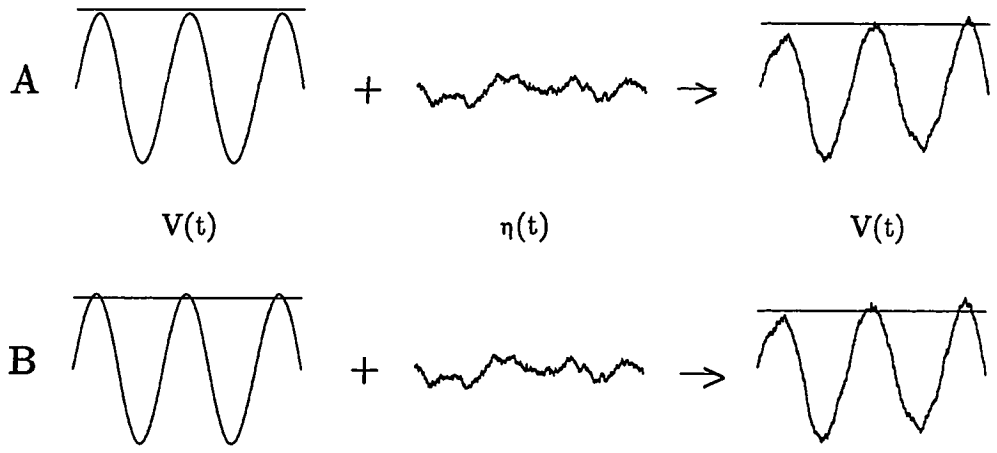

Figure 1.5: A very simplified illustration of the role of noise in skipping (A) Membrane voltage follows a sinusoidal function which amplitude is not large enough to reach threshold (represented by the straight line over the sinusoid). Adding a source of noise to the voltage solution gives rise to threshold crossings. (B) The voltage crosses the threshold at each cycle. Adding noise suppresses some threshold crossings and thus can prevent spikes.

The illustration on top shows a situation where the voltage response amplitude is not large enough to reach threshold (top left). By adding noise to the voltage function, some threshold crossings become possible and the neuron may fire (top right). On the other hand, the bottom illustration shows the case where the noiseless voltage can reach the threshold by itself. In that case, presence of noise may prevent some firings. The part of the periodic function that has a positive slope is more likely to induce an action potential than any other as the potential moves toward the "threshold" when the neuron gets depolarized. Although this is a very simplistic point of view, it constitutes one of the key elements which, combined with synaptic noise, is responsible for skipping patterns in P-type afferents; noise may break periodic firing patterns by preventing/generating spikes and induce skipping. At each cycle, the neuron either "skips" or triggers a spike within a very narrow phase interval.

1.3 Introduction to Neuron Models

We shall first introduce some well-known models from the neuroscience literature in order to address the encoding process going on in P-units. A neuron model is a mathematical description of the processes that lead to spike generation. Most often, it describes the evolution of the potential across the neuron membrane given some stimulus from the outside world or from other neurons. Some models however use other quantities as their state variables such as a dynamic firing probability.

The state of a neuron is given by its membrane potential. A difference between the potential inside and outside a nerve cell due to different ions concentrations causes its membrane to be polarized. The electrical potential inside the cell is in fact lower than the potential outside and the difference is typically -50mV. This potential changes as it is perturbed by exterior stimuli and as ion channels respond to these stimuli by allowing ions to flow in and out of the cell. It also changes due to random openings and closings of channels.

When the neuron membrane undergoes an important depolarization, an influx of positively charged sodium ions enters the cell up to a new potential difference of 40 mV. In response to such a sudden voltage change, potassium channels open and allow positively charged potassium ions in high concentration inside the cell to flow outside, thus reducing the potential to its initial state. Through this process of depolarization and re-polarisation, the potential varies according to a very rapid "spike" which propagates along axons and brings information to the brain. Only the stimuli that are strong enough to generate spikes will be transmitted in some form to other parts of the brain. Spikes can also occur by the action of many concurrent stimuli.

Although very simplified, this description of the spiking mechanism is typical to nerve and muscle fibers in all animals. Numerous numerical models of this process were developed in studies of the nervous system. Some are very complex and describe in great detail the dynamics of numerous variables, while others are very simple and allow fast computation time and easy interpretation of the results. Hence, each one of them is more or less suited to the investigation of a particular feature. Let us introduce two important models for the sake of a simple comprehension of P-afferents dynamics.

Integrate and Fire Model

As a first very simple mechanism, the integrate-and-fire (IF) model represents a neuron as a perfect integrator. Because of its simplicity, it is widely used in applications where the detail of the dynamics is not of great importance such, as may be required in large neural networks. Given an input signal $x(t)$, the dynamics of the IF model potential $v(t)$ is simply given by:

$$\frac{dv(t)}{dt} = \alpha x(t) \tag{1.2}$$

where the parameter α is a constant. Starting from an initial value v_0, the potential changes according to this equation until it reaches a chosen threshold value v_θ; a spike has been triggered. The voltage is then immediately reset to its "rest" value and the integration goes on. Thus spike times in the IF model depend on the height of the threshold — more exactly on the difference between the threshold and rest potentials — and on the dynamics of the input.

The integrate-and-fire model is made more realistic by adding a leaky term to its definition. Indeed, ion dynamics and membrane properties such as leakage and capacitance are such that over long periods of time, information about past stimuli is lost, as the potential decays to its rest value when not stimulated for a certain time. As a result the neuron "forgets" past inputs when left unstimulated. This is not the case for the integrate and fire model. This feature is easily implemented in an integrate and fire model by adding a leaking term proportional to the instantaneous state of the membrane :

$$\frac{dv(t)}{dt} = -\frac{v}{\tau_v} + \alpha x(t) \tag{1.3}$$

where τ_v is the characteristic decay time of the potential to its rest value.

Hodgkin-Huxley Model

The next model we present is based on a less intuitive approach, as it was developed from actual recordings on ions dynamics in the giant squid axon. The most celebrated model from Hodgkin and Huxley published in 1952 describes the variation of the membrane's potential due to the combined effect of various voltage-gated ionic currents [1]. As opposed to the IF model that computes spike time without actually generating a full action potential, the Hodgkin-Huxley (HH) model captures the fast depolarization-repolarization process of the action potential. Its publication has given rise to numerous other models all derived from

the general form:

$$C\frac{dV}{dt} = I_{ionic}(V, W_1, \ldots, W_n) + I(t) \tag{1.4}$$

$$\frac{dW_i}{dt} = \phi\frac{[w_{i,\infty}(V) - w_i]}{\tau_i(V)} \tag{1.5}$$

where the solution for the voltage V is governed by the ionic currents I_{ionic}. Ion channel dynamics are written as a probabilistic description of the open/close state of channels which allow ions to flow in or out of the cell. The W_i's are the fraction of channels of each given ion that are opened/closed and are, in turn, non-linear quantities with respect to the instantaneous membrane potential. The time scale over which the W_i's vary depends on the instantaneous voltage and on a general function ϕ which captures temperature effects and other experimental conditions. The $W_{i,\infty}$'s are the pseudo steady state values of the W_i's i.e. the values to which the W_i's would decay to if the voltage was kept constant. They are called pseudo steady states because they still depend on V. The forcing from external sources and other neurons is represented by the term $I(t)$.

The actual equations of the Hodgkin Huxley model describe the dynamics of the voltage due to the K and Na ions, and to a third set of ions collectively labeled as leak currents referred to with subscripts "l" (mostly chloride channels):

$$C\frac{dV}{dt} = -g_K n^4(V - V_K) - g_{Na}m^3h(V - V_{Na})) - g_l(V - V_l) + I(t) \tag{1.6}$$

$$\frac{dn}{dt} = \alpha_n(1 - n) - \beta_n n \tag{1.7}$$

$$\frac{dm}{dt} = \alpha_m(1 - m) - \beta_m m \tag{1.8}$$

$$\frac{dh}{dt} = \alpha_h(1 - h) - \beta_h h \tag{1.9}$$

$$\tag{1.10}$$

Here α_* and β_* are nonlinear terms of the form

$$\alpha_* = \frac{A(V + B)}{e^{(V+C)/D} + E}, \quad \beta_* = Fe^{V/G},$$

which basically act as thresholds. The g_k, g_{Na}, g_l are the respective ionic conductances and the V_k, V_{Na}, V_l are the equilibrium ("Nernst") potentials for each ion species. The variables n, m, and h are known as voltage dependent gating variables.

Models similar to that of Hodgkin-Huxley may contain many variables if the intention of the investigator is to capture some very specific features of the firing mechanism involving

multiple voltage-gated ion dynamics. Conversely, the number of those variables may be reduced for a simplified model used for say, a statistical study of the input-output rates of a neuron. Such reduction might be achieved by setting to constant some variables which dynamics vary within time scales orders of magnitude larger than that of the voltage. As well, an in-depth phase space analysis of the model dynamics can reveal very similar behavior of two or more variables which may be grouped into fewer and more general variables. Some reductions of the Hodgkin Huxley model are now as widely spread as the original model. Two of them, the FitzHugh-Nagumo and Morris-Lecar models are studied in the present work.

1.4 Understanding the neural code

It was observed from very early experiments on neurons that their response to external stimuli always presents an element of randomness. In an experiment where the exact same stimulus is presented twice to the same neuron, the two resulting spike trains are usually not identical. Thus one may want to quantify the degree of randomness and identify the source of this variability. Moreover, we would like to find a way to characterize the neural response which takes into account the fact that the response is not reproducible.

In order to understand the neural code, we must find the relationship between the spike train and the input stimulus. However, trying to write a "dictionary" — a one-to-one mapping — of the neural responses is not possible because of the random nature of the response. The stochastic element must be included in the description by using probabilistic concepts to describe the code. We present a probabilistic approach using the definitions from [35], which presents a thorough discussion of these issues.

A probabilistic description of the relationship between the spike train characterized by events at times $t_1, t_2, ...t_N$ that we will call $\{t_i\}$ and the external stimulus $s(t)$ should allow a comprehension in both directions. Let the stimulus presented by the experimentalist be taken with probability $P[s(t)]$ from an infinite set of possibilities from the real world and let $P[\{t_i\}]$ describe all the possible spike trains emerging from the neuron. A comprehension in both directions means that one should not only be able to predict the distribution of the possible sets of spike trains given the input $P[\{t_i\}|s(t)]$, but also be able to recover the distribution of input signals that may generate a given spike train $P[s(t)|\{t_i\}]$.

Given these definitions, the most general probabilistic description of the code is the joint probability $P[\{t_i\}, s(t)]$ of finding a given pair $s(t)$ and $\{t_i\}$ in one experiment. It can be

written

$$P[\{t_i\}, s(t)] = P[\{t_i\}|s(t)]P[s(t)] \tag{1.11}$$

or from the point of view of the brain — an incoming spike train is drawn from a distribution of spike trains given by:

$$P[\{t_i\}, s(t)] = P[s(t)|\{t_i\}]P[\{t_i\}] \tag{1.12}$$

Equalities 1.11 and 1.12 lead to a relation through Bayes' rule [32] that relates the two points of view:

$$P[s(t)|\{t_i\}] = P[\{t_i\}|s(t)]\frac{P[s(t)]}{P[\{t_i\}]} \tag{1.13}$$

which implies that if we establish the rules of the code in either one of the ways, we would be able to understand it in both ways. However, the concept of a complete description is not realizable. Earlier experiments have achieved some of the characterization up to the first few moments of the distributions but, as one keeps looking to higher orders, new observed features make the description more and more complex.

In this thesis, we will consider the point of view of the brain in the reduced problem of computing the average input (from the distribution $P[s(t)]$) given the spike train, to the extent that we approximate the neuron as a linear black box. Before doing so, let us explain a few more concepts related to the neural code.

1.4.1 Encoding: the neuron as a transfer function

Neuron dynamics usually involves complex non-linear behavior and can be more easily studied by separating the linear part from the non-linear ones in the neural response function. This can be done using Volterra and Wiener methods to characterize a nonlinear system. Starting with the basic concept of a Taylor series to expand a general function $y = f(x)$ in the vicinity of $x = x_0$ as a series of powers, let's consider the more general case where the input is a time series $x(t)$ instead of a single quantity x. It is described mathematically by the relation $y(t) = F[x(t)]$ called a functional and its expansion is given by:

$$y(t) = g_0 + \int dt' g_1(t')x(t-t') + \int dt' \int dt'' g_2(t', t'')x(t-t')x(t-t'') + ..., \tag{1.14}$$

a series known as the Volterra expansion where expansion terms (g_0,g_1,...) are not independent. Wiener's work showed that if the input is Gaussian white noise, then the functions describing the expansion are statistically independent, allowing us to write:

$$y(t) = h_0 + \int dt' h_1(t')x(t-t') + ..., \tag{1.15}$$

where Wiener kernels (h_0,h_1,...) are independent. This allows one to evaluate the first Wiener kernel h_1 by ignoring correlations between the input and output of higher order than the linear term. More simply, by studying first order correlations between the input and the response, one can find a linear filter that captures all the linear part on the encoding process.

The first Wiener kernel represents the mean feature in the input stimulus that triggers a spike, as if the neuron was "looking for" a particular shape in the signal. Indeed, the value of the convolution integral (eq. 1.15) is maximum when $h_1(t)$ is close to the "preferential feature" and the result is a sharp spike in $y(t)$.

1.4.2 Decoding: linear reconstruction

One way to treat the neural code problem would be to start from the spike train and evaluate a continuous time series as an estimate of the original stimulus. Apart from the fact that the brain does not have access to an entire spike train but only to a small "instantaneous" part of it, this estimation method is somehow implemented by the brain [35]. From such an estimate, one could quantify the quality of the reconstruction by comparing the estimated signal and the real stimulus. That method is called the "linear reconstruction technique" [15, 40, 35].

To do so, one would like to find a "transfer function" similar to eq. 1.15 but this time with the spike train as an input. Considering the probabilistic nature of neurons (one particular spike train may result from different stimuli), one way to achieve this is to compute the average stimulus s_{est} from the distribution $P[s(t)]$ given the spike train. This corresponds to building a linear black box that takes the spike as an input and estimates the stimulus. More technically:

$$s_{est} = \int dt\ h(t)\ x(\{t_i\}) \tag{1.16}$$

where $h(t)$ is an "optimal" decoding filter also called Wiener-Kolmogorov filter. It is defined by the function that, once convolved with the spike train, generates an estimate with minimized mean squared error when compared with the original stimulus.

The detailed steps to evaluate such a filter are presented in section 2.2.1. Briefly, from a neuron response (spike train) to a particular input, one uses correlations between the spike train and the input to evaluate the linear part of the neuron's transfer function. The spike train is then "decoded" via this filter to evaluate an estimate of the input which is compared to the real input. The encoding/decoding process is well illustrated by figure 1.6 from [35].

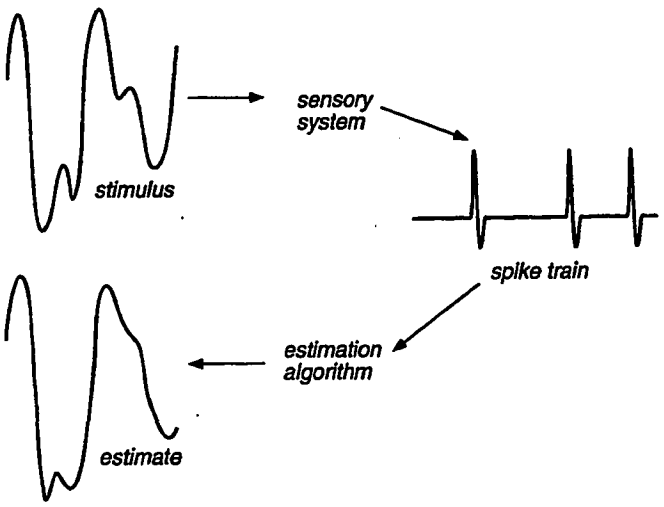

Figure 1.6: The encoding/decoding process. A filter is built from the correlations between the input stimulus and output spike train which captures the linear part of the encoding process. It is used to calculate an estimated stimulus from the spike train. The quality of encoding is quantified by comparing the estimate with the original stimulus. (From [35])

The filter evaluated from the linear reconstruction method is not a universal filter that captures the response of this neuron to any stimulus. It is in fact a little more restrictive because its computation is influenced by the particular stimulus that was used. Thus, the evaluated filter is not a property of the neuron alone but more exactly a property of the neuron given our particular input signal.

1.5 Tools

Throughout the present work, graphical representation of certain variables involved in spiking mechanisms are extensively used. Some of the following tools are very commonly found in the neuroscience literature. We discuss the typical use and appearance of each plots as well as their relevance for the study of signal transduction in skipping in neurons.

1.5.1 Interspike Interval Histograms

An interspike interval histogram is constructed by bining the time intervals between firing events of a spike train. It is intended to reveal the distribution of the stochastic point process of which the spike train is a sample realization.

For a skipping P-unit, interspike intervals are grouped at integer multiples of the carrier's period. It appears as "modes" or peaks in the ISIH as seen in figure 1.4 right(A,B); in this

particular case, the ISIH is said to be multimodal. Often, the magnitude of the modes follow a unimodal relation with increasing interspike interval. The height, width, separation and relative intensities of these modes may provide information about various parameters such as mean carrier amplitude and frequency, noise intensity and distance to threshold. For example, if a neuron operates close to threshold or is forced with a high amplitude EOD, it has a high probability of firing at each cycle and its output rate is high. As a result, the interspike intervals are short and appear at small numbers of EOD intervals in the ISIH. Synaptic noise and conductance fluctuations affect the amount of jitter in the exact phase of the spikes, hence it affects the width of the ISIH modes. The relative amplitude of the modes and their widths is also greatly dependent on the particular dynamics of the neuron and sometimes allows us to identify categories and mechanisms of skipping neurons. As an example, figure 1.4 shows that bursty units are characterized by a unimodal histogram shape (due to intervals between bursts) with an additional peak at an interval of 1 EOD cycle (due to the very short intervals within the bursts).

1.5.2 Tuning Curves

Tuning curves describe the sensitivity of excitable systems in their response to exterior forcing signals. They provide information about the firing threshold of such systems when periodically forced with a given frequency and amplitude. It can reveal some receptor's preferential response to certain frequencies, e.g. in the cochlea. An example of a tuning curve is presented in figure 1.7.

A tuning curve is traced by identifying in the two-dimensional amplitude-forcing frequency (or period) phase space, the limits of regions that exhibit distinct phase-locked firing patterns. Such firing patterns are usually described as n:m (pronounced "n to m") patterns where n and m are integers that represent respectively the number of EOD cycles and the number of spikes within one periodical firing pattern. For instance, a P-units fires 3:1 when it triggers a spike once every 3 EOD cycles.

Experimental investigations have revealed recognizable features in tuning curves of tuberous electroreceptors [43]. T-units are characteristically V-shaped while P-units exhibit L-shaped curves. Such observations point to a possible determinant role of noise in the latter type [28]. Noise lowers the branch of the V-shaped curve in the region of long periods (low frequency) thus effectively lowering the threshold and in turn allowing a better transduction

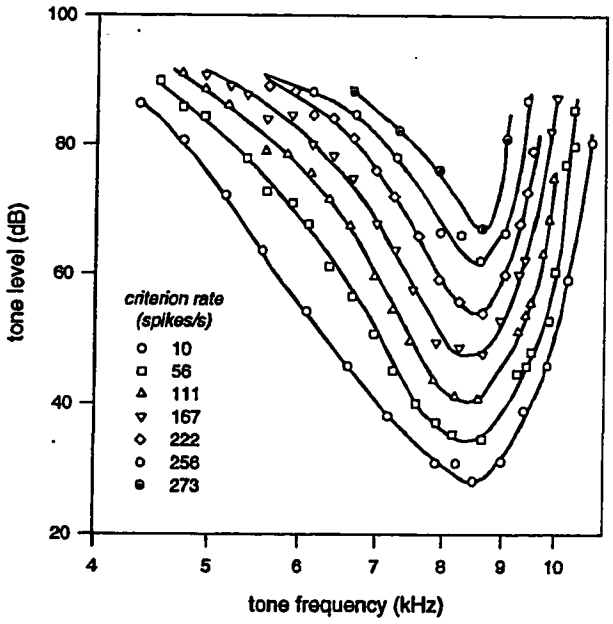

Figure 1.7: Tuning curve of a cell in the cat auditory nerve. Lines are iso-rate contours of the output rate of periodically driven cells. We observe that the cell have a preferential frequency for which a minimum forcing amplitude is needed to achieve a given firing rate. (From [35])

of low frequency stimuli.

1.5.3 Devil's Staircase

In practice, the P value of a unit is a smoothly increasing function of the forcing EOD amplitude (r_0) [40]. In deterministic numerical models forced with only one sinusoidal signal (no noise source, no amplitude modulations) the relation between P and r_0 has a more complex structure. For some intervals of r_0, plateaus of constant P value are observable in the otherwise monotonically increasing function. Those plateaus reveal the phase locking property of P-units models; two distinct values of forcing amplitude may give rise to identical firing probabilities. They are visible at values of P associated with firing patterns of integers numbers of cycles (eg. 2:1, 3:1, 3:2). Such phase locking is expected from periodically driven oscillators (see e.g. Glass and Mackey [19])

The presence of noise in actual P-units, modeled by adding a stochastic signal to the periodic forcing, breaks phase locked firing patterns by randomizing the spike arrival times [5, 18]. As a result, plateaus are washed by the presence of noise and the P vs r_0 is smoothed. Such linearization of the input-output relation may allow for a better signal transduction; a similar effect was presented in a study of stochastic resonance (SR) in the FitzHugh-Nagumo

neuron model [6, 7, 21].

1.6 Recent Work on Information Transfer in P-Afferents

The stimulus reconstruction method was applied to measurements over P-type receptors of the Eigenmannia in a study by Wessel [40]. Their conclusions pointed to an important role of the mean firing rate in the information transmitted by the receptor: basically, more information is transmitted at higher rates. Moreover, the stimulus contrast — i.e. the magnitude of the modulation compared to the mean carrier amplitude — and the frequency content of the stimulus also has an influence on signal transduction, according to their analysis on spike trains recorded from the afferent nerve.

Zador has studied the effect of synaptic unreliability in [42], although this study was not applied to periodically driven neurons but to pyramidal neurons located in the cortex. He considered a model in which a population of unreliable synapses transmitting a presynaptic Poisson process provided the forcing to a simple deterministic integrate and fire neuron model. (A Poisson process is a spike train with exponentially distributed intervals with zero serial correlation between intervals). Using a direct method to evaluate the mutual information transmitted by the model, it was observed that the information rate (in bits/sec) increased monotonically with the probability of the synapse to transmit an incoming Poisson event. Thus, in this particular model, signal transduction gets better as synapses become more "reliable".

An investigation of the role of noise over various information measure was treated by Heneghan [21] through a study of aperiodic stochastic resonance in the FitzHugh-Nagumo model (see chapter 4). In such a model, information transfer from stimulus to response of weak signals appear to be optimized by the presence of noise. Furthermore Chialvo, Longtin [6] have linked this effect to the linearization by noise of the response curve associated to the spiking mechanism.

1.7 Scope and organization of thesis

The present study consists of an investigation of the effect of synaptic and conductance noise on the transduction of minute signals through carrier amplitude modulation. It is done in the context of four published neuron models used here as P-unit models: the leaky integrate-and-fire with dynamic threshold because it captures most of the P-units statistics; the FitzHugh-

Nagumo model, for its realistic voltage dynamics and its popularity in the literature; the Morris-Lecar model for its two possible implementations which operate in the vicinity of two different bifurcations giving rise to repetitive firing as the mean of the stimulus is increased; and the Nelson model for its frequency response approach and simplicity. Through those more or less complex spiking models, we will consider the effect of a stochastic forcing term on information transfer via an investigation in the phase space of the model parameters. For each model, the thesis aims at answering the following questions:

- What are the basic dynamics and the firing statistics of the considered model and how do these apply as a P-unit model considering published experimental measurements on actual P-type electroreceptors?
- What is the effect of the various parameters on P, the probability of firing at each EOD cycle of the P-unit? Remember that the value of P is defined as the mean firing event per EOD cycle when the model is "at rest", i.e. when driven by a constant amplitude EOD (no stimulus).
- What is the effect of P, and thus of the various parameters that determine P, on the quality of information transfer in these models. This will be done using the stimulus reconstruction technique which involves considering the neuron as a black box and evaluating the amount of linear correlation between the input and output signals.

The next chapter presents the numerical methods as well as the analysis techniques used for the thesis. The detailed research over the four models considered in this thesis, namely the Leaky Integrate and Fire model with Dynamic Threshold (LIFDT), FitzHugh-Nagumo(FHN), Morris-Lecar (ML) and Nelson's models are each presented in chapters 3 through 6, respectively. In each chapter, the basic dynamics are illustrated and more elaborate considerations on specifically relevant parameters are discussed using the techniques and language established in the two first chapters. In the light of these discussions, the results of our information measurements are then presented and analyzed. As a conclusion, the last chapter formulates more general statements in the light of the results from all models.

Chapter 2 Method

For the study of information transfer in different numerical models of P-type afferents, the same sequence of numerical techniques was used for each of the models. The calculations consisted of two main steps. In each case, a Fortran code was written to generate a stimulus $s(t)$ and numerically integrate the model's equations driven by a modulated EOD. The output of this program — in the form of a list of interspike intervals along with the stimulus — were then processed through a Matlab algorithm for computation of information measurements. This chapter presents the various numerical methods used and their mathematical justification.

2.1 Simulations

A Fortran code with fixed time step Euler integration scheme was written for each neural model considered. Our choice of a first order scheme was based on a few considerations about the dynamics of stochastic neuron models. First, membrane voltage usually fluctuates over many different time scales. For example, our algorithm must be very precise while integrating a fast varying spike event but could use a much larger time step when the voltage fluctuates around its rest value. However, adaptive methods could not be used because of the stochastic nature of the simulations. Furthermore, accurate methods for numerical integration of noise with order better than 1 demands much more calls to the derivatives which costs a lot of time for some models [10]. For every model considered, the choice of the fixed time step size was done using the techniques discussed in [27]; its value is chosen small enough so that our qualitative results are not changed upon making it smaller.

The routine generates a stimulus $s(t)$ that consists in a Ornstein Uhlenbeck signal filtered by a fourth order low-pass filter characterized by a very sharp cutoff frequency. We refer the reader to section 2.1.3 for more details. It also generates an EOD — approximated by a sine

function — modulated with the stimulus using the following equation:

$$\mathrm{EOD}(t) = r_0\big[1 + s(t)\big]sin(\beta t) \tag{2.1}$$

where r_0 is the mean EOD amplitude (mV) and β the angular frequency of the EOD. This method of multiplying the whole term $\big[1 + s(t)\big]$ with the amplitude r_0 is called constant contrast simulation [40]. It scales the modulation with the amplitude so that the overall aspect of the EOD is unchanged when r_0 is modified. Unless stated otherwise, all our simulations were made at constant contrast.

As a simulation of a particular dynamical model progresses, random numbers are generated; these are used either for the generation of noise signals, stimulus signals or even for taking decisions via a Bernouilli trial. The detailed use of random numbers is specific to each model and will be more thoroughly discussed in each particular case. However, Gaussian white noise and correlated noise are often encountered and the details of the algorithm used are in the upcoming sections 2.1.1 and 2.1.2.

Each model was numerically integrated by a Fortran algorithm that checks for spiking events at each integration step. This is usually done by comparing the membrane voltage with a certain threshold value. When the voltage crosses it with positive slope, an interspike interval is computed and written to an output file.

Certain models include an absolute refractory period. This period represents the minimal time before which the neuron can fire again after having fired. It is due to the inactivation of ionic channels that were activated for spike initiation. It also ensures that the spike handling algorithm does not take into account double crossings due to a stochastic component. Indeed, when the voltage variable gets near the threshold, a fast varying noise source can induce multiple crossings of the voltage threshold in a very short time interval. With refractoriness, when a spike is detected, the program simply keeps integrating if the interspike interval is less than t_{refrac}.

For all simulations, a certain number of iterations were rejected as transients from the beginning of the solution. The chosen number of iterations to be rejected changes across models and is determined based on the longest time constants associated with each model. In all cases, a few multiples of the longest time constant of the system was used as the transient period.

2.1.1 Random Deviate Generation

The uniformly distributed random number generator RAN1 described by [34] was used in all of our routines for generation of any stochastic time series. Its repeating cycle is evaluated at 2×10^8 while our simulations last at most 2×10^7 iterations. This algorithm was proven robust to any correlation test known.

Gaussian deviates when needed were obtained using the well-known Box-Muller algorithm also presented in [34]. Briefly, starting from to uniform deviates β_1 and β_2, two uncorrelated Gaussian random number ξ_1 and ξ_2 with mean zero and variance $\sigma_\xi^2 = D$ are given by:

$$\xi_1 = \sqrt{-2D\ln(\beta_1)}\cos(2\pi\beta_2) \tag{2.2}$$

$$\xi_2 = \sqrt{-2D\ln(\beta_1)}\sin(2\pi\beta_2) \tag{2.3}$$

2.1.2 Correlated noise generator

The release of neurotransmitter from the receptor cell to the afferent nerve is know to be a stochastic process with correlation time comparable to or faster than the time associated with spike generation. Membrane conductance is also known to fluctuate and cause non-linear amplification of synaptic input in neurons. Throughout our work we approximate all stochastic sources with one random process whose correlation time can be adjusted. A Ornstein Uhlenbeck process is a band-limited version of a Gaussian white noise process characterized by an exponentially decreasing autocorrelation. An algorithm to generate such random deviates was proposed by Fox [11] to compute correlated noise.

One seeks an algorithm for numerical integration of the general equations:

$$\dot{x} = f(x) + \eta \tag{2.4}$$

$$\dot{\eta} = -\lambda\eta + \lambda\xi \tag{2.5}$$

where ξ is a Gaussian white noise process with

$$\langle\xi(t)\rangle = 0 \tag{2.6}$$

$$\langle\xi(t)\xi(s)\rangle = 2D\delta(t-s) \tag{2.7}$$

and η a Ornstein Uhlenbeck process with

$$\langle\eta(t)\rangle = 0 \tag{2.8}$$

$$\langle\eta(t)\eta(s)\rangle = D\lambda e^{-\lambda|t-s|} \tag{2.9}$$

so that a sample of the process $\eta(t)$ within a time of the order $\tau \equiv 1/\lambda$ shows significant correlation.

Euler stochastic integration scheme are usually accurate to order 1/2 i.e. as one reduces the integration step by a factor N in order to reduce the error associated with the approximated integral, the error reduction is proportional to $N^{1/2}$. However the algorithm considered here is of order 1.

At each iteration, one generates two random numbers a and b with uniform distribution and computes:

$$h = \sqrt{-2D\lambda(1-e^{-2\lambda\Delta t})\ln(a)}\cos(2\pi b) \tag{2.10}$$

$$\eta_{t+\Delta t} = \eta_t e^{-\lambda\Delta t} + h \tag{2.11}$$

Throughout the thesis we will refer to D as the intensity or "amplitude" of the colored noise. However, the intensity of the noise is usually defined by its variance. In the case of a OU process with correlation time τ, it corresponds to $VAR(\eta) = D\lambda = D/\tau$. Thus, for constant τ, the intensity is simply proportional to D, the intensity of the Gaussian white noise.

2.1.3 Bandlimited Gaussian Random Signal

Typical environmental stimuli detected by the fish are well modeled by a bandlimited Gaussian white noise (modulations of the EOD with very high frequency are not detected) [2]. Hence, our stimulus is generated using Gaussian white noise (see sect. 2.1.1) that is filtered by a fourth order filter with cutoff angular frequency α. Its transfer function is

$$H(\omega) = \left|\frac{\alpha^4}{(\omega-\alpha)^4}\right| \tag{2.12}$$

Following the derivation in appendix A, the following algorithm was used.

$$\dot{s} = z_1 \tag{2.13}$$

$$\dot{z}_1 = z_2 \tag{2.14}$$

$$\dot{z}_2 = z_3 \tag{2.15}$$

$$\dot{z}_3 = -A\alpha z_3 - B\alpha^2 z_2 - A\alpha^3 z_1 - \alpha^4 s(t) + \xi_2(t) \tag{2.16}$$

where $\xi_2(t)$ is a zero-mean Gaussian random signal.

2.2 Quantifying Information Transfer

2.2.1 Stimulus Reconstruction Technique

A Matlab routine originally written by F. Gabbiani (available on the web [14]) was adapted to evaluate information measurements on the simulation results in each model. It uses as input argument the original stimulus $s(t)$ and the resulting interspike intervals, both generated by the Fortran code which simulates the model. From the input and output signal of the neuron, the routine computes a linear estimate $s_{est}(t)$ of the stimulus that is finally compared with the original $s(t)$ to quantify the quality of information transfer. It is done using the linear reconstruction technique via calculation of the Wiener-Kolmogorov filter [15, 40].

The theory due to Kolmogorov and Wiener provides a linear filter that yields the best possible linear estimate (in the mean square sense) $y_{est}(t)$ of a signal $y(t)$ given another observed signal $x(t)$. In our case, the observed signal is the spike train $x(t)$ from which we subtract the mean firing rate x_0:

$$x(t) = \sum_i \delta(t - t_i) - x_0 \tag{2.17}$$

and we seek an estimate $s_{est}(t)$ of $s(t)$ (also with subtracted mean value). The linear reconstruction is achieved by convolving the spike train with an optimal filter $h(t)$

$$s_{est}(t) = \int_0^T dt' h(t - t')x(t'), \tag{2.18}$$

(where T is the total duration of the spike train) and by a choice of this filter so that the mean square error associated to the estimate,

$$\epsilon^2 = \frac{1}{T}\int_0^T dt[s(t) - s_{est}]^2, \tag{2.19}$$

is minimized. From the orthogonality principle, one finds that the expression of the filter in the frequency domain is:

$$h(f) = \frac{S_{sx}(-f)}{S_{xx}(f)} \tag{2.20}$$

where $S_{sx}(f)$ and $S_{xx}(f)$ are the Fourier transforms of the cross-correlation between the stimulus and spike train R_{sx} and the autocorrelation function of the spike train R_{xx}, respectively:

$$R_{sx}(\tau) = \frac{1}{T}\int_0^T dt\ s(t)x(t+\tau) \tag{2.21}$$

$$R_{xx}(\tau) = \frac{1}{T}\int_0^T dt\ x(t)x(t+\tau) \tag{2.22}$$

Thus, $h(t)$ from expression 2.18 can be written:

$$h(t) = \int_{-f_c}^{f_c} df \frac{S_{sx}(-f)}{S_{xx}(f)} e^{-i2\pi ft} \tag{2.23}$$

where f_c is the cutoff frequency of the filter used to generate the stimulus $s(t)$. Here, the integral over all frequencies reduces to the range $[-f_c, f_c]$ because the frequency components of the stimulus are zero for values of $|f| > f_c$.

In practice, the Matlab routine first generates a spike train $x(t)$ (an array of '0's and '1's) from the interspike times t_i, with sample step equal to the sampling rate of $s(t)$. The Nyquist frequency of the sampling was chosen much larger than the cutoff frequency of the bandlimited stimulus in each model to avoid aliasing.

After subtraction of the respective mean values of $x(t)$ and $s(t)$, estimates of $S_{sx}(f)$ and $S_{xx}(f)$ are computed using an averaging method (from the Matlab signal processing toolbox) assuming ergodicity of the process; the power and cross-power spectral densities of equation 2.20 are averaged over windows of 2048 points (with overlap of 1024) from the spike train and stimulus. Each section of the signal is Bartlett-windowed [34] before the spectral density is evaluated. All simulations contained at least 100 000 points so that nearly 100 samples were used for the calculation of a particular $h(t)$.

The optimal filter is first calculated in the Fourier domain using equation 2.20 and converted to the time domain through an inverse FFT routine. Finally, a Matlab algorithm convolves the time version of the filter and the spike train via the frequency domain to yield s_{est}. The coding fraction and mutual information can than be evaluated by comparing the estimate with the original stimulus using the concepts described in the following sections.

2.2.2 Coding Fraction and Information Rate

The deviation of the linear estimate from the actual stimulus can be seen as a "noisy" signal that contaminates the reconstruction. We define the noise $n(t)$ as the difference between the two signals

$$n(t) = s_{est}(t) - s(t) \tag{2.24}$$

and we express the mean square error (Eq. 2.19) in terms of this new quantity

$$\epsilon^2 = \frac{1}{T}\int_0^T dt[n(t)]^2 \tag{2.25}$$

$$= \int_{-f_c}^{f_c} df\, S_{nn}(f) \tag{2.26}$$

$$= \int_{-f_c}^{f_c} df \frac{S_{ss}(f)}{\mathrm{SNR}(f)} \tag{2.27}$$

with the signal to noise ratio $\mathrm{SNR}(f)$ being a measure of the amount of signal power relative to the noise power at any frequency:

$$\mathrm{SNR}(f) = \frac{S_{ss}(f)}{S_{nn}(f)}. \tag{2.28}$$

It is a positive quantity and it takes its minimum value 1 when the contribution to the power at a given frequency is solely due to noise. In the particular case where the estimate is totally uncorrelated with the stimulus, $SNR(f) = 1$ and from the last expression of equation 2.27, the maximum value of the mean square error is $\epsilon^2 = \sigma^2$, the variance of $s(t)$.

The coding fraction γ, a normalized measure of the quality of reconstruction, defined as:

$$\gamma = 1 - \frac{\epsilon}{\sigma} \tag{2.29}$$

takes values between 0 (spike train is totally uncorrelated to the original stimulus, $\epsilon^2 = \sigma^2$) and 1 (the reconstruction is perfect, $\epsilon^2 = 0$). In certain parts of our work, we will be searching for a beneficial effect of internal biophysical noise in the receptor on the quality of encoding via e.g. stochastic resonance [6, 7, 21, 17]. In those cases, we are hoping that by increasing the internal noise of the model, the reconstruction noise $n(t)$ will decrease resulting in a higher coding fraction.

In the particular case where the original stimulus is Gaussian white noise, the rate of mutual information from the stimulus contained in the reconstruction is:

$$I_\epsilon = \frac{-f_c}{log(2)} log\left(\frac{\epsilon}{\sigma}\right) \tag{2.30}$$

It was verified that when processing the spike times through a shuffling algorithm, the coding fraction goes to zero so that our result is not due to signal processing artifacts.

In the present chapter, we have established the numerical recipes that are common to every model treated in the following chapters. Throughout the thesis we refer to the discussed techniques using its section number. Computational aspects that are specific to each model are discussed thoroughly in the implementation section of every chapter.

Chapter 3 LIFDT

We consider the leaky integrate-and-fire model with dynamic threshold (LIFDT) for the study of signal transduction in P-type electroreceptors. First, the basic dynamics are presented and discussed in the region of phase space considered for our study. Then, we quantify the quality of signal reconstruction in LIFDT using the signal reconstruction technique. It is found that signal encoding can be made better through linearization of the model transfer function. Such linearization is achieved in part by the presence of the stimulus itself and in other part by adding a stochastic signal representing synaptic noise and conductance fluctuations in the neuron itself.

3.1 Spiking Mechanism

The very well known and simple leaky integrate-and-fire neuron model (ref. section 1.3) was adapted by Chacron, Longtin, St-Hilaire and Maler [5] to reproduce the first-order and some of the second-order statistics of a P-unit's firing. The key element of the new model is a dynamic threshold variable which overcomes the incapability of a classic leaky integrate and fire neuron to capture the memory feature observed in the P-unit's autocorrelation function. Other neuron models have been proposed along these lines — ours is a simple version.

The leaky integrate-and-fire with dynamic threshold (LIFDT) model is built from a simple LIF endowed with a threshold $\omega(t)$ that changes in time and obeys the following rule: when the potential $v(t)$ becomes greater than $\omega(t)$, the latter is raised by a fixed quantity $\Delta\omega$ and stays at its new value for an absolute refractory period T_{refrac}. It is then allowed to decay exponentially towards a "rest" value ω_0. With such a feature, the threshold tends to get very high when repetitive firings occur in a small time window, thus making the following interval likely to be longer. Similarly, a long interval will allow $\omega(t)$ to "rest", making a short interval more probable. As for $v(t)$, its dynamics follows that of the usual LIF model.

These considerations translate mathematically in the following equations for the potential

and threshold respectively

$$\dot{v} = \frac{v_0 - v}{\tau_v} + i(t) \tag{3.1}$$

$$\dot{\omega} = H(t - t_{last} - T_{refrac})\frac{\omega_0 - \omega}{\tau_\omega} + \Delta\omega\, \delta(t - t_{last}) \tag{3.2}$$

where the post synaptic current $i(t)$ is coupled additively to the potential and δ is the Dirac delta function. The refractory period is implemented by the Heaviside function $H(\ldots)$ with t_{last} being the time of the last spike. Note that the conductance C (see equation 1.4) was set equal to 1 for simplicity.

P-unit features captured by the periodically driven LIFDT with noise are numerous. Not only does it reproduce the autocorrelation function of successive firing intervals measured experimentally (see figure 1.4) with very good agreement (not shown), its baseline firing statistics are also very close to what is observed from actual receptors [5]. Phase locking and skipping patterns are also reproduced by LIFDT and lead to bell shaped histograms with clusters around integer multiples of the carrier period. Proper response to mean EOD amplitude, as observed in [40], is also reproduced, as well as the L-shaped tuning curves [28].

The dynamics of such a model is presented in figure 3.1 along with the principal signals involved in the simulations. The signal on top (A) represents the stimulus that is to be encoded through modulation of the fish's EOD (B). After rectification of the modulated EOD and addition of noise (details in next sections), integration of the post synaptic current leads to the typical dynamics of $v(t)$ and $\omega(t)$ shown in (C). The threshold crossing times $\{t_i\}$ define a spike train (D) made of a sum of delta functions $\delta(t - t_i)$. Notice how the shape of the spike train is affected by $s(t)$ that modulates the firing rate; spikes tend to occur at a higher (lower) rate when $s(t)$ is high (low).

3.2 Numerical Implementation

Signal transduction in LIFDT was investigated with a Fortran algorithm that generates 25 s long simulations with the first 25 ms rejected as transients. The implementation is based on the specifications from [5] and uses the same parameters. The input to the model is an EOD, modulated with the signal to be encoded, along with two sources of noise to mimic the combined effects of synaptic and conductance noise. Interspike intervals are written to an output file when a threshold crossing is detected by the program. We now present the detail of this implementation.

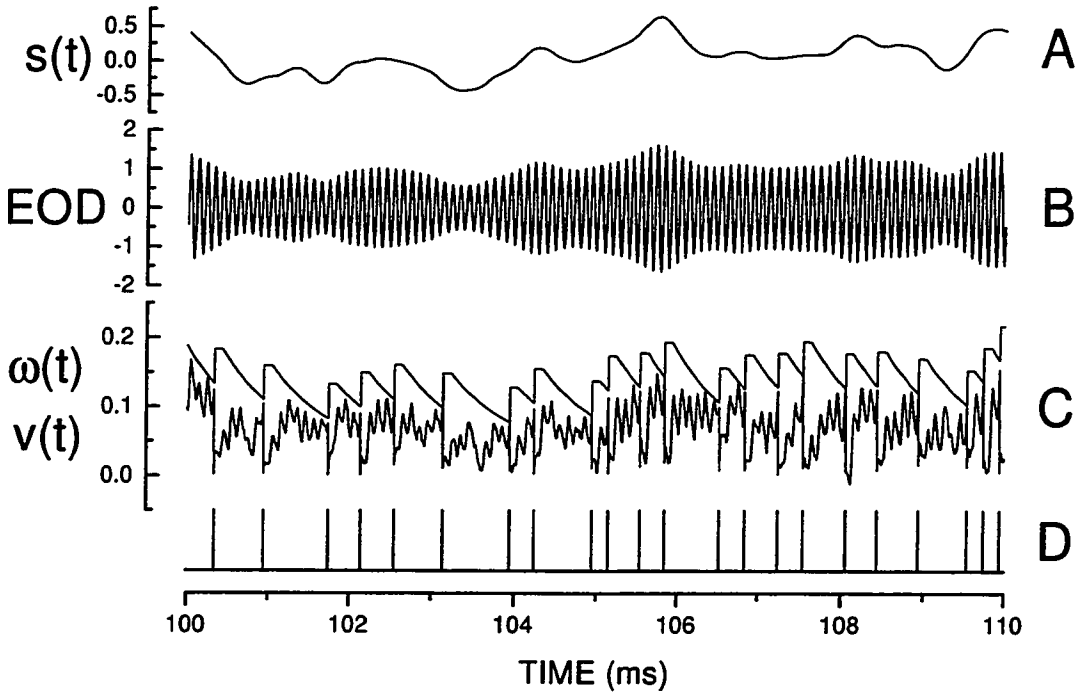

Figure 3.1: Time series of various variables in the LIFDT model. (A) Signal that contains information about the fish's environment. (B) Transdermal potential due to the EOD (carrier) modulated by $s(t)$. (C) Resulting dynamics of the threshold $\omega(t)$ and potential $v(t)$ of LIFDT. (D) The output is a list of spike times defining a spike train of delta functions.

Our routine generates a bandlimited stimulus $s(t)$ using a uniform random deviate generator and the numerical filter described in section 2.1.3. For all simulations the cutoff frequency was set to 100 Hz and the amplitude of the signal was chosen so that its standard deviation was 0.15 of r_0 (based on [40]). A sinusoidal signal of frequency 1 — equivalent to 1 kHz since time units are in ms — is generated and modulated by $s(t)$ with constant contrast (see eq. 2.1).

Two stochastic signals are coupled to the EOD as models of synaptic noise and conductance fluctuations. The resulting signal is then rectified to account for the fact that many neurons (their synapses, to be more specific) perform rectification on forcing signals [13, 12, 25]. Rectification is simply realized by setting to zero all parts of the forcing that correspond to negative values of the sinusoid. Hence the forcing term $i(t)$ of equation 3.1 is written as:

$$i(t) = r_0\big[1 + s(t) + \xi(t)\big]\sin(\beta t)H[\sin(\beta t)] + \eta(t) \tag{3.3}$$

where $H[]$ is the Heaviside function and $\xi(t)$ and $\eta(t)$ are the multiplicative and additive synaptic noises, respectively. Note that $\xi(t)$ is said to be multiplicative only because it multiplies the input which is not the traditional definition where the noise intensity is modulated by the state variable itself. One could say it is multiplicative in this sense if the term $\theta = \beta t$ is included as a dynamical variable with its derivative given by a constant $\dot{\theta} = \beta$ so that $\xi(t)$ multiplies the term in θ.

The Gaussian noise term $\xi(t)$ is constant over one EOD cycle, and induces skipping in the model at rest. It is coupled multiplicatively to the EOD by placing it in the multiplicative term in front of the sine function. This accounts for the fact that noise is proportional to the amount of transmitter release at the synapse [42]. It is realized by generating a Gaussian deviate with variance σ_m^2 (m stands for multiplicative) at each EOD cycle.

The other noise source $\eta(t)$ is a Ornstein Uhlenbeck process with correlation time τ_{add} and variance $D_{add}\tau_{add}$ generated as presented in section 2.1.2. It is added to the current term and its effect is mainly to add more phase jitter and other more subtle correlation effects in the firing data [4]. For our purposes here, it widens the modes in the interspike interval histograms.

At each iteration of the simulation, the program checks for threshold crossing events. Whenever $v(t)$ becomes greater than $\omega(t)$, the voltage is set to v_0 and the threshold is increased by the fixed amount $\Delta\omega$; note that this value is added to the value of threshold at

the (firing) time when it meets the voltage. A new interspike interval is computed from the previous spike time and the value is written to the output file. An absolute refractory period is then implemented by not considering any threshold crossing and by holding $\omega(t)$ to its new value for an interval T_{refrac}.

3.3 Firing Characteristics

We present various aspects of the response from LIFDT to noisy periodic input. In particular, we present the behavior of the P value and of some second order statistics as a function of a limited number of parameters. It will be shown that the firing probability in this model depends mainly on the mean EOD amplitude r_0.

Table 3.1 lists the parameters for LIFDT proposed by [5]. All our simulations were performed using these parameters except for the additive noise amplitude which was set to 0 for simplicity. It was verified that this simplification did not affect our measure of information transfer. For those values, the deterministic (without noise) model baseline firing (at rest i.e.

v_0	0.0 mV
ω_0	0.03 mV
$\Delta\omega$	0.05 mV
τ_v	1.0 ms
τ_ω	7.75 ms
T_{refrac}	1.0 ms
β	2π (1 kHz)
σ_m^2	0.0256
D_a	1.758×10^{-4}
τ_a	0.075 ms

Table 3.1: LIFDT parameter as proposed by [5]

at constant EOD amplitude) shows a 5:1 periodic pattern — one spike occurs every 5 EOD cycles and $P = 0.2$. A sample time course of the voltage and threshold variables for this phase locked pattern is illustrated in figure 3.2 (left panel). $v(t)$ reaches the threshold every five cycles. As a result, all the ISI's fall in the same bin of the ISIH at 5 EOD periods. In this regime, the model is said to be suprathreshold since it is able to trigger action potentials without the presence of noise nor AM.

With added noise ($\sigma^2 = 0.0256$), the 5:1 pattern is perturbed because the voltage time course is no longer purely periodic. As a result, skipping starts occurring (figure 3.2, right

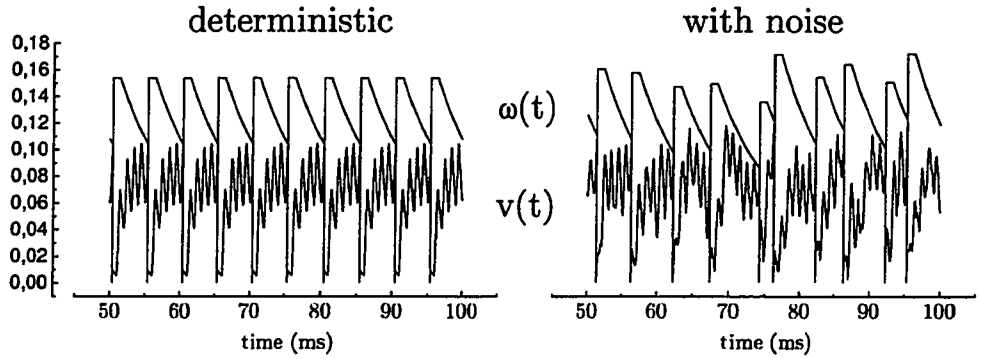

Figure 3.2: Effect of noise on LIFDT dynamics. (Left) Periodic response from constant amplitude forcing (no noise, no AM) with $r_0 = 0.261$. Other parameters as per table 3.1. (Right) The response is no longer periodic when perturbed by the presence of non-zero multiplicative noise intensity ($\sigma_m^2 = 0.0256$).

panel) leading to ISIH's and autocorrelations (not shown, see [5]) closely matching the ones observed on actual receptors (figure 1.4). In particular, the interval histogram is bell-shaped with discrete modes and spreads over a few EOD periods with a mean of 5 cycles.

Figure 3.3 studies the effect of the baseline firing probability per EOD cycle P on the coding quality. As the mean EOD amplitude is increased, P increases (panel A) following a devil's staircase relation [43, 24]. Because of phase locking, the same P value may result from different EOD amplitudes and this is seen as plateaus in an otherwise monotonically increasing function of r_0. *Plateaus are expected to reduce the quality of encoding for they break the one-to-one relation between the input amplitude and the output firing rate.*

Here again we observe that the effect of noise breaks the periodic firing patterns, this time by smoothing out the firing rate relation in the stochastic LIFDT at rest. The dotted line of figure 3.3A was obtained with a non zero multiplicative noise variance of $\sigma_m^2 = 0.0256$.

It is clear from figure 3.3A that, apart form washing the plateaus at high P, noise does not affect the curve significantly. This is further illustrated by plots (B) and (C) where we observe that the mean firing rate is almost constant for our typical values of the noise amplitude ($\sigma_m^2 \sim .0256$ and $D_{add} \sim 0.01$).

Higher order statistics of the spike train are revealed by looking at the ISIH of the LIFDT model. Consider figure 3.4A of the ISIH in LIFDT without noise nor AMs; the model fires periodically every 5 EOD cycles (as in figure 3.2A). In panel B, a multimodal bell-shaped ISIH is obtained by adding noise; the firing is no longer periodic and the intervals spread over a few periods around the mean frequency which stays at approximately 5 EOD cycles. Bottom

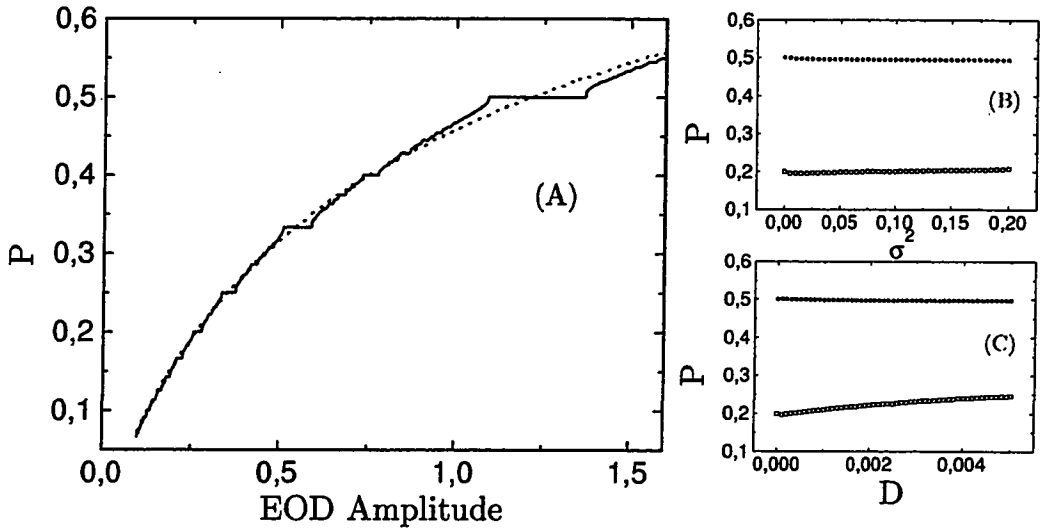

Figure 3.3: P value in LIFDT. (A) The firing probability per EOD cycle as a function of the mean EOD amplitude shows a devil's staircase shape in the deterministic case (solid). Plateaus are wiped out by adding noise to the model $\sigma_m^2 = 0.0256$ (dotted). Each point is evaluated from a 500 ms simulation. For typical values of multiplicative (B) and additive (C) noise amplitude used in our calculations, P is almost constant. EOD amplitudes are : $r_0 = 0.261$ (squares) and $r_0 = 1.2$ (circles).

panels were obtained using the same parameters with the only exception that a random AM was added to the EOD. In particular, panel C shows the interesting fact that, even without noise, a multimodal ISIH is obtained in the simple presence of the AM alone, for the random AM perturbs the deterministic periodic behavior of the voltage. Finally, panel D shows the combined effect of both the AM and noise where the spreading is greater than in each of the preceding individual cases.

An L-shaped tuning curve typical of P-units is reproduced by LIFDT as shown by figure 3.5, as seen experimentally [43]. However, this tuning curve was realized without internal noise and we do not observe the V-shaped curves that we find in deterministic resonators. It appears that LIFDT has no preferential driving frequency, i.e. a frequency with a clear minimal amplitude threshold for firing.

3.4 Results

We present the results of information measurements on spike trains generated by LIFDT using the signal reconstruction technique. The effect of noise amplitude, EOD amplitude and

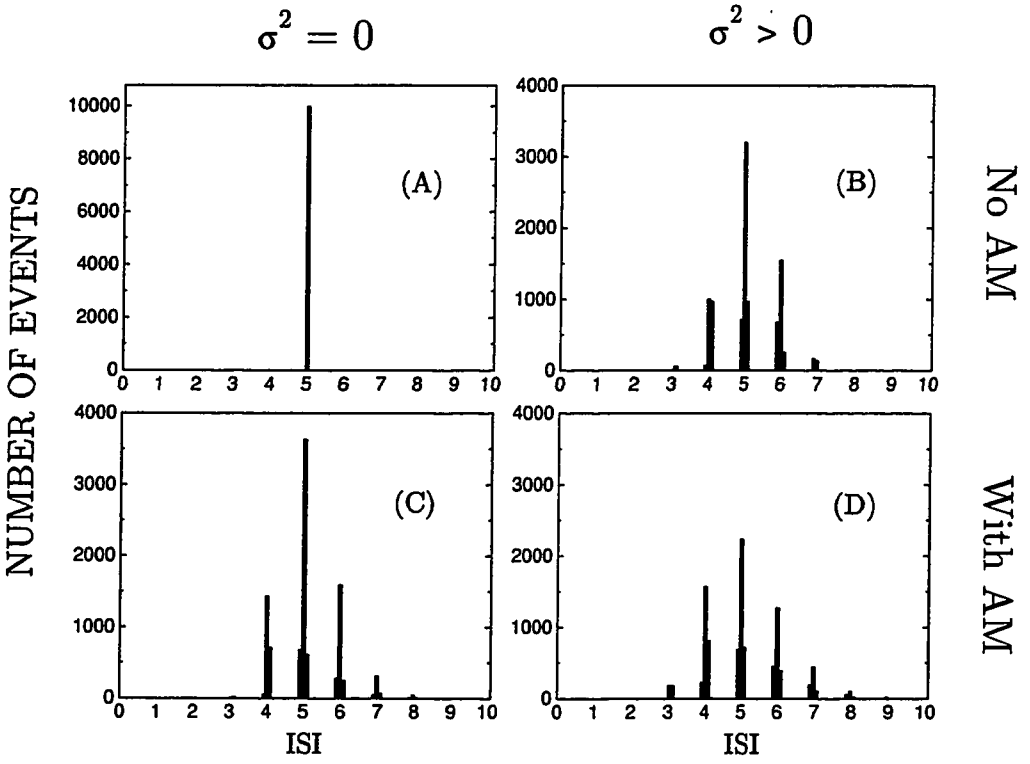

Figure 3.4: Multimodal interval histograms in LIFDT. Top ISIH were computed without AMs while bottom graphics were made with AMs. No multiplicative synaptic noise ($\xi(t)$ in eq. 3.3) was used for histograms on the left while $\sigma_m^2 = 0.0256$ on the right.

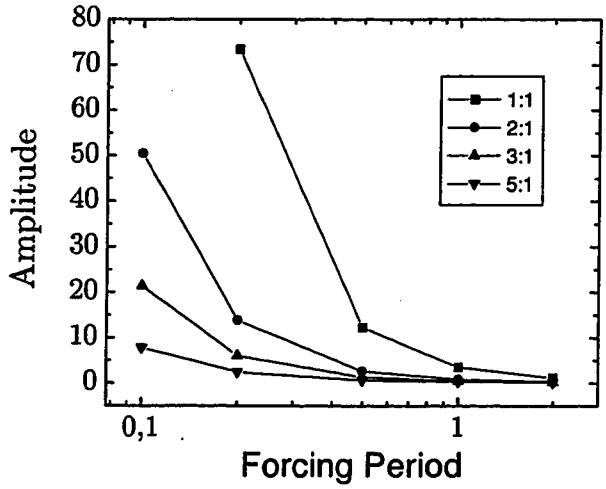

Figure 3.5: Tuning curve of LIFDT. Each curve is obtained by finding the minimum amplitude giving rise to the indicated (n:m) firing pattern for different forcing periods.

P value over the coding fraction are presented. In particular we find that the encoding of very weak signals can be improved by low noise amplitudes. For this entire section we did not make use of the additive noise; it was verified that our qualitative results are not dependent on its presence.

One might expect that the linearization effect of P-unit noise (see figure 3.3A) increase the ability of the model to encode minute stimuli since it makes the input-output transfer function smoother. The effect of increasing noise amplitude on the coding fraction is plotted in figure 3.6. The two curves were obtained in very distinct firing regimes. The top curve shows the result in the 5:1 regime (P=0.2) as studied in the previous section ($r_o = 0.261$) . We observe that the effect of increasing noise in that case always results in a lowering of the coding fraction. In this region the transfer function (figure 3.3) is smooth enough for the AM to induce changes in the firing rate even in the deterministic case. Addition of noise simply randomizes the spike times and lowers the transmitted information.

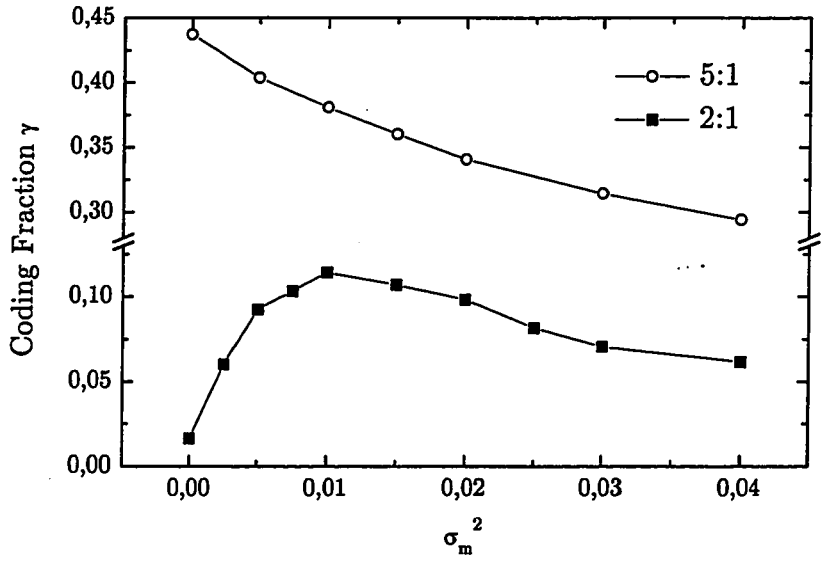

Figure 3.6: Coding fraction vs multiplicative noise variance σ_m^2. The (5:1) curve was obtained with a stimulus standard deviation of $\sigma_{s(t)} = 0.15$ and EOD amplitude of $r_0 = 0.261$. The (2:1) values were $\sigma_{s(t)} = 0.04$ and $r_0 = 1.2$. It was verified that the error on our coding fraction values is of the order of the size of the symbol used for plotting (~ 0.01). Such a value does not affect the overall trend of the curves. The error is evaluated by computing the coding fraction from different simulations with different seeds.

The lower curve was obtained from a regime were the model fires every 2 EOD cycles: the operating point of the model is in the large 2:1 plateau of the devil's staircase relation (figure 3.3). A small enough stimulus ($\sigma_{s(t)} = 0.04$) was used so that in the absence of noise,

the modulation is not enough to perturb the periodic phase locked pattern. We find that the coding is almost zero in the deterministic case i.e. at $\sigma_m^2 = 0$ (a few digressions from 2:1 were actually generated). With increasing multiplicative noise, the transfer function is smoothed out and the model starts coding. In other words, internal synaptic noise helps coding in this case. Note that this effect is not stochastic resonance, since the stimulus is suprathreshold in the absence of noise. At some point (in this case $\sigma_m^2 \gtrsim 0.01$), too large a noise amplitude generates many irrelevant spikes and the coding fraction decreases. Note that the lower coding fraction values compared to the 5:1 case are due to a lower amplitude of the stimulus hence to a smaller contrast.

For fixed noise amplitude, we now present the effect of the EOD amplitude on the coding fraction. As the carrier mean amplitude r_0 increases, the output rate of LIFDT increases monotonically in the presence of noise and AM. The increase translates into a better sampling rate of the input signal, thus into a greater coding fraction as shown in figure 3.7. Both curves of the figure are done with distinct values of the noise variance. The result is in agreement with measurements by [40]; the coding fraction first increases and then saturates with increasing EOD amplitude although in [40] the internal noise could of course not be changed as we do here. We also find that the curve associated with the larger noise amplitude has lower coding fraction; this was already observed in figure 3.6 (5:1 case).

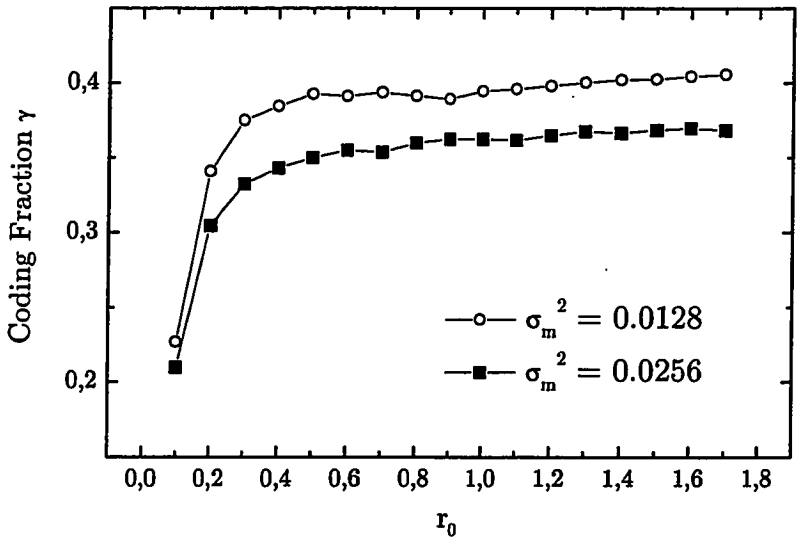

Figure 3.7: Coding fraction vs r_0 in LIFDT

From the known relation between the mean EOD amplitude r_0 and the P-value (measured

at rest i.e. without AM), the results of figure 3.7 are easily presented as a plot of the coding fraction vs P (figure 3.8). Again, we find an asymptotically increasing function which is also expected from the experiments in [40]. What is of particular interest here is that for a given P value, there is no unique value of the coding fraction. Thus P does not completely determine the quality of information transfer in this model of a P-unit. It also depends on e.g. the synaptic noise strength and other model parameters.

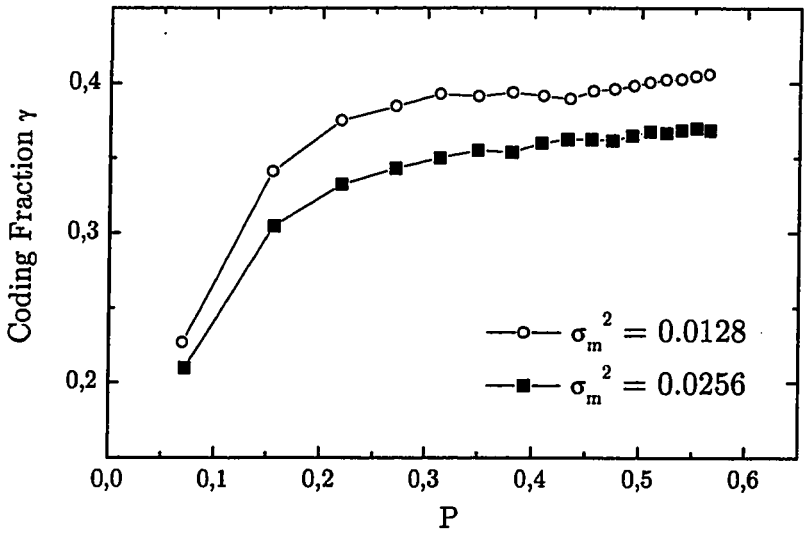

Figure 3.8: Coding fraction vs P in LIFDT. The results are from the same simulations as for figure 3.7; they are simply plotted as a function of P

3.5 Discussion

The LIFDT constitutes an interesting P-Afferent model for it reproduces an important number of spike train statistics measured from actual receptors. All regimes considered for our study of weak AM encoding in LIFDT were suprathreshold i.e. firing occurs even without noise and amplitude modulations. Moreover, the transfer function of the deterministic model is almost monotonically increasing with very few plateaus. The models thus produces an intrinsically monotonic (except for a few plateaus) transfer function. For the set of parameters proposed by [5] and which match the in-vivo measurements very well, we found that the information transfer is always better in the deterministic case since the stimulus-response curve is almost monotonic in that region of parameter space; adding noise only randomizes the spikes times and reduce transduction quality.

A beneficial effect of the noise was found in the case where a small amplitude modulation falls within a plateau of the $P - r_0$ relation. Its presence allows transitions to non periodic firing patterns, thus allowing information from the stimulus to be encoded. This effect is somehow similar to stochastic resonance effect seen in FHN [6, 21, 7] although stochastic resonance does not involve suprathreshold forcing as is the case here.

We have found the important result that the quality of information is not completely determined by P. Two coders with the same P values may have different coding fractions given the distribution of their associated ISIH. This is because P itself depends on the synaptic noise strength and other parameters such as the frequency of the EOD.

For a simple treatment of the effect of the distribution the reader is invited to refer to [16] where a very simple integrate-and-fire model with gamma-distributed ISI distribution is used as an example. The study points out that a wide ISI distribution results in low coding fraction because its output is more random. This is interestingly conflicting with the concept that we do want to randomize the output to break periodic firing pattern. We must seek the right balance between the two effects of the internal noise whenever the coding is occurring on a phase locking plateau.

The particular choice of a rectified forcing and of the noise sources were made following the specifications from [5]; it was verified that this choice did not affect our qualitative results. The waveform of the voltage response is most important in the portions that are close to threshold; these are mostly responses to the portions of the EOD not affected by the rectification. For this reason, the other models considered in this work do not make use of such rectification.

More recent developments have lead to an even more accurate model which reproduces for instance the behavior of the Fano factor, a measure of the dispersion of the ISI distribution [4]. We expect that the new development would have negligible effect on our results since they simply use additive noise as well, with a very long correlation time and very low intensity.

Chapter 4 FitzHugh-Nagumo

The model studied in this chapter[1] is the FitzHugh Nagumo model, a reduction of the Hodgkin-Huxley model. It is described by a voltage variable that actually captures the depolarization-repolarization process of the action potential dynamics. We first present the effect of various model parameters on its firing statistics in two distinct operating regimes: one with subthreshold forcing and a second regime with suprathreshold forcing. We then present the effect of those parameters on our measure of information, in the two same regimes. As part of our results, we observe that the coding fraction can be optimized with low synaptic noise amplitude in the subthreshold regime.

4.1 Spiking Mechanism

The two dimensional FitzHugh-Nagumo (FHN) neuron model has been widely studied because of both its simplicity in comparison to Hodgkin-Huxley and its capacity to produce biophysically reasonable action potentials. It is a reduced description of the Hodgkin-Huxley conductance-based model and its state is defined by a (fast) voltage variable v and a (slow) recovery variable w whose dynamics are governed by [9, 8]:

$$\epsilon \dot{v} = v(v-a)(1-v) - w + I_{bias} \tag{4.1}$$

$$\dot{w} = v - dw - b \tag{4.2}$$

where ϵ is the conductance of the membrane and I_{bias} is a bias current used to tune the fixed point of the model. Note that (a,b,d,ϵ) are constant parameters. This system is similar to the Bonhoeffer - van der Pol relaxation oscillator [38].

The FitzHugh-Nagumo model when used as a modeled P-unit (i.e. when periodically forced) exhibits spiking dynamics typical of so called type II membrane. We refer the reader to the next chapter for a comparative discussion on the dynamics of type I and II membranes.

[1] The results presented in this chapter were the object of a publication by Longtin and St-Hilaire in 2000 [30]

In type II membranes, the generation of action potentials is possible thanks to the presence of a Hopf bifurcation (see e.g. [38]) in the vicinity of its operating point; a significant change in the bifurcation variable I_{bias} may give rise to the onset of a periodic solution with a non-zero frequency at the onset. Thus, the periodic solution is characterized by a limit cycle and the model acts like a resonator around its preferred frequency.

The response of the FHN system to periodic input exhibits many features observed in the P-units such as skipping patterns, realistic tuning characteristics [28] and proper baseline firing statistics at mid-to-high frequencies. However, it was verified (not shown) that the negative autocorrelation at first lag observed by Nelson [31] in the measurements on P-units is not reproduced by this model; the autocorrelation of FHN fluctuates around zero (no correlations between the firing intervals) for all lags.

4.2 Numerical Implementation

Encoding characteristics of the FHN model are investigated by numerical integration of equations 4.1 and 4.2 via a Fortran algorithm. A Euler first order algorithm with small time step (0.001) is used in the light of the discussion in section 2.1. For each set of parameters, a 25 s spike train is generated (10 ms were rejected as transients) using a simulation of 2.5×10^7 time steps during which interspike intervals are saved to an output file along with a sampled version of the signal $s(t)$ for latter analysis. We solved the following set of equations:

$$\dot{v} = v(v-a)(1-v) - w + I_{bias} + r_0[1+s]\sin(\beta t) + \eta \tag{4.3}$$

$$\dot{w} = v - dw - b \tag{4.4}$$

where the EOD term and synaptic noise term η are both coupled additively to the voltage variable. Note that the model is forced with constant contrast as the EOD r_0 multiplies the modulation term [1+s] (see equation 2.1). s is the band-limited Gaussian white noise stimulus generated as per the specifications of section 2.1.3. η is a source of exponentially correlated noise with characteristic time τ_η and amplitude D representing the combined effect of synaptic noise and conductance fluctuations; it is generated as presented in section 2.1.2.

When the potential crosses a threshold value θ with a positive slope, a firing has occurred. In reality, the threshold in FHN is defined by a curve in the (v, w) phase space rather than by a single value θ. However, for our set of parameters, $v > \theta = 0.5$ indicates clearly that a spike has occurred. An absolute refractory period is implemented by rejecting interspike

intervals smaller than T_{refrac} which in our case is set to 0.4 time units. Note that T_{refrac} was estimated numerically by choosing a value close to the duration of an action potential. This same time constant scales the model by comparison to the fish's real refractory period ($\sim$ 1msec); in order to link our results to the actual data of the P-unit, one should scale the model by comparison of the refractory periods. Thus by comparing our value of T_{refrac} with the actual value for the fish, we find that the time units of our model are roughly 10^3 times slower than that of the actual P-unit in seconds.

The parameters used through our study are listed in table 4.1 and unless otherwise stated they apply to all our results. With this set of parameter, the threshold input amplitude is $r_0 = 0.0128$ at 1 cycle/time unit; when forced by a fixed constant amplitude sinusoid, without EOD and amplitude modulation, the deterministic model will not fire unless $r_0 > 0.0128$. For any amplitude below this value, the forcing is said to be subthreshold since it cannot induce firing alone. Conversely, all amplitudes over it induce firing and are called suprathreshold.

a	0.5
b	0.15
I_{bias}	0.04
ϵ	0.005
τ_η	0.001
T_{refrac}	0.4

Table 4.1: FitzHugh-Nagumo model parameters

The intensity of the modulation was set so that the standard deviation of the stimulus was approximately 0.15. From equation 4.3, this represents 15% of the EOD amplitude, a value similar to that used by Wessel [40].

4.3 Firing Characteristics

In FHN, the probability P of firing at each EOD cycle depends on a couple of the model parameters. Varying r_0 — to capture the fact that each receptor "feels" a different effective EOD amplitude — or the synaptic noise amplitude affect P, and their effect is different depending on whether the forcing is subthreshold or suprathreshold. We first discuss the specific effect of those parameters on the basic firing characteristics of the model driven with constant sinusoidal input.

Throughout this section, we consider two forcing regimes defined by their EOD amplitude

and distinguishable by their firing response in the deterministic case, i.e. without synaptic noise and amplitude modulations. An EOD amplitude of $r_0 = 0.010$ is used for the subthreshold forcing regime; in the absence of stochastic forcing, an EOD with $r_0 = 0.010$ is not large enough to generate spikes in FHN. In this regime the firing rate is zero, hence the associated P is zero. Another amplitude of $r_0 = 0.014$ is chosen for the suprathreshold case. In this regime, FHN fires one spike every 2 cycles (2:1 firing pattern) and the associated $P = 0.5$. As a reminder, the threshold amplitude separating the two regimes is $r_0 = 0.0128$. The chosen value of $r_0 = 0.014$ for the suprathreshold regime is larger than the threshold but still reasonably close so that we expect that the noise and amplitude modulations might prevent some firing events by keeping the voltage below threshold.

The sharp separation between the two forcing regimes is observable in the plot for the probability of firing per EOD cycle as a function of the EOD amplitude in figure 4.1. In the deterministic case (solid line) the firing probability is the P-value of the neuron and the curve has a devil's staircase structure (see section 1.5.3). The dotted line was obtained with a non zero value of the noise amplitude. The presence of noise linearizes the transfer function and the plateaus of the devil's staircase are washed out. A similar effect was found in the LIFDT model (previous chapter).

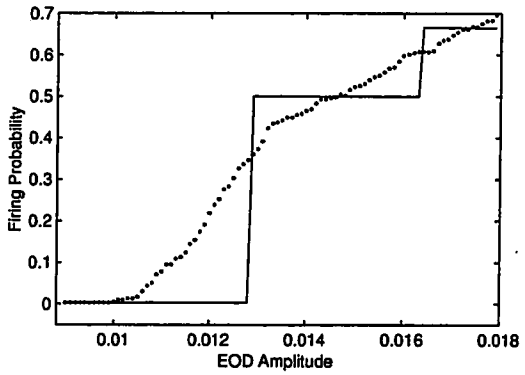

Figure 4.1: Devil's staircase of the FHN model. The solid line was obtained without synaptic noise; a value of $D = 5 \times 10^{-8}$ was used for the dotted curve. All other parameters as per table 4.1.

We then consider the role of synaptic noise in the skipping dynamics of periodically driven FHN. Figure 4.2 presents voltage time series and associated interspike intervals for the firing at rest in the two considered regimes. Note the effect of the periodic forcing in the voltage solution; $v(t)$ fluctuates around its rest potential with an almost periodic function. In the subthreshold case, the model would not fire in the absence of synaptic noise. Here

the presence of noise allows subthreshold forcing to reach the threshold and fire with the resulting interspike interval shown in panel B. In the suprathreshold case the deterministic model fires every 2 cycles (2:1 pattern). In the presence of noise, this pattern is perturbed and we find the distribution shown in panel D. Due to a higher output rate, the interspike intervals are shorter on average and thus the ISIH is shifted to the left in comparison with the subthreshold ISIH.

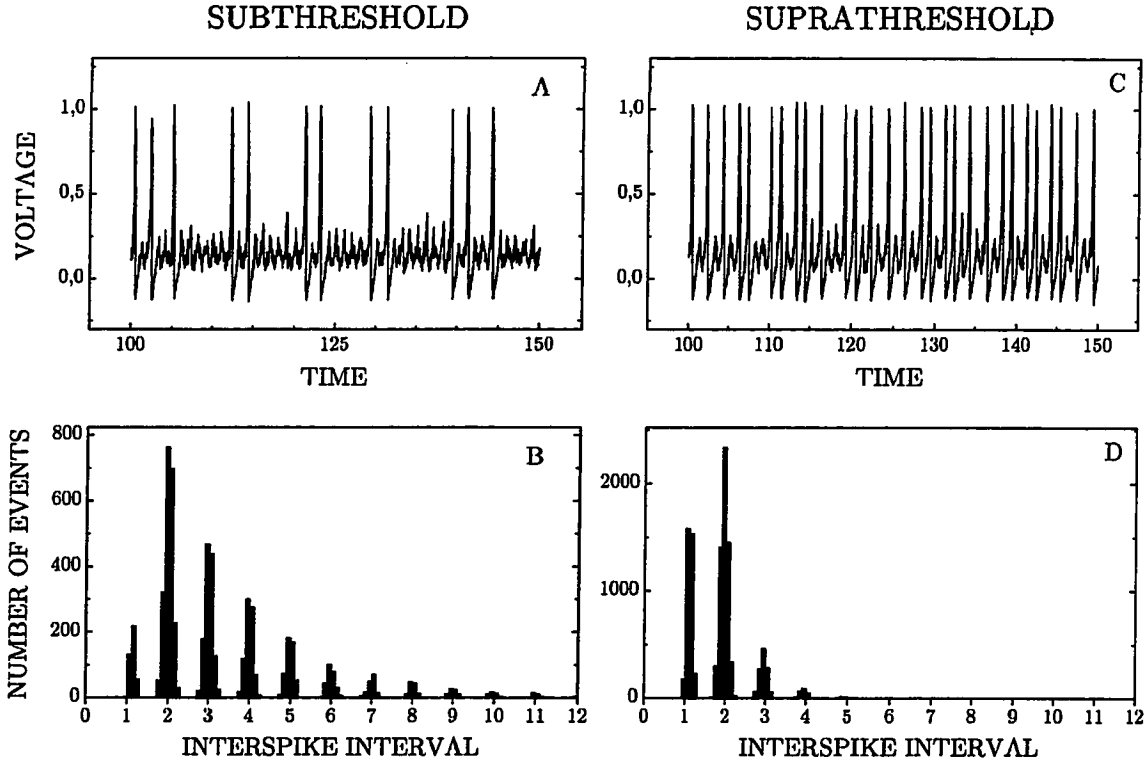

Figure 4.2: Voltage response and ISIH in FHN at rest. (Left panels) Voltage response (A) and ISIH (B) of the model forced with subthreshold EOD amplitude ($r_0 = 0.010$). (Right panels) Voltage response (C) and ISIH (D) of the model forced with suprathreshold EOD amplitude ($r_0 = 0.014$). Note that the scaling in (D) is different from that in (B). All other parameters as per table 4.1.

We now apply a stimulus — a random EOD modulation — and look at the voltage response to understand how the modulations are encoded in the spike train. Figure 4.3 presents such voltage responses for increasing fixed intensities of the noise in the subthreshold regime. The top panel (A) shows the forcing EOD. In the noiseless case (panel B) we clearly see that the voltage response is modulated by the presence of the stimulus. In the sample time series shown, the voltage does not reach the threshold and no spikes are generated; very few spikes were actually generated in the whole simulation. Even if the amplitude modulation

has zero mean, the positive portions of the AM allow the model to reach threshold and thus the FHN model with subthreshold input starts firing; we say that the AM brings the system closer to threshold. Panel C and D are realized at increasing noise amplitudes ($D = 1 \times 10^{-7}$ and $D = 5 \times 10^{-7}$ respectively). We observe that the output rate increases with increasing synaptic noise; noise also brings the system closer to threshold in the subthreshold regime. Finally, notice how the output rate is modulated by instantaneous amplitude of the EOD as spikes are more likely to occur when the stimulus is high.

The same analysis was made for the suprathreshold regime and plotted in figure 4.4. In the noiseless case (panel B) we find that the 2:1 firing pattern is perturbed by the presence of the modulation as negative fluctuations of the modulation prevent spikes from begin fired every 2 cycles. For increasing values of the noise (C and D) the output rate increases as well and some irrelevant spikes start occurring at very large noise. Note that the increase in output rate is only possible because the model is "near" suprathreshold regime. For much larger EOD amplitudes, the effect of noise is no longer an increase in output rate; its presence only randomizes the spike arrival times (not shown).

The effects of AM and synaptic noise on the firing statistics are further illustrated by plotting the ISIH of realizations similar to those presented in figures 4.3 and 4.4. Figure 4.5 reveals that increasing noise in the subthreshold regime raises the output rate in both the presence and absence of AM. Left panels are obtained from constant amplitude forcing and their associated P value is the inverse of the indicated mean ISI (P is defined without AM). Thus P becomes larger with increasing noise. The presence of AM's also shortens the interspike intervals and the output rate increases accordingly despite the fact that the modulation has zero mean; they bring the system closer to threshold in the subthreshold regime. However in the near suprathreshold case (figure 4.6), the presence of AM's decreases the output rate of FHN. The lower rate is due to the negative portions of the AM which are encoded by deleting spikes. However we still observe that the noise raises the output rate in the suprathreshold case.

We conclude our discussion on FHN firing statistic with the tuning curve of the model, presented in figure 4.7. The V-shape reveals the resonant behavior typical to type II membranes. A thorough discussion on the tuning properties of FHN can be found in Longtin [28] with the same parameters used here. In particular, his results show that the effect of noise on these tuning curves is to lower the branch in the large period region (not shown here). We

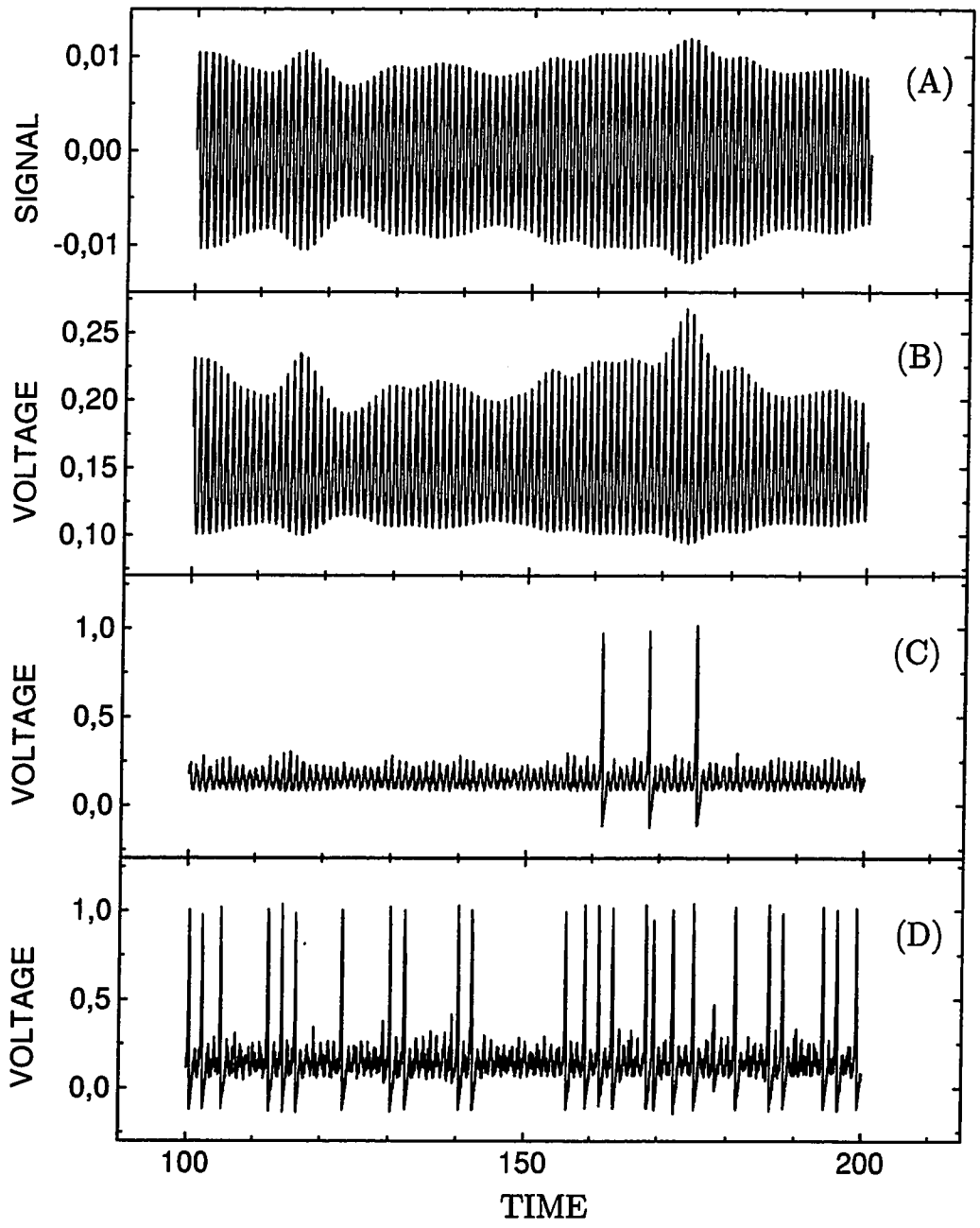

Figure 4.3: Encoding an amplitude modulation in the FHN model, in the subthreshold regime ($r_0 = 0.010$). (A) EOD with band-limited random amplitude modulation. Other panels are the voltage responses for noise intensities $D = 0$ (B), $D = 10^{-7}$ (C) and $D = 5 \times 10^{-7}$ (D).

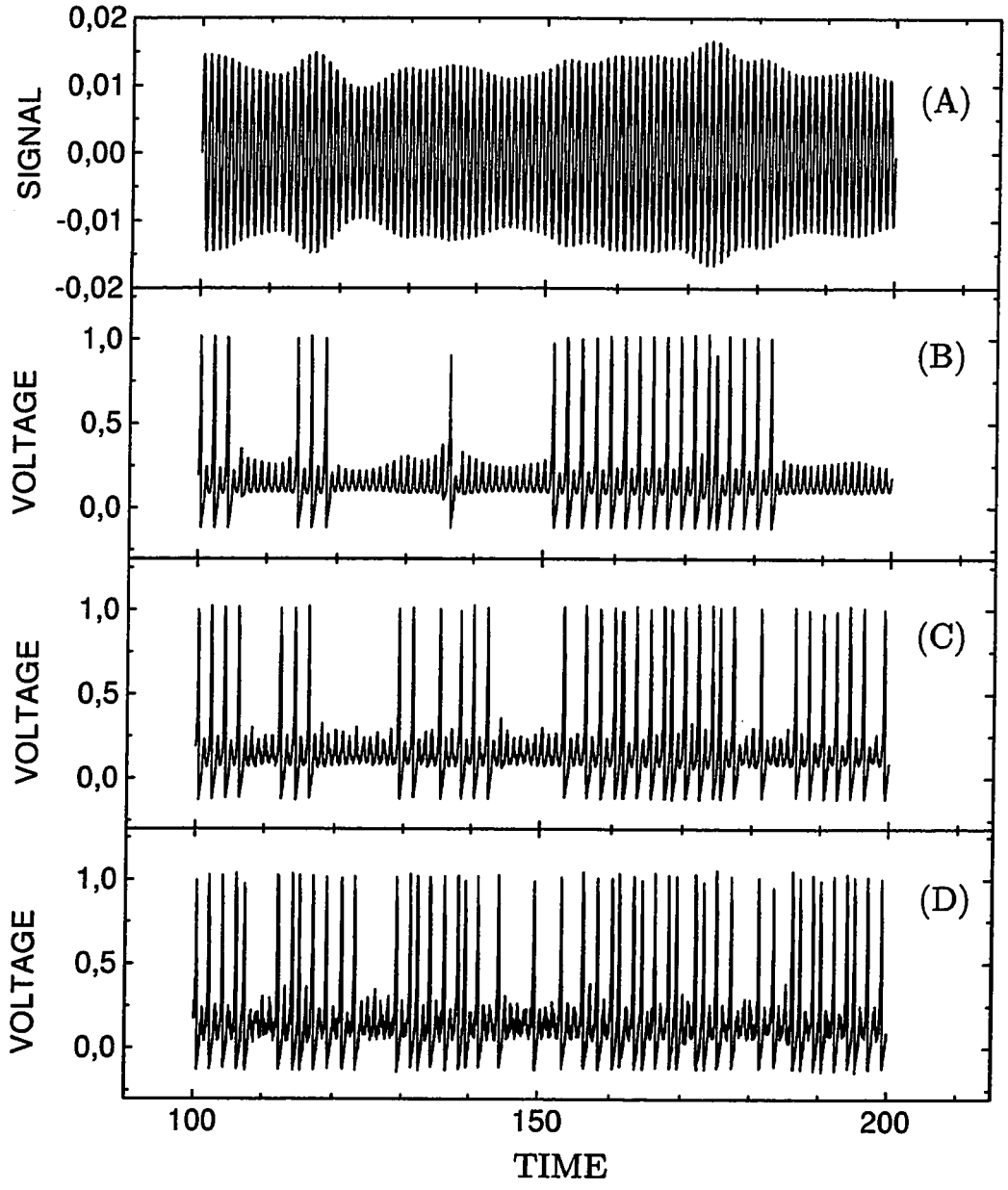

Figure 4.4: Encoding an amplitude modulation in the FHN model, in the suprathreshold regime ($r_0 = 0.014$). (A) EOD with band-limited random amplitude modulation. Other panels are the voltage responses for noise intensities $D = 0$ (B), $D = 10^{-7}$ (C) and $D = 5 \times 10^{-7}$ (D).

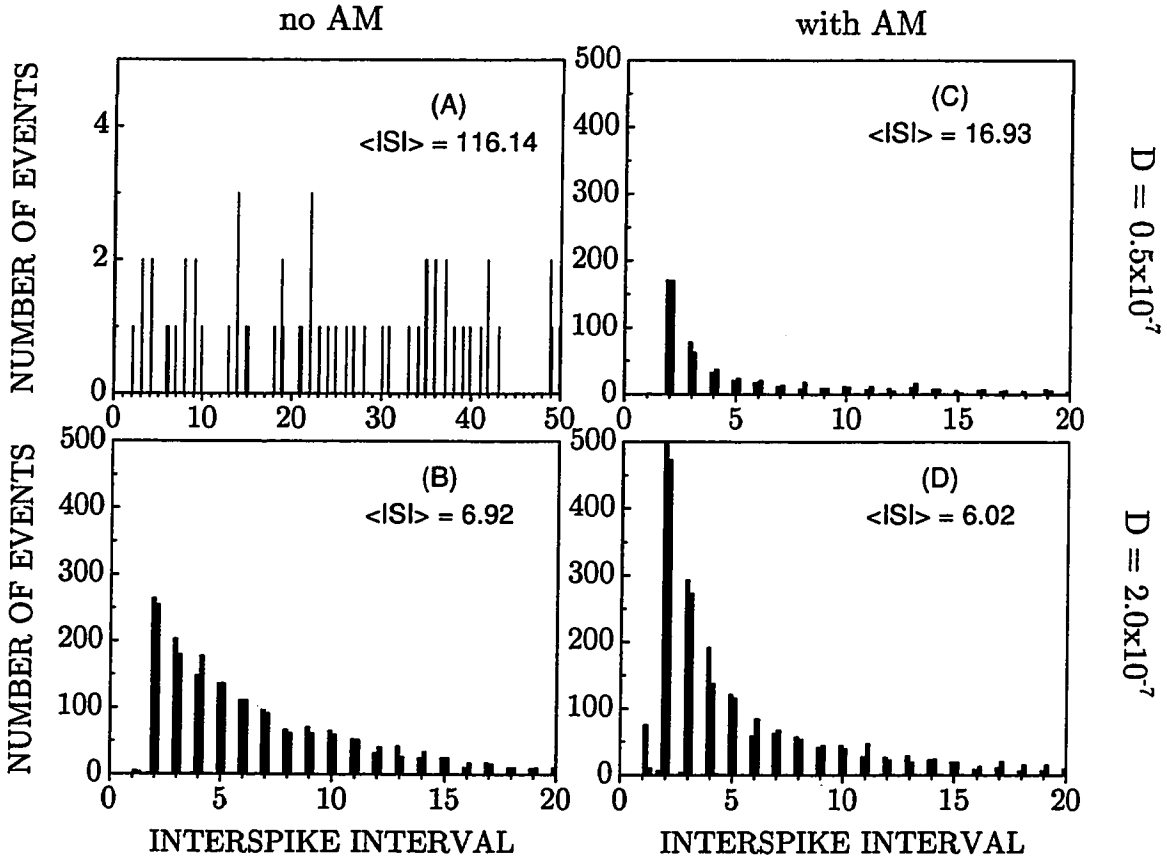

Figure 4.5: Interspike intervals histograms in the FHN model, in the subthreshold regime ($r_0 = 0.010$). The upper panels are for $D = 0.5 \times 10^{-7}$, and the lower ones, for $D = 2.0 \times 10^{-7}$. A constant amplitude EOD was used for the left panels (no AM's) while the right panels are realized with AM's. The average interspike intervals are given in units of the carrier period. Note that the scales of (A) are different from the others due to very few events in that case.

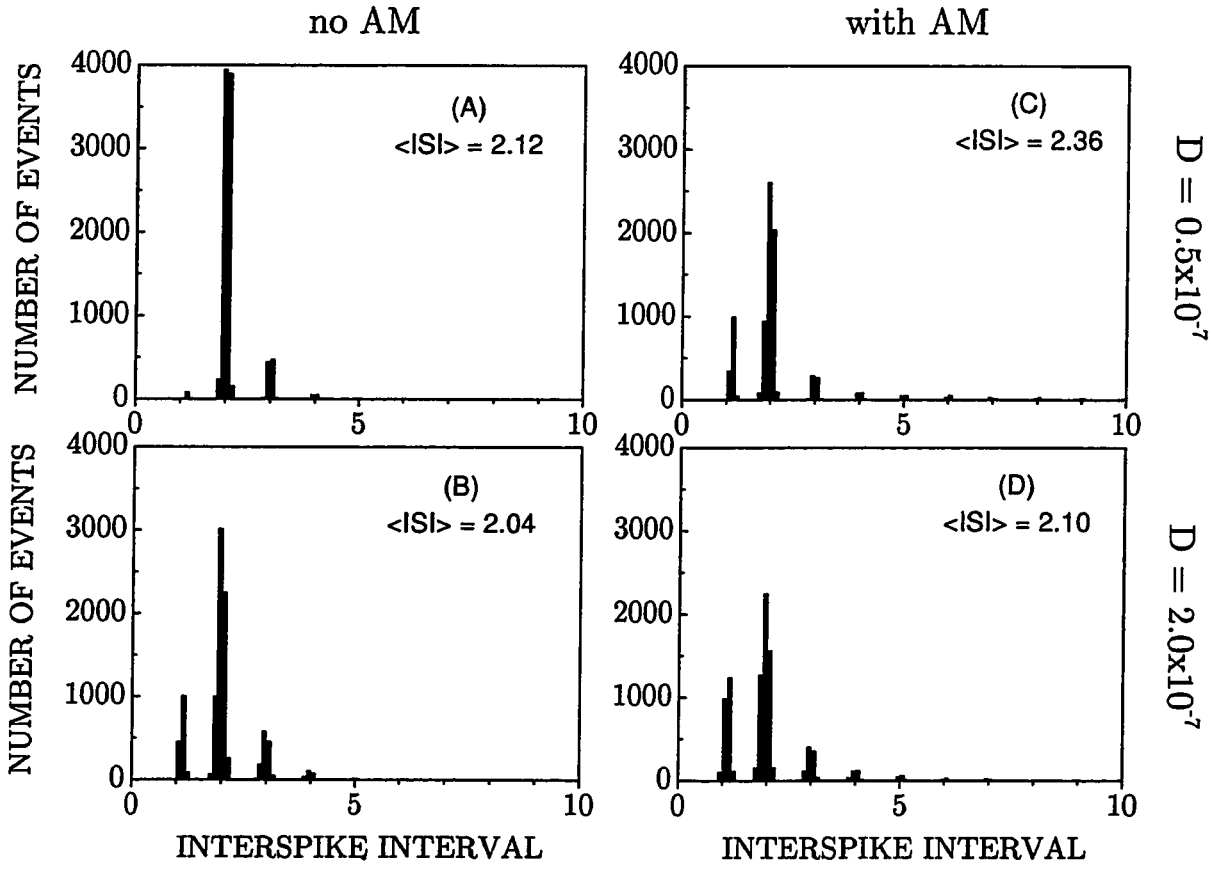

Figure 4.6: Interspike intervals histograms in the FHN model, in the suprathreshold regime ($r_0 = 0.014$). Details as for previous figure 4.5.

expect this effect to be beneficial for encoding slowly varying modulations, as it lowers their associated threshold.

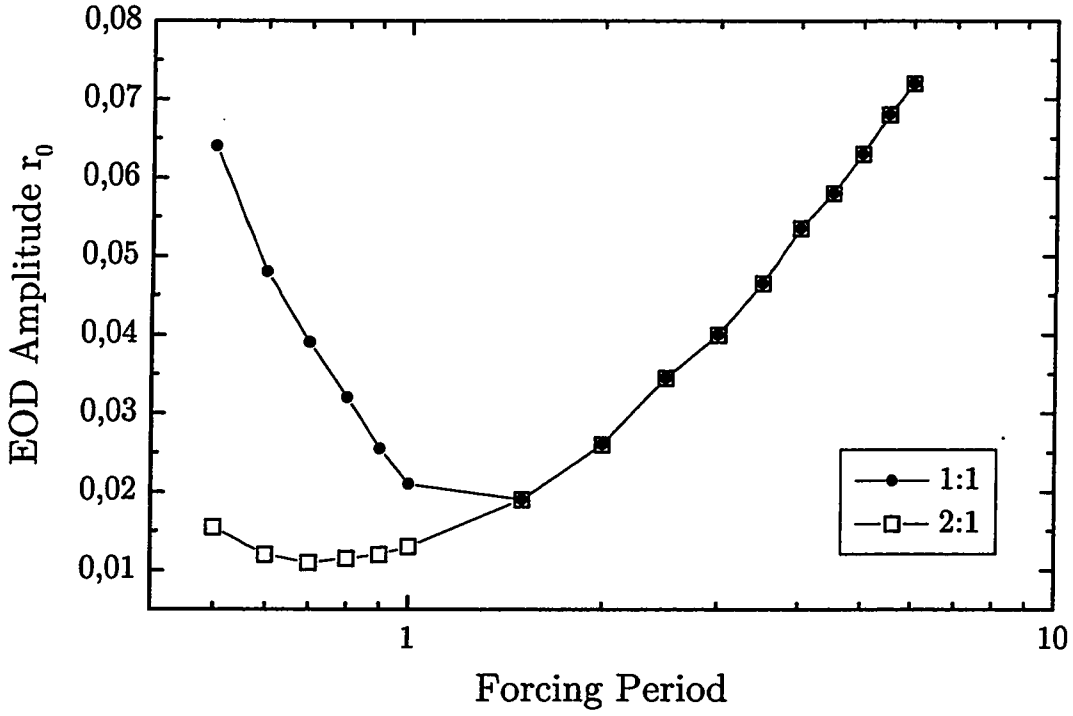

Figure 4.7: Tuning curve in the FHN model. Each curve is obtained by finding the minimum amplitude giving rise to the indicated (n:m) firing pattern for different forcing periods.

4.4 Results

In order to characterize the encoding capability of a given P-unit we present the effect of synaptic noise amplitude D and mean EOD amplitude r_0 — the two parameters which influence most the value of P — on information transfer. In each case, the interpretation depends on whether the model is in the subthreshold or suprathreshold regime.

In the subthreshold regime, synaptic noise can enhance information transfer in FHN. This is illustrated by a plot of the coding fraction as function of the noise amplitude for various mean EOD amplitudes (figure 4.8). We first observe that all curves have a non-zero coding fraction at D=0. This is due to a few AM local maxima going above threshold even though the model is subthreshold. We also observe that the lines associated with EOD amplitudes in the subthreshold regime ($r_o \lesssim 0.0128$) show a maximum for some optimal noise amplitude. In such regimes, increasing D first increases the coding fraction and the effect is two-fold.

As D is increased, spikes occur more often, thus enhancing information transfer because of a higher sampling rate of the AM (Note that this sampling rate is done at random times, and differs from the usual sampling done e.g. by an A/D converter). Also, increasing D linearizes the transfer function of the neuron (figure 4.1) and allows the portion of the AM that are mostly below but near threshold to be encoded to some extent. The coding fraction then reaches a maximum and starts decreasing monotonically as the stochastic element becomes too important and spikes start occurring at irrelevant times.

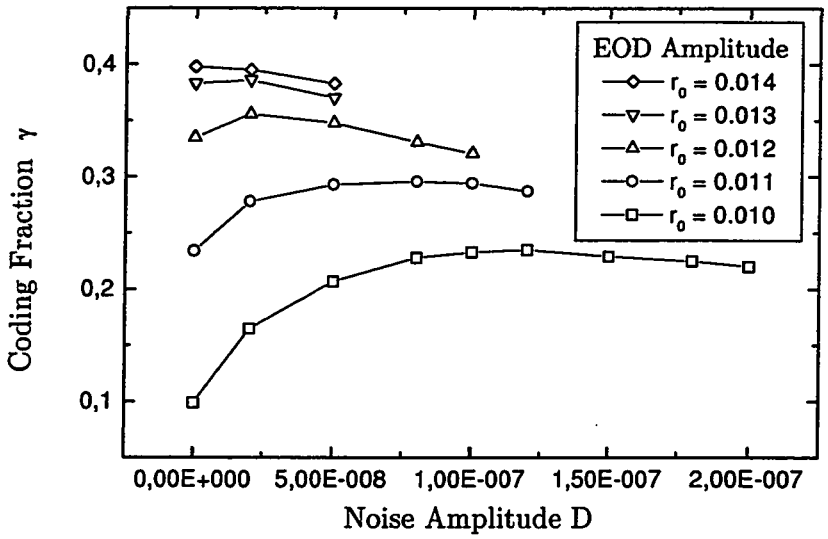

Figure 4.8: Coding fraction vs synaptic noise amplitude in the FHN model.

As r_o is increased towards the threshold, the value of D for which the coding fraction is maximum decreases, since less noise is needed to reach threshold and the curves are shifted to the left. At the same time, the whole curve gets shifted to higher coding fraction values as the increase in amplitude increases the apparent AM fluctuations (constant contrast). The beneficial effect of the synaptic noise is observable up to near suprathreshold amplitude, after which the effect of noise is mainly a randomizing one. At $r_o = 0.014$ and higher amplitudes, the coding fraction is optimal for the deterministic simulation and decreases monotonically with increasing D.

Figure 4.9 illustrates our results from another point of view. Now each curve is realized at a fixed noise amplitude by varying the EOD amplitude. Once again, the behavior depends on the operating regime of the model. For subthreshold amplitudes ($A < 0.128$), the coding fraction increases rapidly as r_0 is brought closer to threshold. It is due to the increasing

sampling rate combined with an increase of the apparent AM fluctuations. The coding fraction then seems to saturate for suprathreshold EOD amplitudes. Still a significant increase is observable, probably due to the amplified modulations. Finally, at very large amplitude, saturation effects reduce the coding fraction, since the model cannot fire more than once per EOD cycle. The spike train becomes almost periodic and contains much less information about the input. Nevertheless, a few skips in firing associated with various minima are responsible for the non-zero value of γ. Here, the AM minima become very important, since they are being encoded.

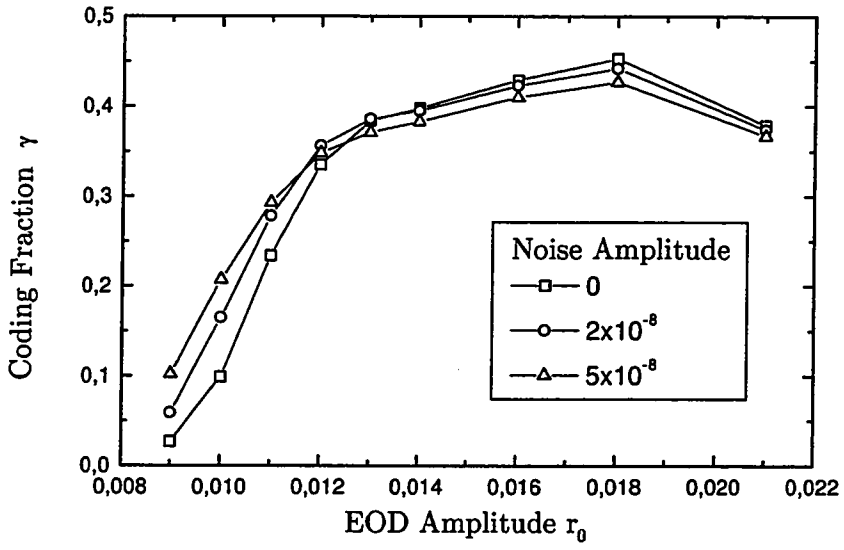

Figure 4.9: Coding fraction vs mean EOD amplitude in the FHN model.

Since different sets of parameters in FHN can lead to identical values of P, one cannot find a one-to-one relation between the encoding quality of a P-unit and its associated probability of firing at each per EOD cycle. Figure 4.10 maps the simulations with different A and D on the P axis whose individual values lead to multiple values of the coding fraction. The points on each curve were actually evaluated from simulations at EOD amplitudes r_0 of $\{0.009, 0.010, 0.011, \ldots 0.014\}$. We observe that for each P, multiple values of the coding fraction are possible, depending on the intensity of the noise. In particular, the three points at $P = 0$ are from simulations with $r_0 = \{0.009, 0.010, 0.011\}$ and synaptic noise of intensity $D = 0.2 \times 10^{-7}$. In the absence of AM, the system almost never reaches the threshold at such forcing amplitudes thus $P \approx 0$ for the three cases. However, in the presence of AM, the model forced with subthreshold amplitudes starts coding and a distinct coding fraction value

is obtained for each EOD amplitude.

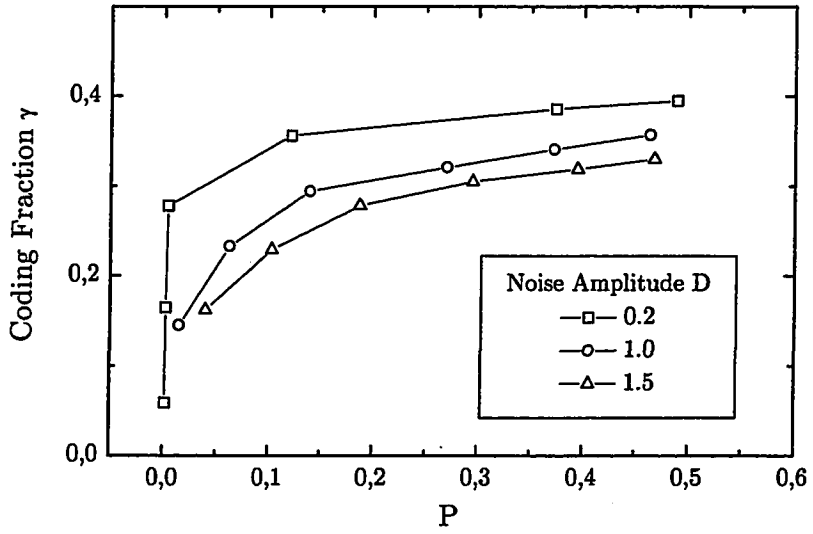

Figure 4.10: Coding fraction vs P in the FHN model. It was verified that the error on the coding fraction values is of the order of the size of the symbol used for plotting (~ 0.01).

We also investigate the effect of the carrier frequency on the coding fraction in FHN. Figure 4.11 results from simulations at amplitude $r_0 = 0.011$ and reflects the tuning characteristics of the model. Indeed, we find that the coding fraction is non negligible over the range off frequencies $F = \beta/2\pi \sim [1.0, 2.5]$. A closer look at the response shows that the model fires with a rate of 0.5 spikes per EOD cycle in this region (not shown). We know from the 2:1 (P=0.5) tuning curve in figure 4.7 that FHN with EOD amplitude around 0.011 only fires significantly at forcing periods in the range [0.5, 1.0]. This interval correspond to frequencies [1.0, 2.0] closely matching what we observe from the coding fraction. Outside this range, the model triggers too few spikes to transmit information.

4.5 Discussion

Even though it is a simplified version of the conductance based Hodgkin Huxley model, the FHN model constitutes a simple yet biologically relevant spiking mechanism. When forced with sinusoidal input it reproduces a lot of features of P-type electroreceptors such as tuning characteristics, baseline firing statistics at mid-to-high frequency and proper behavior while changing the mean input amplitude.

We find the interesting result that one cannot establish a one-to-one relation between the encoding quality of FHN and its associated probability P to fire at each EOD cycle. Although

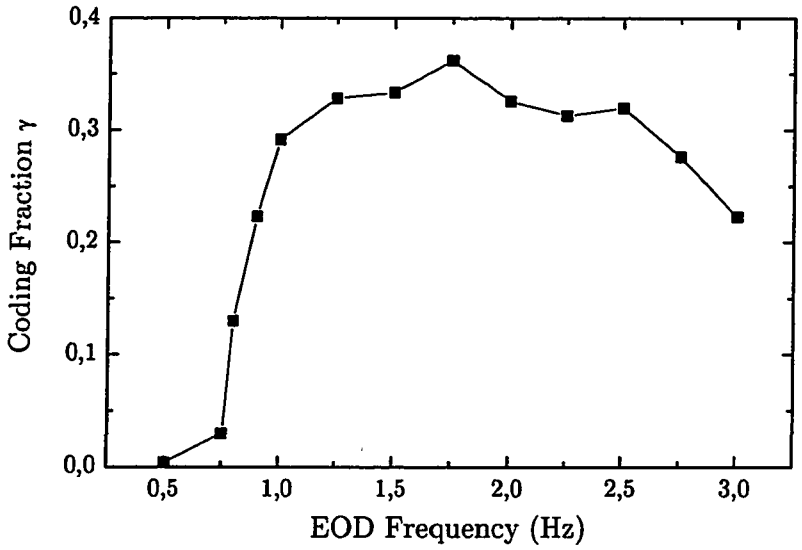

Figure 4.11: Coding fraction vs carrier frequency in the FHN model. All points were obtained with EOD amplitude $r_0 = 0.011$ and $D = 8 \times 10^{-8}$. This value of the noise intensity corresponds to the maximum of the curve at $r_0 = 0.011$ in figure 4.8.

this was also found in the LIFDT model studied in the previous chapter, the value of P in the present model is not only dependent on the forcing amplitude. For that reason we studied the individual effects of the mean carrier amplitude and of the exponentially correlated noise amplitude on the information measurement. Their effect was investigated in two distinct forcing regimes: subthreshold and suprathreshold.

We have found that noise can enhance the information transfer in the subthreshold regime. Its effect was presented in terms of the linearizing effect of the noise on the transfer function and of its tendency to raise the sampling rate in the subthreshold regime. From [28], we also know that the effect of synaptic noise on the tuning properties of FHN is to lower the threshold at large forcing period. Thus, in terms of frequency, slowly varying amplitudes produce a larger effective modulation of the output rate of the model when noise is present.

A beneficial effect of the noise on signal encoding by FHN was similarly found in studies of stochastic resonance — associated to subthreshold forcing by definition — with slowly varying input signals in [6, 7, 21]. However in those studies the signal was directly applied to the model and no carrier signal was involved. The presence of a carrier in our study does not seem to alter the linearizing effect of the noise on the transfer function of FHN. But the sensitivity of the FHN model to the carrier, specifically via the tuning curve, does determine the overall magnitude of the modulation and thus of the coding (figure 4.11).

In the suprathreshold regime, the qualitative effect of synaptic noise is the same as our result from the previous chapter. The presence of the AM's alone is sufficient to induce transitions between neighboring region of phase locked firing in the phase space. Additional synaptic noise simply randomizes the firing times and reduces the coding fraction.

Our results of the effect of EOD amplitude on the coding fraction (figure 4.9) is similar to that of Wessel [40] from their measurements on artificially forced P-units. Their results showed that by increasing the forcing amplitude and thus by raising the output rate of the neuron, the coding fraction increased and saturated a very high output rates. However, the decrease at very high rate was not observed in their study, although they did not study firing rates greater than ~ 0.5 spikes per EOD cycle.

Finally, our last result on the coding fraction vs the forcing frequency points to an important role of the resonant behavior of type II membrane on the encoding quality. Although we might expect the limit cycle of resonant models to interfere with rate coding, we find that amplitude modulations are best encoded near the preferred forcing period. This interesting result will be further discussed in the next chapter as we compare type I and type II membranes dynamics in two implementations of the Morris-Lecar model.

Chapter 5 Morris-Lecar

Another reduction of the Hodgkin-Huxley model, the Morris-Lecar model, is now considered for our study of signal transduction. This particular model exhibits an important variety of dynamical behaviors by simply adjusting input parameters. We will use this behavioral richness to investigate the encoding of weak electrical signals using two distinct sets of parameters for which the model operates in the vicinity of two different bifurcations between resting and periodic firing. We compare the results obtained from a spiking mechanism underlying a Hopf bifurcation (type II membrane) to those from a mechanism that involves a Saddle-Node bifurcation (type I membrane). Our results suggest that although the underlying dynamics of the two coders is quite different, their ability to encode weak random amplitude modulations are qualitatively, and in fact, even quantitatively very similar. We are not aware of any comparison of the coding capabilities of these two important neuron classes.

5.1 Spiking Mechanism

The model developed by Morris-Lecar (ML) was first used in the context of a study of the barnacle muscle fiber. It is a hybrid between the Hodgkin-Huxley and FitzHugh-Nagumo models, thus its equations have the same general form as expressed by equations 1.5. It involves two voltage-gated ionic currents: one Ca^{2+} channel and one K^+ channel.

$$C\dot{v} = -g_{Ca}m_\infty(v)(v - V_{Ca}) - g_K w(v - V_K) - g_L(v - V_L) + I \tag{5.1}$$

$$\dot{w} = \phi\frac{[w_\infty(v) - w]}{\tau_w(v)} \tag{5.2}$$

where

$$m_\infty(v) = \frac{1}{2}\left[1 + \tanh\left(\frac{v - V_1}{V_2}\right)\right] \tag{5.3}$$

$$w_\infty(v) = \frac{1}{2}\left[1 + \tanh\left(\frac{v - V_3}{V_4}\right)\right] \tag{5.4}$$

$$\tau_w(v) = 1/\cosh\left(\frac{v - V_3}{2V_4}\right) \tag{5.5}$$

w and m represent the fraction of open channels for K^+ and Ca^{2+} respectively and the infinity subscript indicates the pseudo steady state of the variable, similar to HH. Due to the dynamics of m being much more rapid than that of the voltage over the considered time scales, the model assumes that m always reaches its pseudo steady state value (m_∞) instantaneously. It is called pseudo steady state because it still depends on v. As for w, its dynamics is governed by a characteristic time τ_w which in turn is dependent on the transdermal potential. Note that ϕ is a general function that captures temperature-like effects.

The behavioral richness of the Morris Lecar model was well demonstrated by Rinzel and Ermentrout in [36]. Their investigation revealed that such a model can exhibit various non-linear dynamics and, in particular, the appearance of periodic solutions via two distinct bifurcations as the bias current I is increased.

In [36], they first present the phase space analysis of the model with a set of parameters that admits a periodic solution in the vicinity of a Hopf bifurcation. The periodic solution arising from such a bifurcation typically emerges with a well-defined, non-zero frequency, thus a finite oscillation period. This mechanism of spiking in a neuron model is known in the literature as type II membrane. A finite-period limit cycle makes these coders recognizable by their typical resonant-like v-shape of their tuning curves. The FHN model studied in the previous chapter is of this particular type.

Rinzel and Ermentrout then analyzed the dynamics for a different set of parameters, for which the system can also exhibit a periodic solution although, in that case it emerges via a saddle-node bifurcation. This second mechanism is usually referred to as type I membranes. Here the onset of the periodic solution can appear with arbitrary small frequency. No resonant behavior are observed in deterministic type I membranes.

We now present in further detail the dynamics of both type II and type I ML based on plots reproduced from [36]. We refer to [36] for a more in-depth discussion of the two mechanisms. We assume that the reader is familiar with some elements of non-linear dynamics analysis which can be found in introductory textbooks such as [38].

Type II

Figure 5.1A and B presents the response of type II ML to a brief current impulse (square pulse). According to plot A, the time course of the membrane potential depends dramatically on the current pulse intensity. Note that a very subtle change in the initial current pulse can

make the difference between an action potential being triggered or not. In all cases though, all the trajectories end up decaying to one fixed resting state. Plot B depicts the same four current pulse experiments, this time in the v-w phase space where the v and w nullclines are represented by dotted lines.

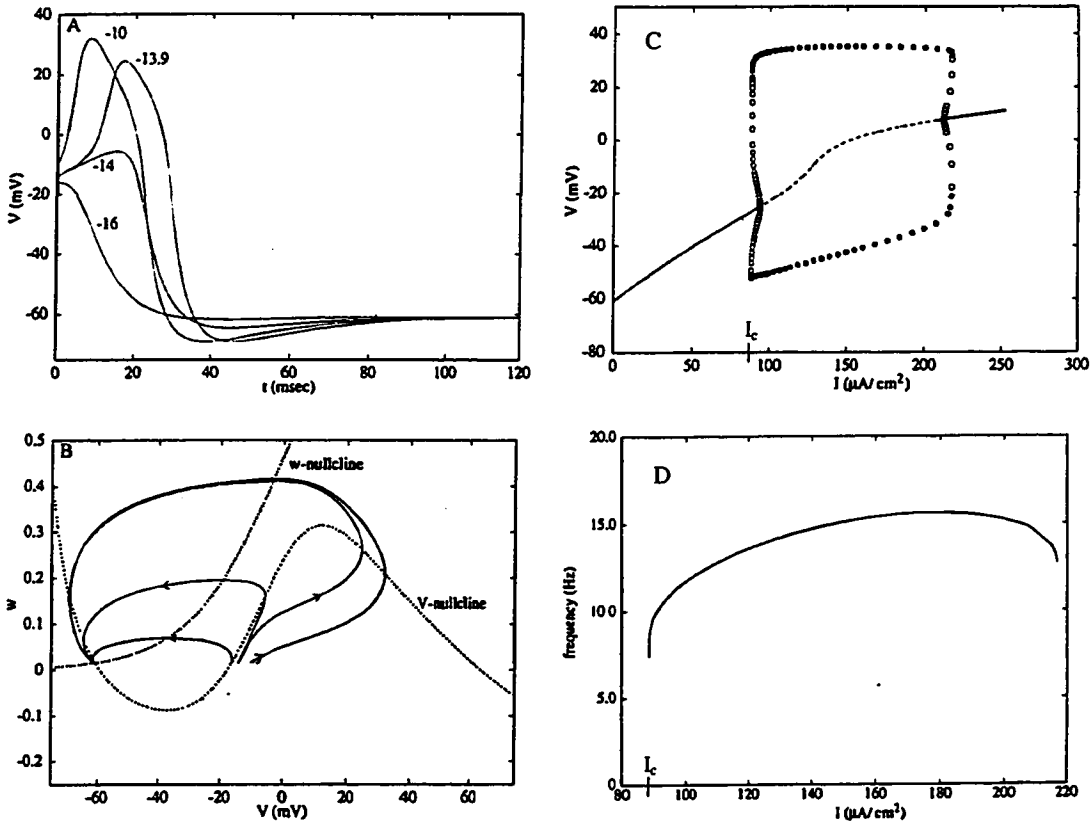

Figure 5.1: Dynamics of type II Morris-Lecar. LEFT: (A) Voltage response to various current impulses with amplitude indicated alongside the corresponding curve. (B) The same responses are shown in the v-w phase plane. Dashed lines represent the v and w nullclines. RIGHT: (C) Bifurcation diagram of steady state voltage vs I (no EOD). The branches plotted with circles represent the extrema of the periodic voltage solution. (D) The frequency of the periodic solution as a function of I, the bifurcation parameter. Note that the parameters differ from ours; plots are for qualitative description only. (From [36])

For the particular set of parameters used to produce figure 5.1B, the intersection of the two nullclines is a stable fixed point. This is where the system decays to when no external stimuli is applied. Upon the application of a sudden current impulse, the system becomes depolarized, which translates into an almost instantaneous shift to the right in the v-w phase space. The path to the fixed point then depends on the actual size of the shift and is dictated by the phase space, in particular by the nullclines.

This particular arrangement of the nullclines and the stable fixed point can be disturbed by the simple addition of a constant current. Through linearization and analysis of the flow around the fixed point, one can show that the fixed point of figure 5.1B loses its stability and a periodic solution (repetitive firing) appears. The occurrence of this Hopf bifurcation is represented as a function of the bifurcation parameter in panel C. The lower and upper branches beyond I_c on this plot of the steady state value of v vs the applied current are the extremum reached by the voltage in its periodic trajectory. Note from panel D that the periodic solution emerges at I_c with non-zero minimum frequency and that the frequency is somehow constant over the whole periodic solution interval. The presence of such a limit cycle characterizes all type II membranes.

Although it is beyond the scope of the present work, note that for a very small interval of current I near the bifurcation point, type II Morris-Lecar exhibits bistability; when I becomes slightly greater than I_c, the bifurcation diagram exhibits three fixed points in a small interval of bias currents. In this narrow region a stable fixed point and a stable limit cycle coexist and the dynamics depends on the initial condition. Given the starting point in the phase space, the state of the system will either decay to the stable fixed point or approach the stable limit cycle. For even greater values of I, all initial conditions will lead to a periodic solution.

Type I

The second Morris-Lecar implementation of interest is a model of type I membrane with parameters as given by table 5.2. The equivalent to figure 5.1 in this new model is plotted in figure 5.2. The time course of the voltage in response to brief current impulses is presented in the top left plot. The dynamics for the same experiments is also presented in the v-w phase plane (B). Notice in this phase plane the three intersections of the v and w nullclines, revealing three fixed points. From left to right those fixed points are (R) a stable rest state, (T) an unstable saddle node and (U) an unstable spiral.

Upon a small displacement to the right from R — not passed the threshold T — the system decays to the rest state. However, if the displacement is large enough to bring the state of the system passed the saddle threshold T, the return to the rest state happens via an action potential.

In comparison with the dynamics of type II ML, the major difference in dynamics is due to the presence of the saddle fixed point. For initial conditions very close to the stable and

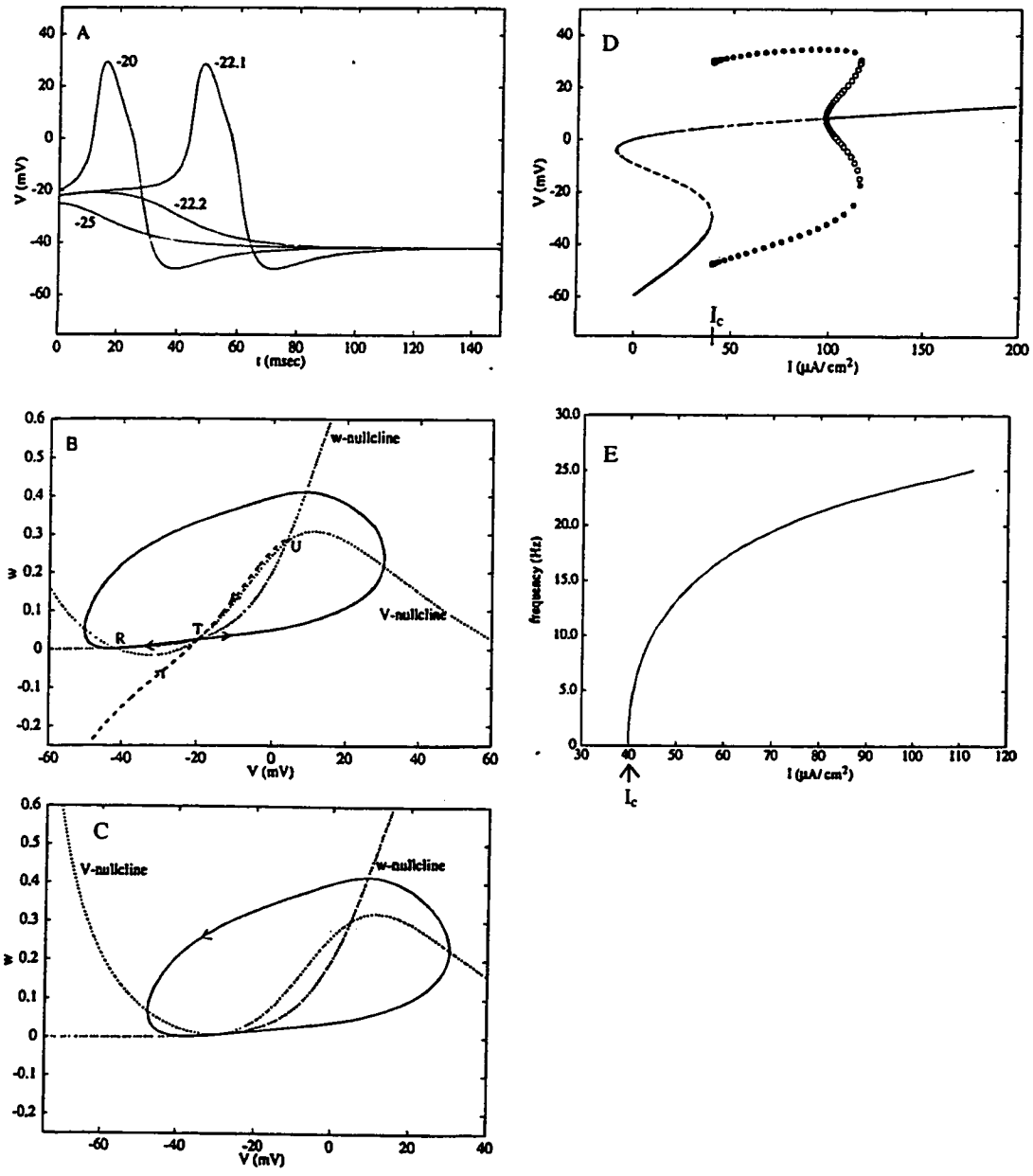

Figure 5.2: Dynamics of type I Morris-Lecar. LEFT: Voltage response to various current impulses (A) in time and (B) in the v-w phase space. Dashed lines represent the v and w nullclines. (C) Periodic solution in the v-w phase space. RIGHT: (D) Bifurcation diagram of steady state voltage vs I (no EOD). The branches plotted with circles represent the extrema of the periodic voltage solution. (D) The frequency of the periodic solution as a function of I is zero at the critical current. Note that the parameters differ from ours; plots are for qualitative description only. (From [36])

unstable manifolds — the two crossing nullclines at T — the dynamics is very slow and it takes the system a long time to either decay to the rest state or trigger an action potential. Because of this particularity, action potential can occur over arbitrary long periods. This property is not observed in type II coders.

A periodic solution is also observable in type I ML by tuning the input current I of the model. Figure 5.2D illustrates the three fixed points (for $I < I_c$) discussed above in a bifurcation diagram of v as a function of the applied current; the corresponding dynamics in the phase space is shown in panel C. As the current is raised, the stable rest state and the saddle-node threshold coalesce giving rise to a periodic solution whose dynamics is very slow near the coalesced fixed points. Thus the onset of repetitive firing in type I can occur with arbitrary long period as illustrated by a null frequency at I_c (Panel E). Note that the second bifurcation observed in panel D will not be considered in this study of a type I membrane as it is a (reverse) Hopf bifurcation.

5.2 Numerical Implementation

The transduction of weak signals by the Morris Lecar model was investigated using a Fortran algorithm. Each simulation used 2×10^7 time steps of size dt=0.025 ms. The first 10^5 iterations were discarded as transients.

The voltage variable was forced additively with constant contrast (see eq. 2.1) using the following EOD implementation:

$$\mathrm{EOD}(t) = r_0\big[1 + s(t) + \eta(t)\big]sin(\beta t) \tag{5.6}$$

where r_0 is the mean EOD amplitude, $s(t)$ is the band-limited random amplitude modulation and η is the synaptic multiplicative noise term. The latter is implemented as an Ornstein Uhlenbeck process with correlation time τ_{mult} and variance $D_{mult}\tau_{mult}$ generated as discussed in section 2.1.2. The multiplicative coupling of η to r_0 accounts for the synaptic noise being proportional to the instantaneous amount of synaptic transmitter [42]. This is a reasonable property for point processes that represent the sum of spikes at the neuron's input.

The choice of the parameters was based on Rinzel and Ermentrout's analysis in the first and second editions of [26]. The set of parameters in the second edition was renormalized, and slightly changed. Since some of our work had already been done based on the scheme of the first edition of [26], we kept the renormalization scheme of the first, and made the

slight adjustments to reflect the dynamics from the most recent publication. The resulting parameters are slightly different than those of the first edition and are shown in table 5.2.

Parameter	Type II	Type I
V_1	-0.01	-0.01
V_2	0.15	0.15
V_3	0.167	0.01
V_4	0.25	0.145
V_{Ca}	1.0	1.0
V_K	-0.7	-0.7
V_L	-0.5	-0.5
g_{Ca}	1.1	1.0
g_K	2.0	2.0
g_L	0.5	0.5
C	1.0	1.0
ϕ	0.2	0.333
τ_{mult}	0.025	0.025

Table 5.1: Morris-Lecar parameters for type II and type I spiking mechanisms. All quantities are unitless (see first edition of [26] for details of the nondimensionalization).

5.3 Firing Characteristics

The present study involves forcing the Morris-Lecar with an amplitude modulated sinusoidal signal (EOD), using the two sets of parameters presented in table 5.2. We first present the firing characteristic of the two implementations of the model at rest i.e. when forced with a constant amplitude EOD (no AM). In particular, the effect of the bias current and of the limit cycles are shown and discussed.

Type II

When forced with a simple, constant current term I (no EOD), our implementation of type II Morris Lecar undergoes a Hopf bifurcation at a critical bias current value $I_c = 0.183$. For any currents below I_c, the model converges to a rest state dependent on the actual value of the current; it does not fire in this steady state. For currents above I_c — and up to another critical value which is not of interest here — type II ML exhibits a periodic solution which appears as periodic firing with a period of approximately 32 ms.

When forced with a I below the critical I_c and with an additional constant amplitude sinusoidal term (adding the EOD), type II Morris-Lecar responds in a phase locked manner. It is illustrated by the devil's staircase structures in plots of P vs r_0 in figure 5.3 for two

distinct bias current values. The respective I currents for plots (A) and (B) are 0.135 and 0.149; thus we say that the top case is further away from the bifurcation. The relative distances from the threshold for the 2 models is different here since case (A) must be forced with a greater carrier amplitude to exhibit a non zero firing probability.

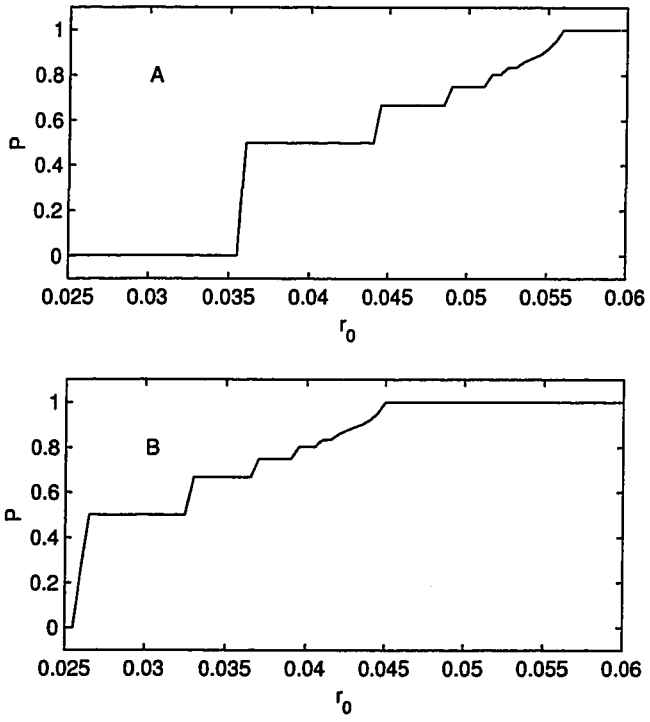

Figure 5.3: Devil's staircase of type II Morris-Lecar. Bias currents I are 0.135 (A) and 0.148 (B). All other parameters as per table 5.2 (without synaptic noise).

Notice for the top plot that any EOD amplitude below $r_0 = 0.036$ will not produce any firing unless noise or a random amplitude modulation is added. Those amplitudes are said to be subthreshold. Conversely, amplitudes above $r_0 = 0.036$ are said to be suprathreshold as they give rise to firing without any other forcing. The equivalent threshold carrier amplitude for the bottom plot is $r_0 = 0.026$.

The large plateaus seen in figure 5.3 reveals an important phase locking phenomenon in Morris-Lecar type II. One can easily distinguish plateaus at phase locking patterns of 2:1, 3:1, 4:1 and even 5:1. Such plateaus are "washed out" when adding synaptic noise to the model (not shown) and the current-frequency transfer function is linearized as we have found for LIFDT and the FHN model. Phase locking is also observable in ISIHs of type II ML (fig. 5.4) for two different currents yielding two distinct regimes. Both histograms are realized

with the same EOD amplitude; the subthreshold and suprathreshold regime were obtained by changing the distance to the Hopf bifurcation using to distinct bias current values of 0.135 and 0.149. Synaptic noise of amplitude D = 0.06 was applied as well.

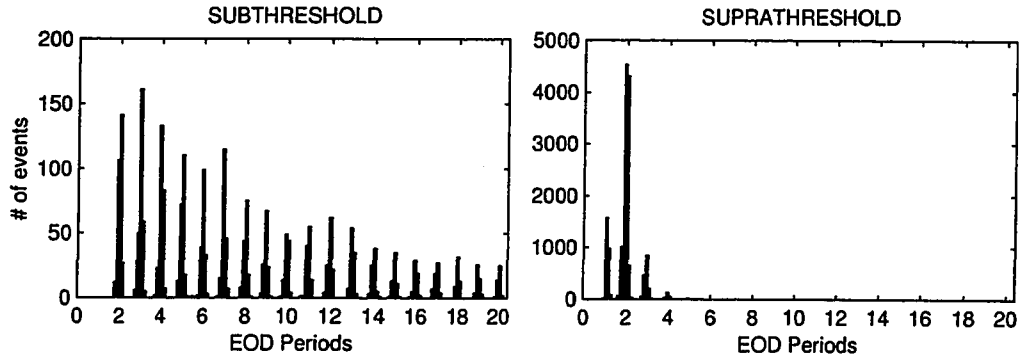

Figure 5.4: Interspike Interval Histogram of type II Morris-Lecar with constant amplitude periodic forcing. Both panels are realized with $r_0 = 0.03$ and noise intensity $D = 0.06$. The subthreshold and suprathreshold regimes are obtained using two current values of 0.135 and 0.149, for the left and right histograms, respectively. Fluctuations in mode heights are statistical; for longer simulations, the ISIH is expected to decay monotonically.

In the subthreshold regime, the model would not fire in the absence of synaptic noise. The addition of a stochastic component allows firing and the resulting gamma-distribution shape of the ISIH is typical of histograms found in mid-to-high frequency units — in contrast with Gaussian-shaped histograms found in low frequency units. The frequency of the forcing being f=60Hz, we find clusters of intervals around multiples of t=16.66ms equivalent to 1 EOD period.

In the suprathreshold regime, firings happen at a greater rate, hence the interspike intervals are reduced on average and the modes are shifted to the left of the histogram. In the absence of synaptic noise, this regime exhibits a 2:1 firing pattern (one spike every 2 cycles). Notice the different scales indicating a greater number of events in the suprathreshold case.

We conclude on type II firing statistic with a tuning curve realized at $I = 0.135$ shown in figure 5.5. It has the characteristic V-shape of type II membrane and its minimum is located slightly to the left of the period associated with its limit cycle (31.2 Hz). Notice the location of the period chosen for our study (16.6 ms, 60 Hz) at about half the period of the limit cycle. Because of its resonant behavior, we expect signal transduction in type II ML to be lower because of its tendency to fire at the frequency of its limit cycle, rather than according to the AM fluctuations of the EOD.

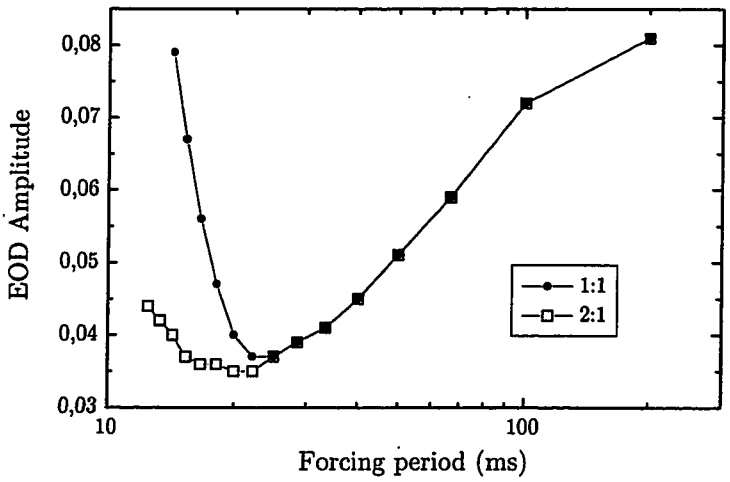

Figure 5.5: Tuning curve of type II Morris-Lecar. Each curve is obtained by finding the minimum amplitude giving rise to the indicated (n:m) firing pattern for different forcing periods.

Type I

The critical bifurcation current of type I ML as illustrated in figure 5.2 is $I_c = 0.083$. We recall that when I is increased passed this critical value, a stable fixed point and a saddle node coalesce through what is called a saddle-node bifurcation. For $I > I_c$ periodical firing emerges with zero initial frequency.

Periodically driven type I ML exhibits the devil's staircases presented in figure 5.6 with bias current values 0.0718 and 0.0736. The latter values are below I_c and the first of the two being smaller, it is further away from the bifurcation. As expected, panel A reveals that a larger EOD amplitude r_0 is needed to induce firing than when the system is placed closer to the bifurcation. Phase locking is apparent in the devil's staircase of type I, although the plateaus are smaller than for type II. Also, we find that the slope of the r_0-P transfer function is steeper than in the type II case. Thus we expect the range of EOD amplitudes that are potentially encoded by type I to be smaller. Conversely, the steeper transfer function should encode minute modulations better since they induce larger changes in the firing probability per EOD cycle.

The modes in the interspike interval histograms of type I are broader than those of type II, although the distribution is roughly the same. The suprathreshold case is also a perturbation of the 2:1 firing pattern, and intervals are also shifted to the left in comparison with the subthreshold case. We remark that the type I model allows more spikes in the first mode

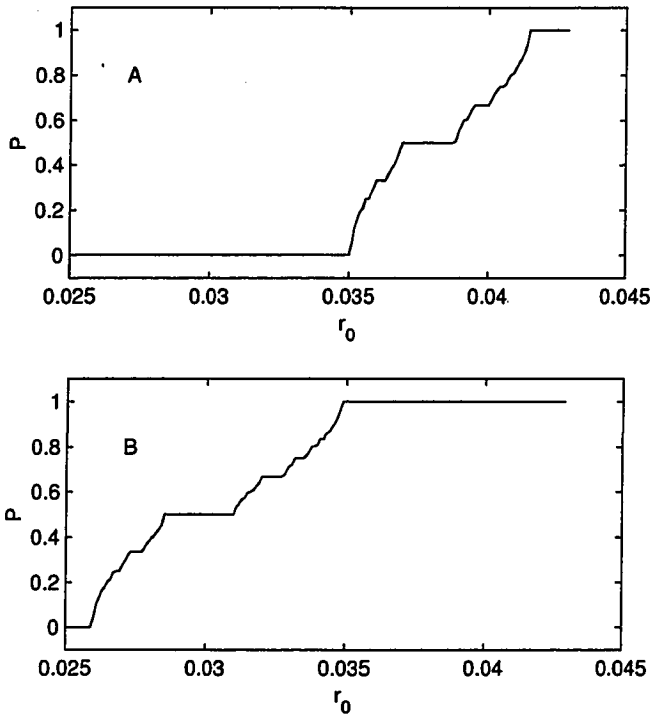

Figure 5.6: Devil's staircase of type I Morris-Lecar. Bias currents I are 0.0718 (A) and 0.0736 (B). All other parameters as per table 5.2 (without synaptic noise).

(ISI's of one EOD cycle) than type II does in both sub and suprathreshold regimes.

The most important difference between the type I and II models is found by comparing the tuning curves of the two. The type I tuning curve is monotonic everywhere in the range of forcing periods plotted in figure 5.8. The L-shape of the curve reminds the tuning curve found in LIFDT (chapter 3). The almost-constant and low threshold amplitude in the region of long forcing periods (low frequency) signals suggests that slowly varying modulations should be well encoded in that type of membrane model.

5.4 Results

Matching P responses

Our investigation consists in a comparative study of the transduction of weak signals by the Morris-Lecar model operated in the vicinity of two different bifurcations. Given that our information measurement is greatly dependent on the P-value, the comparison only makes sense if both cases exhibit similar output frequencies in response to the combined fixed EOD and noise amplitudes. Moreover, we want the responses to show similar P-values over the

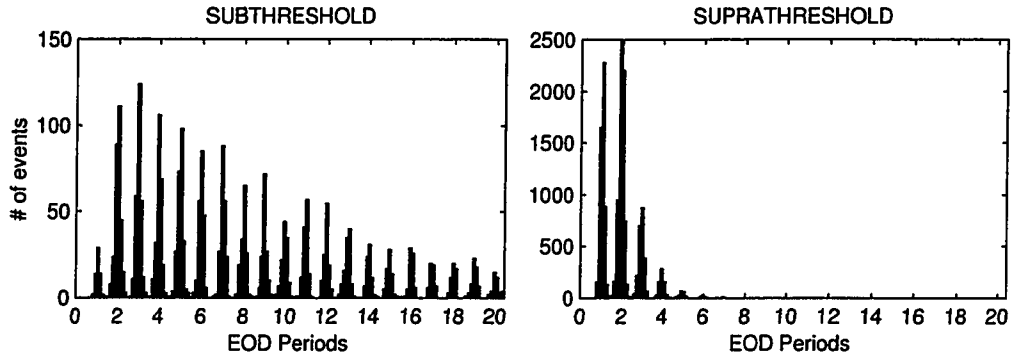

Figure 5.7: Interspike Interval Histogram of type I Morris-Lecar with constant amplitude periodic forcing. Both panels are realized with $r_0 = 0.03$ and noise intensity $D = 0.06$. The subthreshold and suprathreshold regimes are obtained using two current values of 0.0718 and 0.0736, for the left and right histograms, respectively. Fluctuations in mode heights are statistical; for longer simulations, the ISIH is expected to decay monotonically.

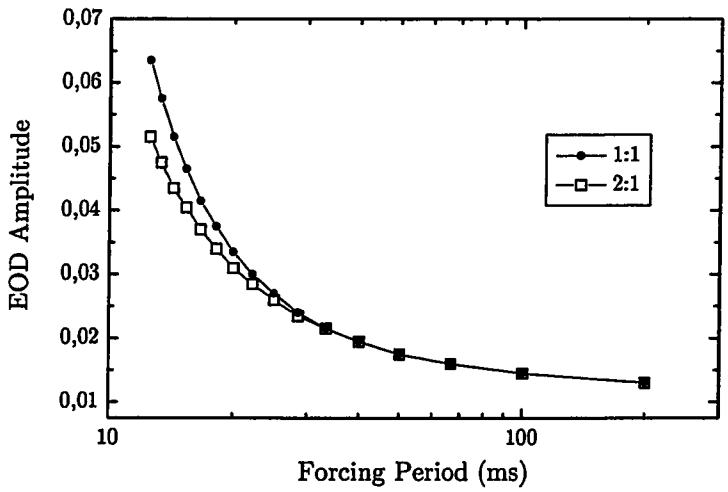

Figure 5.8: Tuning curve of type I Morris-Lecar. Each curve is obtained by finding the minimum amplitude giving rise to the indicated (n:m) firing pattern for different forcing periods.

range of noise amplitudes considered for our information transfer study. This can be achieved by tuning the bifurcation variable I for each model in order that the distance of the operation point of each model from their respective bifurcation is approximately the same.

P values of both type II and type I models forced with a constant EOD amplitude of 0.03 (no AM) are plotted over the same interval of noise amplitudes in figures 5.9 and 5.10. Each curve is computed for a fixed bias current. We recall that P is defined as the probability of firing per cycle without a stimulus; values of P were obtained from the average firing rate of a 25 s simulation. It is expected that for low current values, the operating point is far from

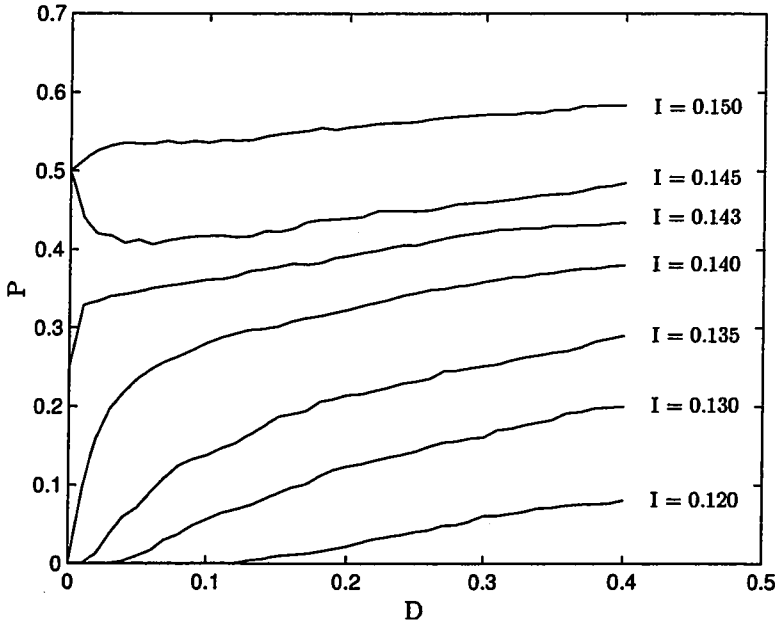

Figure 5.9: P vs D for different input current values in TYPE II Morris-Lecar. One point was generated every $D = .001$ from the average interspike interval of a 25 seconds simulation. All parameters are as per type II parameters listed in table 5.2.

the bifurcation and the resulting P value is low. Increasing synaptic noise brings the system closer to threshold and P increases. Also expected is the fact that output rate increases as the input current approaches the bifurcation critical value.

Each model was tuned so that they could both be compared in the subthreshold regime as well as in the suprathreshold regime. For both regimes, two sets of similar P-D relations are shown in figure 5.11. They were obtained after a close investigation of figures 5.9 and 5.10 by generating such plots at more closely spaced current values. It was found that both models have a similar curve, in the subthreshold regime, for current values of $I = 0.0718$ (type I) and $I = 0.135$ (type II). Note that when the noise amplitude is zero, their P value

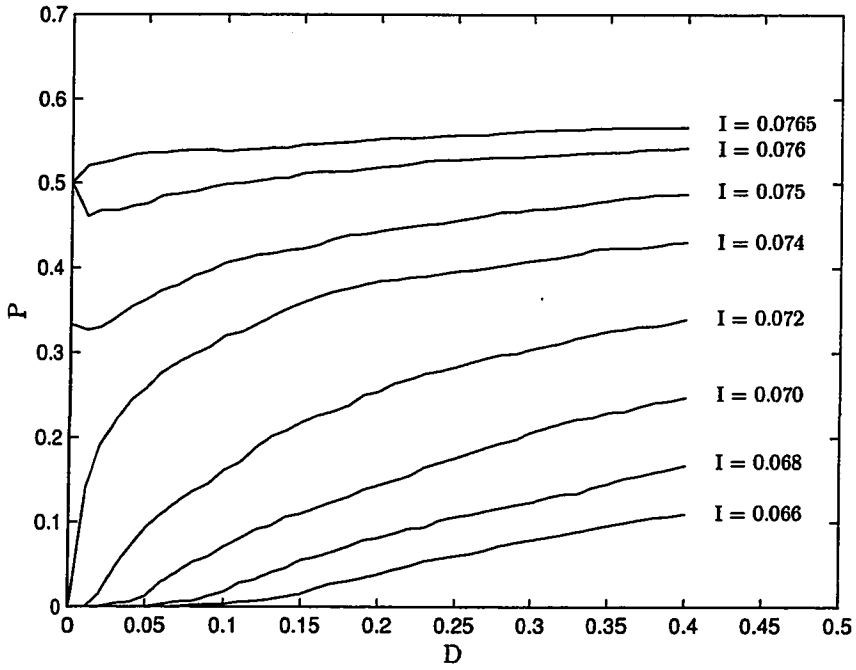

Figure 5.10: P vs D for different input current values in TYPE I Morris-Lecar. One point was generated every $D = .001$ from the average interspike interval of a 25 seconds simulation. All parameters are as per type I parameters listed in table 5.2.

is 0 and that is why they qualify as subthreshold cases. The two curves are especially close for values of $D < 0.1$. Values for greater D are of lesser importance; this choice of parameter will become clear when comparing coding fractions, as their maximum coincide in the low D region. In the suprathreshold case, current values of $I = 0.0763$ (type I) and $I = 0.149$ (type II) lead to very similar curves in the whole interval considered. Note that the output rate is close to constant at a fairly high value of 0.5 (far suprathreshold regime) and that the noise has very little effect on the mean rate in those implementations.

Comparing Coding Fraction

Using the set of parameters that yield closely matching P-D curves, we then simulated the response of both models to an EOD with random amplitude modulation of standard deviation set to 17% of r_0 based on [40]. We wish to characterize, as in previous chapters, the effect of increasing synaptic noise on the coding fraction, in the two types of amplitude coders each for two specific regimes: subthreshold and suprathreshold.

Results for both models in the subthreshold regime are presented in figure 5.12 for the coding fraction as a function of the synaptic noise amplitude. Each point is obtained using

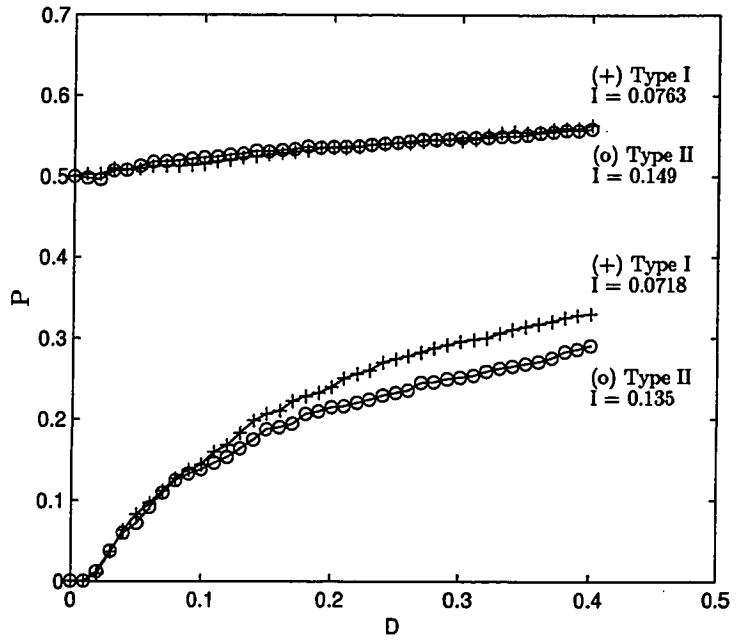

Figure 5.11: Comparative P-D curves for both subthreshold and suprathreshold cases. Specification and parameters are as for figures 5.9 and 5.10. Circles (o) identify the type II model and plus signs (+) are used for type I coders.

the linear stimulus reconstruction technique (ref. section 2.2.1) . The error on each point is found by evaluating the coding fraction from multiple simulations with different initial seeds; it is of the order of ± 0.01 for each point. Interestingly, the result for the two models is very similar, although the coding fraction of type II is everywhere slightly better than that of type I except for the deterministic case (D=0). The reconstruction quality for both models first increases with increasing noise from a low value, and goes through a maximum at roughly the same noise amplitude of $D \cong 0.06$. This can be understood as follows, as in section 4.4 for the subthreshold FHN model; low noise amplitude brings the system voltage closer to threshold and raises the mean firing rate, thus the coding quality is enhanced. However, noise at amplitudes greater than $D \cong 0.06$ has more of a randomizing effect and the coding fraction starts decreasing.

We have performed the same simulations in the suprathreshold case using bias current parameters for the matched P-D curves in the suprathreshold regime. Results are in figure 5.13 which shows that the quality of the reconstruction diminishes with increasing noise amplitude in both ML implementations. The error on each point is of the order of ± 0.01. Here again we find that type II is better that type I for most of the range of noise intensity

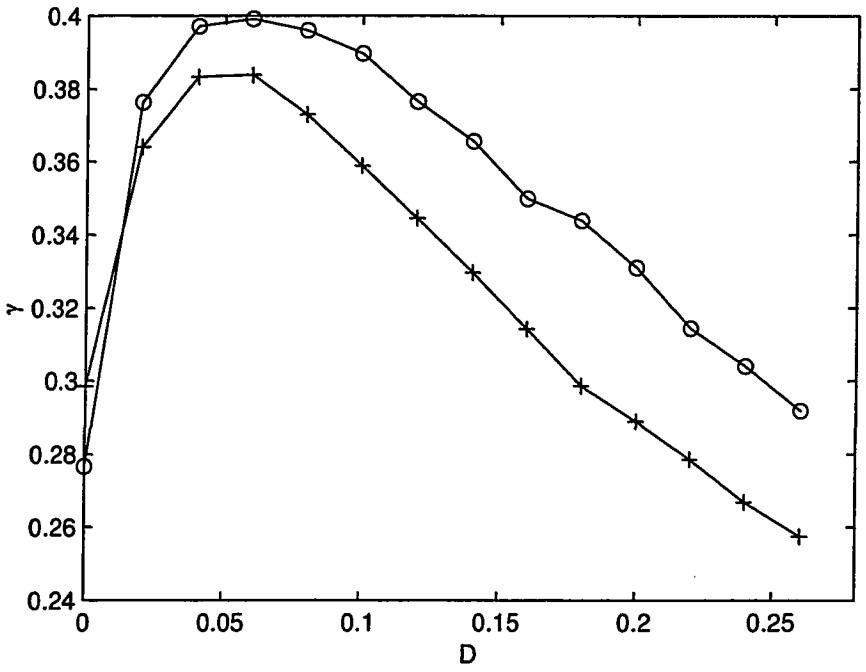

Figure 5.12: Coding fraction vs noise amplitude in the subthreshold ML model. Circles (o) identify the type II model and plus signs (+) are used for type I coders.

we have investigated, except at very low noise values where type I encodes better. This result is also similar to the result from the suprathreshold FHN (section 4.4).

We also present preliminary results on the dependence of γ on the distance to the bifurcation, based on the study of neural firing probability in type I of Ermentrout in [20]. It is not clear how to quantify the "distance to a bifurcation" especially in the case of periodically driven models as its definition is somehow different in every model. One might express it as the relative distance to the bifurcation (e.g. $(I - I_c)/I_c$ but due to the complex equations of non-linear models, this quantity is hard to relate to the driving amplitude. For example, resonance effects in type II ML reduces the effective distance to threshold and our two models won't exhibit the same firing rates in response to the same EOD. An attempt at comparing the distance to threshold is found in [20] where the distance is simply defined as the absolute distance to the threshold (e.g. $I - I_c$). Using absolute distance though is highly vulnerable to a renormalization of a model. Nevertheless we have used this method and we present the effect of the distance to threshold on the coding fraction in figure 5.14. It was obtained from simulations over a range of bias current values (with all other parameters constant) and plotted as a function of $I - I_c$. We recall that critical values are $I_c = 0.183$ and 0.083 respectively

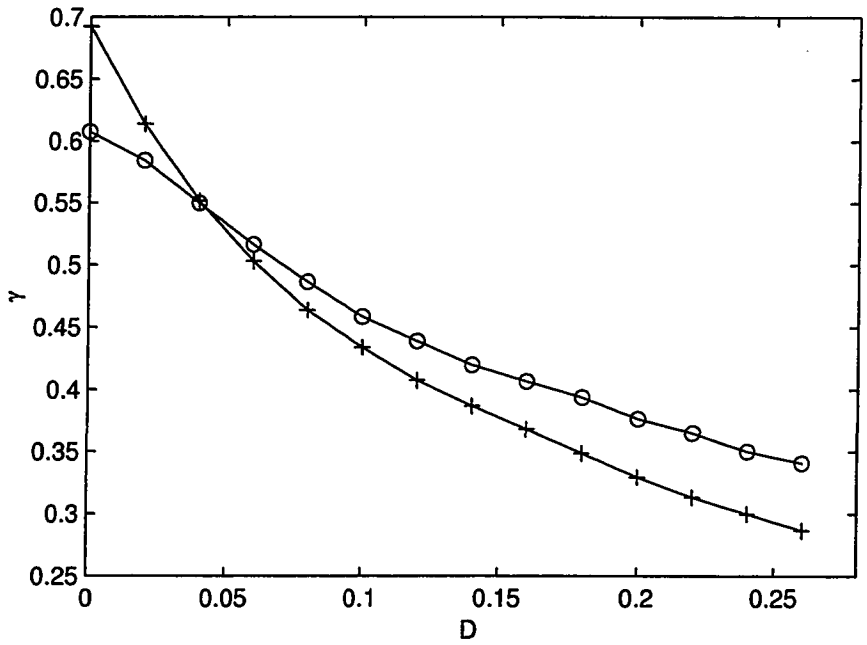

Figure 5.13: Coding fraction vs noise amplitude in the suprathreshold ML model. Circles (o) identify the type II model and plus signs (+) are used for type I coders.

for type II and type I ML. A noise amplitude of $D = 0.06$ was used for all simulations which corresponds to the maximum of the coding fraction in the subthreshold case (figure 5.12).

We find that the maximum coding fraction for both models (peak values) are very similar, although they do not appear at the same distance from their respective bifurcations. The interval for which the coding fraction is high is larger and flatter in type II and further away from the bifurcation.

5.5 Discussion

We have studied the transduction of weak signals via carrier amplitude modulations in two implementations of numerical Morris-Lecar model as a P-type electroreceptor. We have reviewed the basic spiking mechanism of the model operating (A) in the vicinity of a Hopf bifurcation (type II membrane) and (B) near a saddle-node bifurcation (type I membrane). We have observed that for both types, the ISIH for subthreshold EOD amplitude with no modulations and with synaptic noise are similar to those observed for mid-to-high frequency electroreceptors [41, 37]; ISIH's for suprathreshold carriers are concentrated on the first few EOD periods due to a higher output firing rate (reduced mean ISI).

We have shown that in both type II and type I models, noise of synaptic origin may

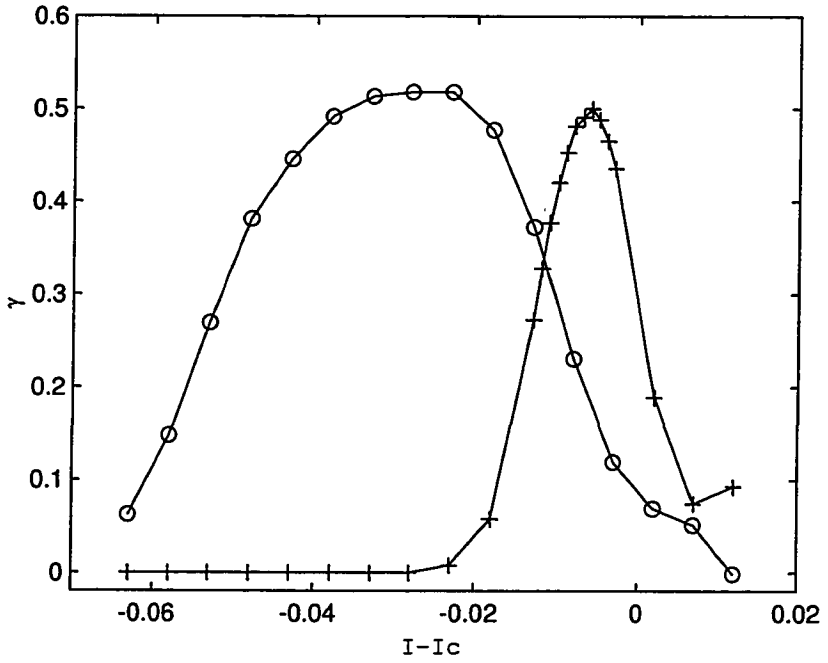

Figure 5.14: Coding fraction vs distance to bifurcation. Circles (o) identify the type II model and plus signs (+) are used for type I coders.

increase the quality of signal transduction in the subthreshold regime near the threshold. Low noise amplitude raises the sampling rate of the model by bringing it closer to the threshold and reduces reconstruction noise. In the suprathreshold case, noise was found to always reduce the quality of transduction by comparison with the noiseless case as in FHN and LIFDT.

The performance of both types of coders was strikingly similar indicating very little influence of the onset mechanism for the limit cycle on the coding quality, at least in this ML model. Nevertheless we do observe the following differences. In both the subthreshold and suprathreshold case, type I ML has a significantly larger coding fraction than type II in the low noise region. However, at larger noise amplitudes, we found type II to be a slightly better coder despite the fact that it has a slightly lower sampling rate, as shown in figure 5.15. This plot shows in fact that, although both models have approximately the same P (defined without random EOD modulations), the firing rate of type I is higher than that of type II when AM's is present.

The fact that both models code similarly in subthreshold and suprathreshold regimes is likely a consequence of the fact that the synaptic noise, and the on-going transients induced

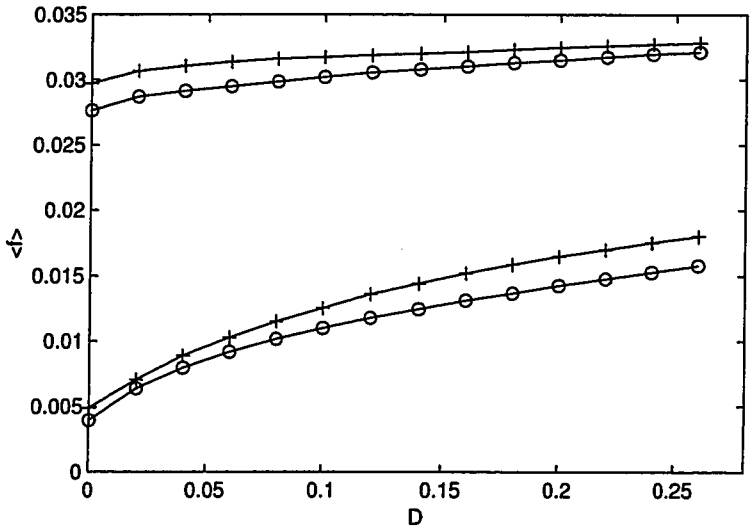

Figure 5.15: Mean firing rate vs noise amplitude. Circles (o) identify the type II model and plus signs (+) are used for type I coders. Curves on top are from the suprathreshold regime while those at lower frequency are from the subthreshold regime.

by the AM's, cause a linearization of the ML transfer function.

The differences between the two curves in figure 5.14 are interestingly addressed by analyzing the effect of resonance in ML type II on the coding fraction. For example, we observe that the maximum of the curve for type II is further away from the bifurcation and wider than for type I even if the same amplitude modulation was used for both models. It appears that the subthreshold response is heightened by the intrinsic resonance in type II. Also, type II may saturate more quickly above the threshold which is why the best coding occurs below and around threshold.

The effect of resonance on amplitude modulation transduction is two-fold. We expect the resonance to increase information transfer as it increases the effective amplitude of the AM. On the other hand, a resonant model tends to fire at the frequency of its limit cycle, thus lowering its coding quality. Our study points to a more beneficial effect of the resonance as type II encodes as well as the non resonant type I. However, the limit cycle does reduce the coding fraction as observed in figure 5.14 around the bifurcation. Indeed, as I reaches the critical value I_c (i.e. at $I - I_c \sim 0$), the response is governed by the limit cycle and the coding fraction is greatly reduced. This is further expected in the type II model which could explain the position of its maximum, on the left of the maximum for type I, i.e. for relatively more subthreshold signals.

Chapter 6 Nelson

The model investigated in the present chapter was proposed by Mark Nelson [31]. By studying the response of in-vivo P-afferents to sinusoidal amplitude modulations at various frequencies, Nelson established the parameters of a linear filter that captures the frequency response of these receptors. This filter can be used in a simple model of a P-unit to transform the bandlimited stimulus $s(t)$ into a "firing probability" signal which serves as the input to a stochastic spike generator. We investigate the effects of the baseline firing rate and the spread of the interspike interval histogram on stimulus encoding in this model. We also discuss the effect of a clipping nonlinearity included in the model.

6.1 Spiking Mechanism

The model of a P-unit proposed by Nelson [31] in 1997 is not based on the response of a voltage variable to a modulated EOD as were previous models in this thesis. Instead, its dynamics is described by a time-varying spiking probability calculated from the stimulus alone (without a carrier). Its mechanism is made of (1) a linear filter that captures the P-units' frequency response to AM's, (2) a clipping non-linearity which incorporates the effect of firing rate rectification and saturation and (3) a stochastic spike generator that converts a firing probability into a binary spike train.

The first processing step of the model consists of filtering the stimulus with a linear filter. The response characteristic of such a filter was determined by Nelson, by averaging the response of a population of electrosensory afferents (from the gymnotiform species *Apteronotus Leptorynchus*) to AMs of different single frequencies (the AM's are of an actual EOD).

In practice, P-units were stimulated with imposed sinusoidal AMs at various discrete frequencies between .1 and 200 Hz. It was found that P-afferents show a sinusoidal modulation in their firing rate around their baseline (average) rate. Indeed, a phase histogram of the firing times built from the response spike train revealed a sinusoidal shape, with the maximum of

this sinusoid corresponding to a preferential phase in firing times. The gain and preferential phase value were dependent on the fixed frequency of the AM. A fit of the sinus-shaped phase histograms allowed a determination of the gain and phase response of the selected units. These values were then fitted to reveal an AM transfer function that is high-pass in character and characterized by two time constants. The transfer function can be represented by a system of two first-order high-pass filters and one constant gain filter placed in parallel. Two time constants τ_a, τ_b and three gain terms G_a, G_b and G_c are combined to write the total filter as:

$$H(s) = \frac{G_a s}{s + 1/\tau_a} + \frac{G_b s}{s + 1/\tau_b} + G_c \tag{6.1}$$

where s is the complex frequency $(\mu + i\omega)$. Figure 6.1 shows the AM transfer function and illustrates the contribution of the three terms of the filter.

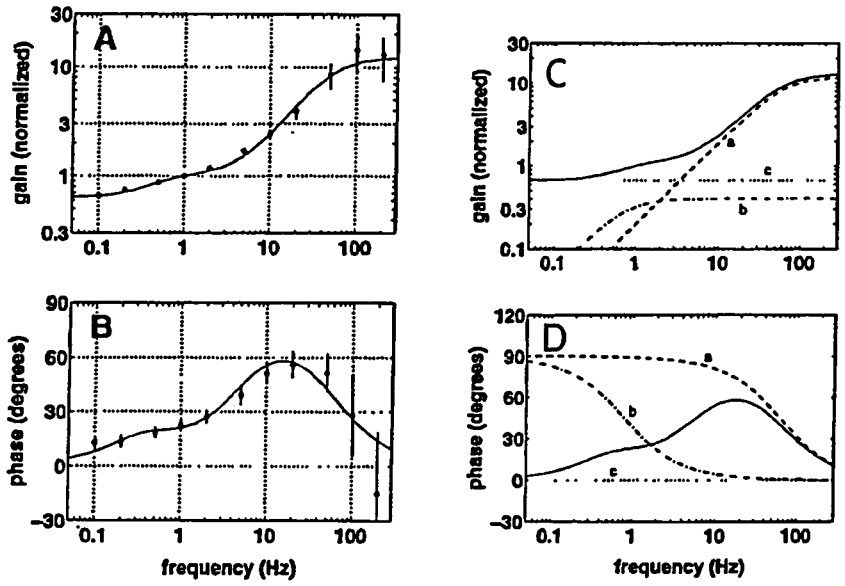

Figure 6.1: The population-averaged P-unit response characteristics. (LEFT) Mean normalized gain (A) and mean phase (B) versus AM frequency. (RIGHT) Individual contributions of the three linear filters to the overall gain (C) and phase (D) response. Each of the terms from equation 6.1 are identified with lower case a, b and c. (From [31])

The input stimulus is processed through the filter using eq. 6.1. The filter output represents the modulation in P-unit firing rate. To this modulation, the mean firing rate — a constant term — is added to obtain a time-varying firing rate which fluctuates (due to the AM) around its predicted mean.

Before converting the newly computed firing rate into a binary spike train, a clipping

nonlinearity is added, which captures both firing rate saturation (firing rate cannot exceed the EOD frequency f_{EOD}) and rectification (firing rate cannot be less than zero) observed in the P-units. This non linearity is based on the experimental observation that (1) the response rate to a weak AM stimulus scaled almost linearly with stimulus amplitude, and that (2) strong AMs gave rise to clipping (saturation or rectification) hence to a non-linear response in firing rate. A deeper numerical analysis revealed that the non-clipped portions of this nonlinearity is well approximated by a linear response function (a slightly better approximation can be obtained with a power law function — not shown). Consequently, the clipped firing rate is obtained by setting to zero any negative value of the rate and by setting to f_{EOD} any value of the rate that would exceed f_{EOD}.

The last processing step consists in translating the clipped firing rate into a binary spike train. The stochastic spike generator is based on a simple random number generator with uniform distribution between 0 and 1 (thus to a certain constant between 0 and f_{EOD}). At each interval of one EOD period, a uniform deviate is generated and compared to the clipped firing rate. Since the latter is bounded between 0 and f_{EOD}, one simple implementation of the stochastic spike generator is to trigger a spike whenever the deviate is lower than the computed firing rate.

The model accurately describes the frequency response over the range of AM frequencies that are relevant for electrolocation [31] and also captures with good agreement the adaptation of a unit in response to a step AM [41]. However, it was verified that it does not capture the autocorrelation seen in the P-unit data, nor can it reproduce the tuning curve since it is not periodically driven; only the AM counts in the modulation of the firing rate. Nevertheless we consider it because it is a commonly used class of model.

6.2 Numerical Implementation

Simulations were performed on a Unix machine running a Fortran code based on a stochastic Euler integration scheme (see section 2.1) with integration step $t = 0.005$ ms. For each parameter set, a binary spike train of total duration 50 s — excluding 500 ms discarded as transients — was simulated. Each series — a set of simulations differing by only one changing parameter and represented by the same symbol in the results plots — were realized using a "frozen noise stimulus", i.e. the same stimulus was used for all simulations, as in the actual experiments in [40]. The stimulus was generated throughout the simulation by the Fortran

algorithm itself and was written to a file with a sampling rate of .5 ms. Once again the last 4 equations of the set of equations 2.13 with $\alpha = 2\pi F = 2\pi/10$ ms^{-1} were used and the resulting signal was sent in parallel to the three components of the second order linear filter.

Numerical implementation of the filter described by equation 6.1 is achieved by solving the following differential equations with $s(t)$ being the stimulus.

$$\dot{x}_a = -\frac{x_a}{\tau_a} + \frac{G_a}{\tau_a} s(t) \tag{6.2}$$

$$\dot{x}_b = -\frac{x_b}{\tau_b} + \frac{G_b}{\tau_b} s(t) \tag{6.3}$$

$$\dot{y} = -x_a - x_b + (G_a + G_b + G_c) s(t) \tag{6.4}$$

where gains and time constants are as presented in table 6.1 along with other relevant parameters. The output to this filter is $y(t)$ which represents the modulation in firing rate. The

r_{base}	300 Hz
τ_a	2.6 ms
τ_b	210 ms
G_a	14.1
G_b	0.47
G_c	0.67

Table 6.1: NELSON model parameters

baseline firing rate of the neuron r_{base} is added to $y(t)$ so that the firing probability $r'(t)$ will fluctuate around this mean value:

$$r'(t) = y(t) + r_{base} \tag{6.5}$$

Since the model was built based on receptors of the species *Apteronotus Leptorynchus*, a realistic "typical" value of the mean firing rate is 300 Hz. On the basis of this value, the amplitude of the incoming stimulus was chosen so that its filtered version (the non-clipped firing probability) would present a standard deviation of 18% of the 300Hz baserate based on [40].

Saturation and rectification effects were then applied using the following implementation of the clipping non-linearity:

$$r(t) = \begin{cases} 0 & r'(t) < 0 \\ r'(t) & 0 \leq r'(t) \leq f_{EOD} \\ f_{EOD} & r'(t) > f_{EOD} \end{cases} \tag{6.6}$$

so that the firing rate $r(t)$ never exceeds the EOD frequency and never takes negative values. Therefore, one can define a normalized time-varying spiking probability from the ratio:

$$p(t) = r(t)/f_{EOD} \tag{6.7}$$

which is bounded between 0 and 1.

The final processing step, a stochastic spike generator, is implemented to capture the phase locking phenomena observed in experimental measurements (see figure 1.4A, right). For this purpose it checks for spiking events at intervals equal to the EOD period. In practice, the algorithm computes the instantaneous probability of firing $p(t)$ by integration of the model equations until time reaches a multiple of the EOD period. Then a random uniform deviate β is generated and compared to the firing probability $p(t)$ at that time. If $\beta < p(t_i)$, a spike is triggered.

Before computing the resulting interspike interval from the new spike time, some jitter is added using a random Gaussian deviate, to match the quality of phase locking observed in laboratory. From the analysis of the experimental data, a Gaussian distribution with zero mean and standard deviation equal to 8% of the EOD period is chosen. Such a distribution yields the correct width of the modes in the ISIH.

Finally, an absolute refractory period equal to one EOD cycle is implemented based on observations over a population of P-units that no intervals are present within the first cycle in the interspike interval histogram (see figure 1.4A, right). It is simply done by setting to the value of one EOD period any smaller interval.

An enhanced version of the stochastic generator includes an additional constant m that has an effect over the spread of the ISIH. As in Nelson [31] we define an integer m such that, at each EOD cycle, the program generates m Bernouilli trials (instead of only one) given the firing rate at that time. A spike is triggered only when m successful events are encountered and we keep track of the number of positive results from one period to another. Suppose for example that at the first cycle, n of the m trials were successful. Then, if $(m - n)$ events are also successful at the next cycle, a spike will be triggered. If not, the cumulative number of successes is reported to the third cycle and so on.

Since the EOD carrier wave is not implemented in Nelson's model, one issue that did not need to be considered in previous models now arises. Note that the driving signal in other models was implemented with constant contrast, i.e. with the mean amplitude multiplying

both the carrier and stimulus amplitudes (eq. 2.1). In the present model however the stimulus $s(t)$ acts of the mean firing rate r_{base} by adding its filtered version to the constant r_{base}. Its amplitude is set so that the standard deviation of the probability modulation $y(t)$ would represent a fixed percentage of the mean probability r_{base}. For this contrast to be constant, whenever r_{base} is scaled from the "standard value" of 300Hz, the stimulus entering the filter must also be scaled by the same ratio. Thus, when r_{base} is increased, the amplitude of the input is also increased; in the special case where the baseline firing probability would be set to 0, the input stimulus would also be set to zero amplitude.

Our work distinguishes the following two implementations: constant contrast amplitude simulations and constant stimulus amplitude simulation. The first type is as described above. The second type is implemented by not rescaling the input stimulus amplitude with r_{base}; if r_{base} is increased, the amplitude of the input stays fixed.

6.3 Firing Characteristics

Two parameters are of particular interest in Nelson's model for our study of stimulus encoding. The constant baserate r_{base} and the value of m in the enhanced version of the spike generator act on the firing rate by changing its first moment, P, and its second moment, the width of the interval distribution. We present their effect on the basic firing characteristics for the two versions of the model, namely the constant contrast and constant stimulus amplitude versions.

When the model is integrated without any stimulus the output firing rate is equal to the constant value of the baserate as expected. The linear behavior of the model without any input is expressed by the transverse line in graphs 6.2 and 6.3 of the value of P as a function of the additive constant r_{base}. As a reminder, P is defined as the probability of firing without a stimulus; thus its value is simply given by r_{base} in Nelson's model.

Figures 6.2 and 6.3 also show the firing response of our two versions of the model, respectively the constant contrast and the constant stimulus amplitude version, for two non-zero values of stimulus amplitude. It is observed that the firing rate is mainly affected — or diverges from the linear response — in regions where the baserate is near its extreme values 0 or f_{EOD}, and even more so for larger stimulus amplitudes. These regions are where the clipping non-linearity has an effect on the rate r(t).

A closer look at figure 6.2 for the constant contrast version shows firing rates that increase

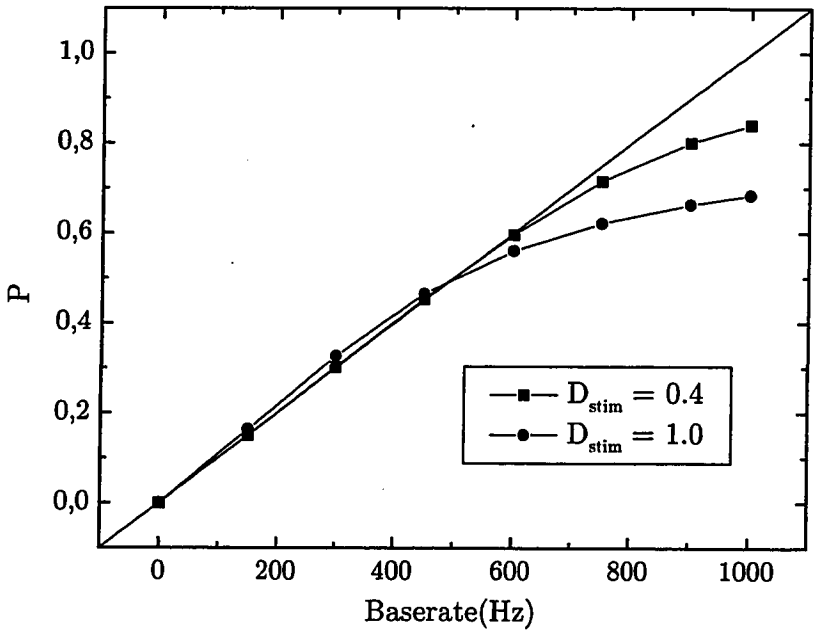

Figure 6.2: P vs baserate in Nelson's model with constant contrast stimulation. Each points was obtained from the mean ISI of a 50 seconds simulation. All parameters as per table 6.1

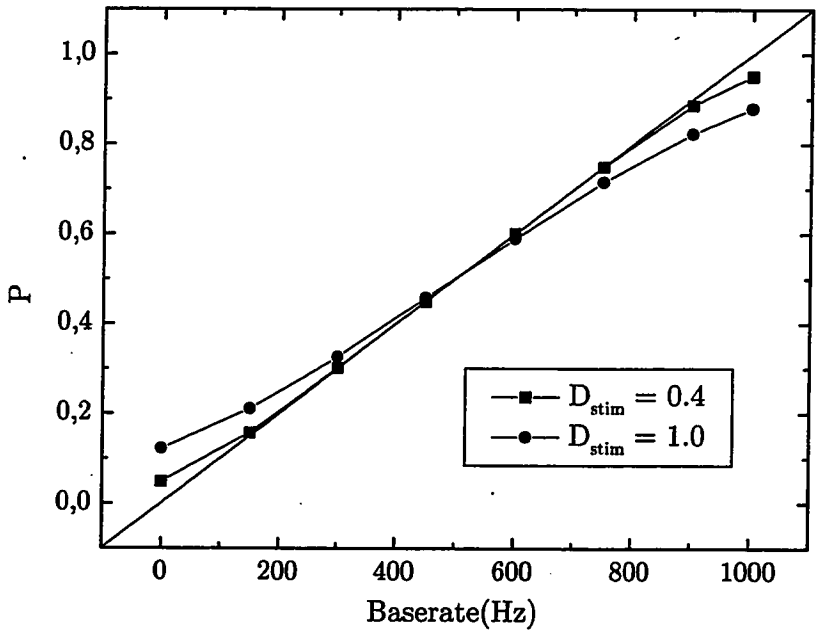

Figure 6.3: P vs baserate in Nelson's model with fixed stimulus amplitude. Details are the same as for figure 6.2

linearly starting from zero at null frequency, and this for reasonably small values of r_{base} (in the plotted case, $r_{base} \lesssim 600$ Hz). Such behavior is expected since the stimulus amplitude is scaled by the ratio $(r_{base}/300)$ which itself increases linearly starting from zero. This combined with the fact that our stimulus fluctuates around a zero mean — and thus when averaged over the whole realization has no effect on the mean firing rate — explains the nearly linear behavior of the firing rate in this region. However, for large values of the baserate, the spiking starts diverging from the linear behavior due to the presence of the non-linearity. When the baserate is near its maximum value, positive portions of the stimulus are clipped by the non-linearity and thus are not encoded as well. In counterpart, the negative portions of the stimulus are not affected in this region, resulting in a negative overall firing rate modulation. Thus, as the baserate approaches f_{EOD}, the firing response of the contant contrast model diverges from the linear function. Such divergence is observable at even smaller r_{base} for larger stimulus amplitudes because of the nature of the non-linearity.

With a constant stimulus amplitude, the model reacts differently to the presence of a stimulus. Figure 6.2 shows that the firing rate as a function of the baserate is linear for values of r_{base} in the midrange values, once again due to the fact that small amplitude modulations fluctuate around a mean value and do not affect the mean firing rate. However, the effect of the non-linearity is observed now at both ends of the graph and they are "symmetric"; the divergence at high firing rate towards smaller values of r_{base} presents the same shape as the divergence at low rate towards greater values of r_{base}. The amplitude of the stimulus being kept constant for all simulations, it is not affected by the actual value of r_{base} but rather by the "distance" of r_{base} to the non-linearity. At high firing rates, the positive portions of the stimulus are clipped and P is reduced. Conversely, the negative portions of the stimulus are clipped at very low rate, thus increasing the P value. Here again, the divergence is more important as the chosen stimulus amplitude is increased.

The parameter m associated with the enhanced version of the stochastic spike generator affects the width of the interspike interval histograms as shown in figure 6.4. The spread of the ISI distribution is sometimes quantified with the coefficient of variation $CV = \sigma/\bar{t}$ where σ is the standard deviation and $\bar{t}$ the mean of the distribution. At $m = 1$, which corresponds to the basic version of the generator, the shape of the ISIH is similar to histograms observed in mid-to-high frequency receptors; they are characterized by a large number of events in the first mode and monotonically decreasing modes at longer intervals (CV is large). Similar

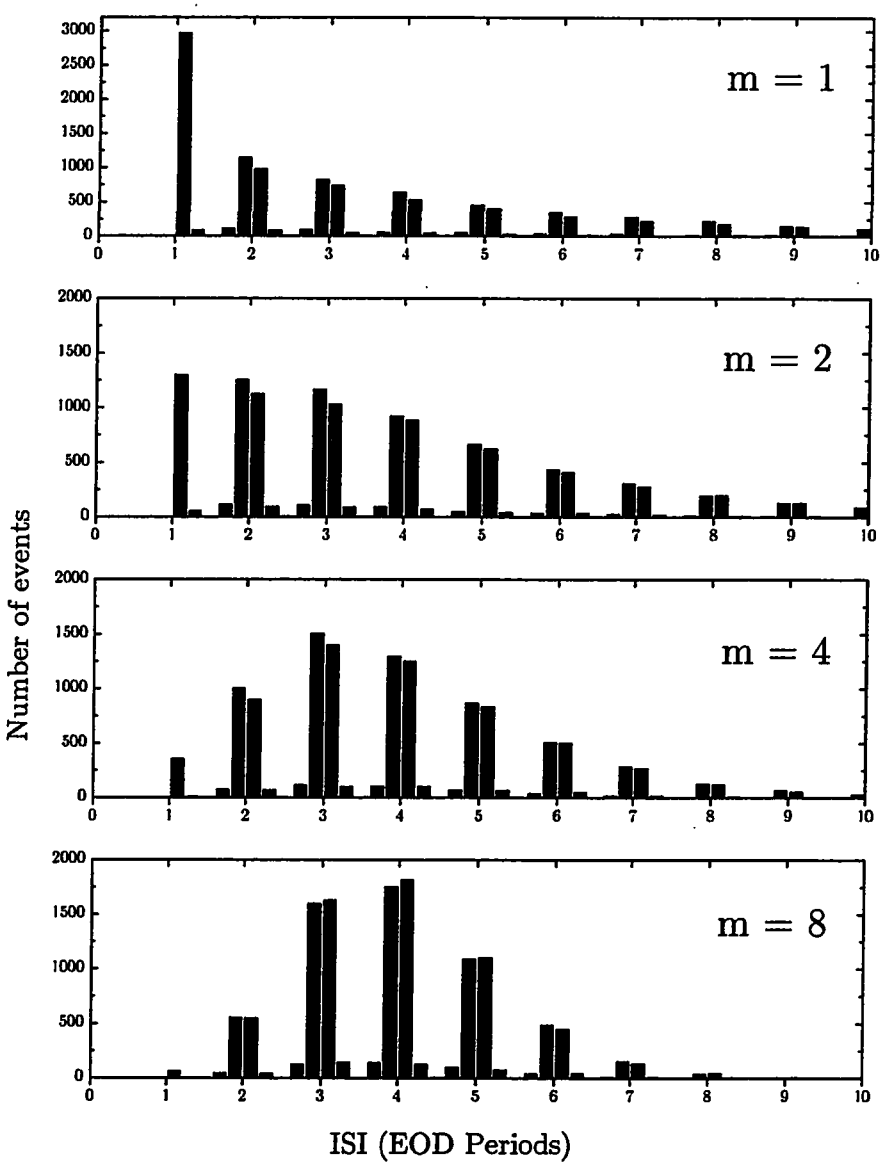

Figure 6.4: Effect of m over interspike interval histogram in Nelson's model. The average ISI has a value of 4 in all cases. Note that the top histogram is shown at a different scale because of the large number of events in the first bin.

histograms were observed in our study of the FitzHugh-Nagumo (Chapter 4) and Morris-Lecar models (Chapter 5).

As m is increased, the mean firing rate remains the same but the width of the distribution narrows around the mean value (CV decreases). At $m = 8$ the bell-shaped ISIH appears more like the histograms observed in the LIFDT model and those measured from P-units by Nelson in [41] (see figure 1.4). Thus m is an interesting parameter as it allows one to observe the effect of the second moment of the distribution while keeping the probability P constant [16]. It is even more interesting since our measurement of information transfer is affected by P itself.

6.4 Results

We present the effect of the baserate and m on the coding fraction and the mutual information in the model of a P-unit proposed by Nelson [31]. Their effects and interpretation depend strongly on whether the amplitude of the input is kept constant or scaled with the baserate for maintaining constant contrast.

The first part of our study consisted in generating a few simulations with all parameters equal, except for r_{base} which was set to pseudo-random values between 0 and f_{eod}. All parameters are as presented in table 6.1 with $m = 4$.

According to figure 6.5 for the constant contrast case, the coding fraction and information rate (see section 2.2.2) are zero at null baserate, since the stimulus is scaled to zero; there is simply zero input to the spike generator. As the stimulus amplitude is scaled with increasing baserate, the probability fluctuations become larger at the generator input. As a result the modulations are better encoded by the spike generator; the quality of the reconstruction and thus of information transfer increases monotonically. However, when r_{base} becomes large enough for the positive parts of the stimulus to be clipped by the saturation non-linearity, the coding fraction goes through a maximum and start decreasing. As r_{base} closes in on its maximum value, the lowered firing rate — negative fluctuations are no longer counterbalanced by the positive firing probability fluctuations (fig. 6.2)— combined with the fact that nearly half the fluctuations are simply not encoded, produces a decrease in coding fraction.

The baserate being a constant value added to the spike generator input, it acts as a noise source that raises the baseline stochastic firing rate. From this point of view, the effect observed here is similar to what was found in the FHN model. A moderate noise intensity first

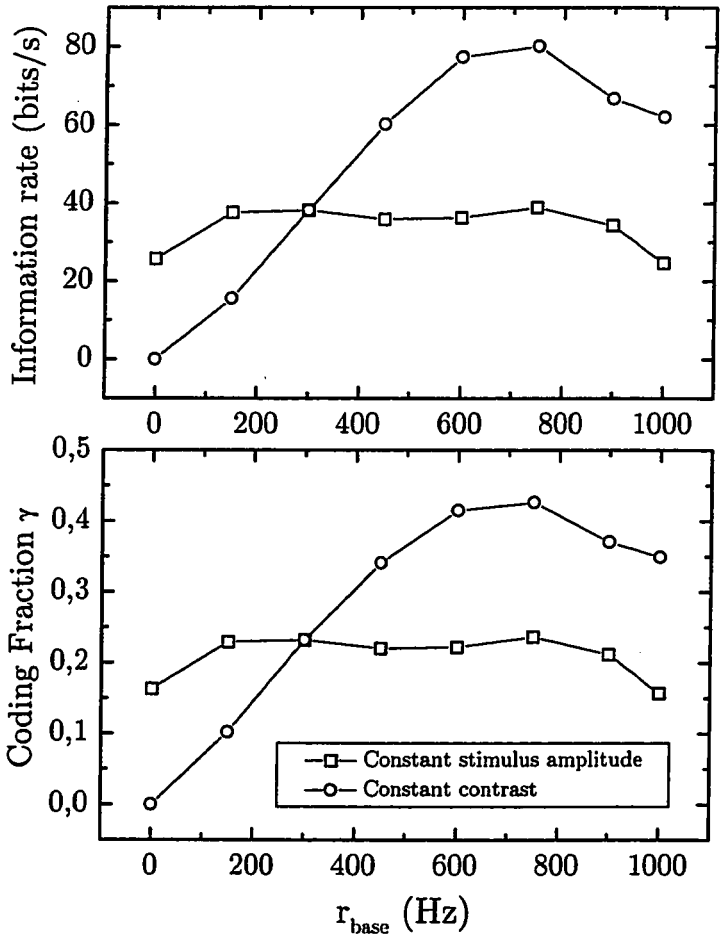

Figure 6.5: Coding fraction and information rate vs baserate in Nelson's model.

raises the firing rate, which results in a better encoding. We also observe an optimal value of the noise term for which the coding fraction and information rate are maximum. Finally, the quality of the reconstruction decreases as the noise gets too important and irrelevant spike times dominate the response.

The other curves of Figure 6.5 reveal a very different behavior of information transfer for the constant stimulus amplitude simulations. It is found that the coding fraction and mutual information rate now have a non zero value at null baserate. With r_{base} set to zero, the negative portions of the fixed amplitude modulation are clipped by the lower limit of the nonlinearity. Nevertheless, its positive portions are encoded resulting in a low yet non-zero coding fraction. Then for increasing values of the baserate, the effects of the non-linearity become less and less important and information transfer increases. At the same time, the contrast between the stimulus amplitude and the baserate diminishes and more spikes start occurring at irrelevant times. When this latter effect becomes more important, both the coding fraction and information rate go through a maximum and start decreasing (around 300 Hz).

Note that the curves for fixed stimulus amplitude are nearly symmetrical around 500 Hz: when r_{base} either increases from 0 to 500 Hz or decreases from 1000 to 500 Hz, the coding fraction and information rate first increases, then goes through a maximum and starts decreasing. This suggest that the removal of spikes by negative fluctuations at high rate has the same effect on encoding properties as the addition of spikes at low rates.

Information per spike (see section 2.2.2) as a function of the baserate is also very different for the two versions of the model (see figure 6.6). For fixed stimulus amplitude, information per spike decreases monotonically as the baserate increases. The curve results from dividing the information rate curve from figure 6.5 by the fast increasing function of the firing rate (1/ISI) shown in figure 6.3. The fast increasing number of spikes compared to the slowly varying coding fraction underlies this monotonic decrease. In the case with constant contrast, each spike carries a maximum amount of information around the value $r_{base} = 500$Hz, or half f_{EOD} right in the middle of the linear coding range, as expected.

As a second part of our investigation, the effect of m on the information measurements is presented in figure 6.7, based on simulations at constant $r_{base} = 300$Hz with m changing from 1 to 8 (see also Figure 6.4). Remember that P, the mean of the ISIH distribution, is not affected by the value of m. As the number of successful events that are necessary to

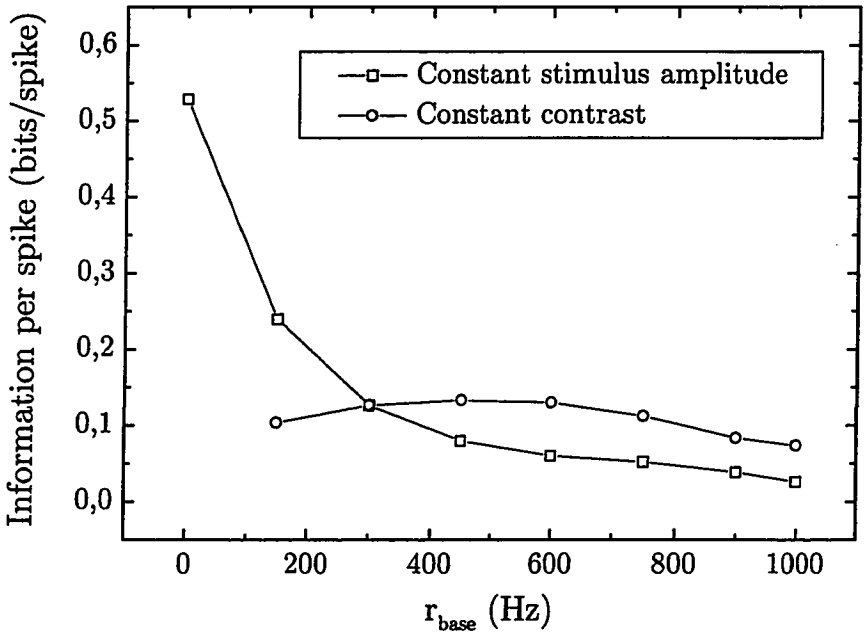

Figure 6.6: Information per spike vs baserate in Nelson's model. Each points were obtained by dividing results in *bits/s* from figure 6.5 by their associated firing rate at each value of r_{base}.

trigger a spike increases, the fluctuations in the time intervals between successive spikes are averaged out and the model output becomes more regular (smaller coefficient of variation); the ISIH becomes narrower ($m = 8$). As a result, the information transfer is improved. Since P is constant for all m, the change in information transfer (figure 6.7 B and C) is solely due to the change in the information that every single spike carries (figure 6.7 A), as the three similar traces suggests.

6.5 Discussion

We investigated the quality of AM coding in the model of a P-type electroreceptor proposed by Mark Nelson in [31]. The model uses an AM transfer function that was derived from measurements on actual P-units, to compute a time varying firing probability from the stimulus $s(t)$. The resulting probability passes through a clipping non-linearity and then serves as the input to a stochastic spike generator. Such a model is known to capture both the frequency response over a range of AM frequencies relevant for the fish and the adaptation of a unit's firing rate in response to a step AM [41].

Two variants of the models were investigated. In the first version, the stimulus was scaled

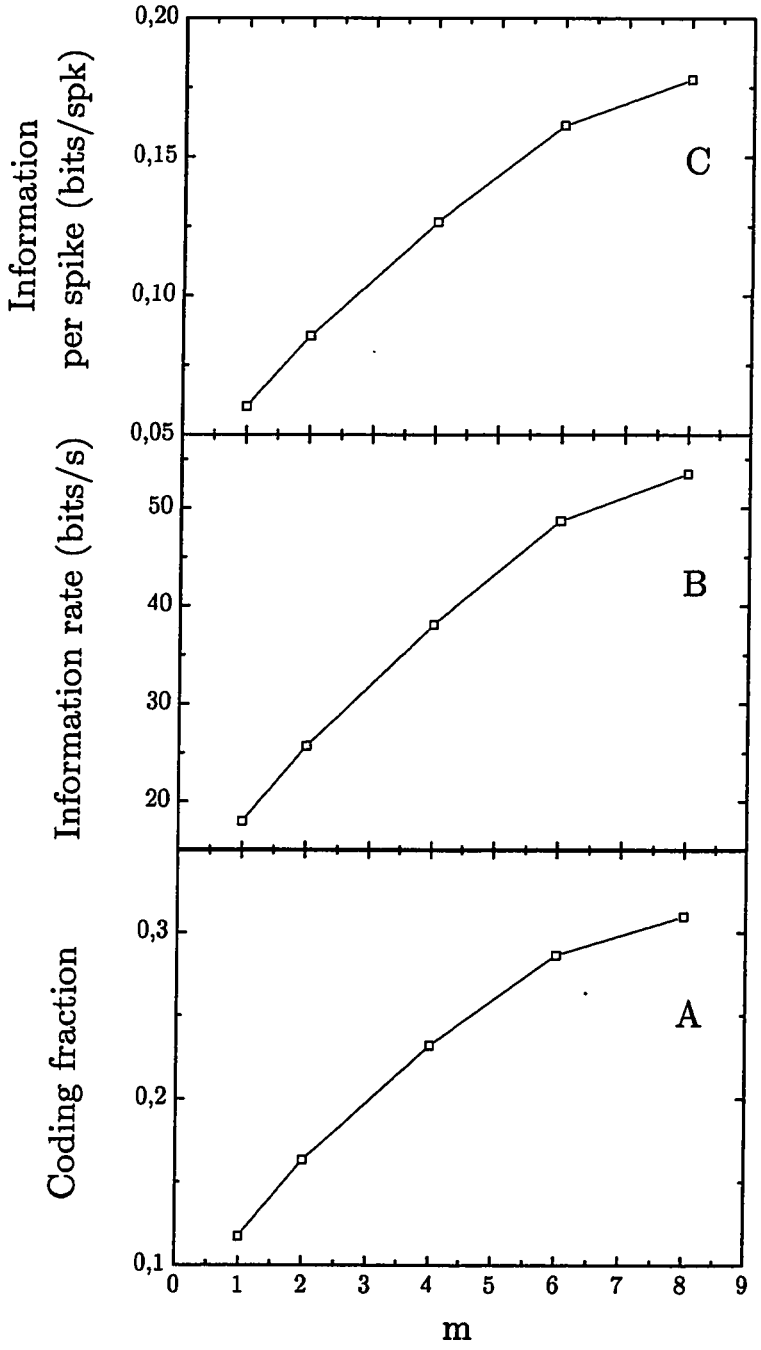

Figure 6.7: Coding fraction, information rate and information per spike vs m in Nelson's model.

with r_{base} ($\propto P$) to keep a constant contrast at the spike generator's input for consistency with other models investigated in this thesis. It was found that the quality of the reconstruction increased with the baserate except near the saturation non linearity were it started decreasing.

In the second version, the stimulus was not scaled with r_{base}, as originally done by Nelson, although he was not looking at information transfer. We found that stimulus reconstruction quality behaved "symmetrically" for the two manifestations of skipping: information can be carried by either triggering spikes at low rate or by strategically preventing some spikes to be triggered at high rates.

The enhanced version of the stochastic spike generator ($m > 1$) revealed interesting results by allowing the variation of the width of the interval distribution without changing the mean interval. As m increased and the coefficient of variation CV is decreased, the model became more reliable and each spike would carry more information for an overall beneficial effect on the transfer of information from stimulus to spike train.

The monotonically increasing curves in figure 6.7 mimick those observed in the simpler numerical model in [16] where the random threshold integrate-and-fire models were used. In these models, the value of the threshold is not fixed but rather chosen randomly from a given distribution at each firing event. The variability of such neurons (width of the ISI distribution) can be set by adjusting the distribution from which random thresholds are picked. In [16], it was found that the coding fraction increased as the variability of the ISI distribution decreased.

We know from the other models considered in this thesis that increasing synaptic noise induces a shift of the interspike intervals to the left of the ISIH, but that it also makes the modes broader. Thus we see how this important class of models behave from the point of view of coding, but we also see that, in order to get biophysical insight into what really influences coding quality, the dynamical models are preferable. Both however predict to a similar extent that a higher mean firing rate is good for coding, at least in the linear regime.

Chapter 7 Conclusions

We have investigated the encoding of minute electrical signals in P-type tuberous receptors of the weakly electrical fish. For this purpose, we have studied the encoding of biophysically relevant stimuli in numerical models of those receptors. Spike trains were obtained from the response of four published numerical neuron models to a periodic carrier with random amplitude modulations. In each model, the basic dynamics responsible for the skipping response to a periodic input was analyzed for a prior understanding of the effect of relevant parameters and variables on first and second order firing statistics. Based on the work by Wessel [40], we have used the linear stimulus reconstruction technique to calculate the coding fraction — a measure of the amount of information linearly encoded in the spike train, about the amplitude modulation — as a function of the parameters of interest. In particular, we have paid special attention to the effect of synaptic and conductance variability on the coding fraction, because the presence of noise is believed to be an essential feature of signal transduction in those receptors. In the light of our analysis of the spiking dynamics, we have discussed our results and proposed novel investigation and interpretation methods.

The four models were chosen based on their importance in the existing literature and their relevance as models of P-type electroreceptors. Each model offered a different point of view, i.e. it allowed different aspect of stimulus encoding to be addressed. We find that our results and their interpretation depend on the particular dynamics of the models. In certain cases, they even differ for distinct operating regimes of the same model. We now summarize our work with an overview of the important results.

One of the main question we addressed is, what is the role of the P value, the probability of firing per EOD cycle, in information encoding, and how is this P value affected by biophysical parameters. This is important because there are many P-units, each with its particular P value.

The leaky integrate and fire model with dynamic threshold proposed by Chacron [5],

an improved version of the well-known leaky integrate and fire model, was used because it exhibits several firing characteristics of actual P-units. Although this model is described by a voltage variable, its dynamics cannot reproduce the de-polarization-repolarization process of real neurons. P depends on the mean amplitude of the applied EOD and internal noise affects higher-order statistics. Our implementation of the LIFDT model involved suprathreshold forcing, i.e. the EOD alone (the sinusoidal forcing) yields firings for the parameters we have chosen.

LIFDT's response to periodic input is characterized by an almost-smooth input amplitude-output frequency transfer function, hence the deterministic model is very good at encoding amplitude modulations. However, internal synaptic noise is required in this model to produce proper firing statistics. This noise was found to be usually detrimental to stimulus encoding. Interestingly, noise was also found to improve signal transduction when weak amplitude modulations are not reflected in the output rate, due to the presence of phase locking in the deterministic transfer function. Finally, we found that the quality of signal transduction was not uniquely determined by P, but depended on other biophysical parameters as well.

The widely studied reduction of the Hodgkin Huxley model by FitzHugh and Nagumo is a model of type II membrane that exhibits simple yet biologically relevant dynamics. The important aspect here is that the voltage state variable of this model does capture the dynamics of action potentials. It also has a resonance. Its value of P depends on both the forcing amplitude and the intensity of internal noise. It was studied in the two distinct regimes of subthreshold and suprathreshold forcing.

In FHN, the coding fraction was found to be optimal at low internal noise amplitudes for subthreshold forcing amplitudes up to near-suprathreshold amplitudes. The effect of a stochastic source is to bring the subthreshold FHN closer to threshold as well as to linearize its abrupt transfer function. Here again, it was found that the coding depends on first-order statistics as well as on higher-order ones.

Another reduction of the Hodgkin Huxley model, the Morris-Lecar model was chosen for the richness of its dynamics which permitted an investigation of the effect of the bifurcation underlying the nonlinear dynamics of spike generation, on signal transduction. This model was also capable of reproducing action potential dynamics. Model of type I and type II membranes were compared by tuning the two models to show similar output rates in response to identical inputs. A Hopf bifurcation in type II membrane may give rise to a periodic

solution with fixed frequency at the onset. In contrast, a periodic solution may appear with initial zero frequency in type I membrane thanks to the presence of a saddle-node bifurcation. In each model, both subthreshold and suprathreshold forcing regimes were considered.

As in FHN, we found a beneficial effect of the noise in the subthreshold regime of both type I and type II ML. Strikingly, the noise amplitude leading to the optimal coding fraction was approximately the same in both models and the coding fractions themselves were very similar (see figure 5.12). We found that the type II resonator coded as well or even slightly better than the type I membrane. One could have expected that the resonator would tend to fire more in synchrony with its resonance frequency rather than with AM's, but this is not the case. Noise linearizes the transfer function in both cases, and furthermore, converts a type II resonator to a type I membrane. Thus it is not surprising both models perform similarly with noise. Further, for low noise where type II still acts pretty much like a resonator, type I does code a bit better (figures 5.12 and 5.13). To our knowledge, our method of tuning the two models so that they would exhibit the same response rate to identical input is novel. Our comparison of type I and type II ML also revealed a potentially important role of resonance effect in P-units. This was partially observed in an interesting discussion on the effect of the distance to a bifurcation on the encoding quality in both models.

Finally, the model proposed by Mark Nelson was studied, because it captures the frequency response of P-units and it is described by a firing probability variable, a commonly used type of model in the literature. It reproduces the saturation and rectification effects due to P being limited to values between 0 and 1. It was studied in two distinct forcing regimes: constant contrast and constant stimulus amplitude.

As a very interesting result, we have observed that the encoding of the negative portions of the stimulus, via deletion of spikes at high rate, may be as important as the encoding of the positive portions at low rate. The parameter m also provides interesting results regarding the effect of the width of the interval distribution or "reliability" on the coding fraction.

The skipping dynamics in models of P-type electroreceptors was often found to be due to a perturbation by a stochastic signal of a periodic (or null) firing pattern. In the LIFDT, FHN and ML models, the multimodal ISIH were obtained by forcing the model with a sinusoidal waveform and adding either the synaptic source or the AM. The effect of both stochastic signal was to break periodical firing pattern by smoothing the limits of the regions of phase locked pattern in the phase space of input signals. In the case of the Nelson model,

the multimodal ISIH were artificially reproduced by forcing the spikes within a fixed phase interval.

As a very important result, we found that there is no one-to-one relation between the value of P — a first-order statistic — and our measure of information, and this is true across all models investigated here. We find that higher-order statistics have an important influence on signal transduction. Further, a given P value can be obtained for different sets of biophysical parameters, and the coding quality will not necessarily be the same across these sets. Also in every model, we were able to find a case in which increasing the internal noise intensities resulted in a decrease in reconstruction noise.

Although noise can help coding in some cases, its presence is never purely beneficial because of its very definition: it introduces randomness which most of the time is unwanted in reliable systems. Consequently, we find that sufficiently large noise intensities always reduce information transfer. In the suprathreshold regimes of LIFDT, FHN and ML, even low noise amplitude reduced the coding fraction because the presence of the AM alone already linearizes the transfer function and optimizes information transfer. However, in other cases such as subthreshold FHN, noise does help the encoding via stochastic resonance.

The choice of the coding fraction as a measure of information did not allow a comparison of the encoding quality across the different models studied here. Indeed, the coding fraction is dependent on various parameters that were not constant in all models, especially on the forcing parameters such as the cutoff frequency of our stimulus. Nevertheless a quantitative comparison was possible between the two type of coders studied in the Morris-Lecar model.

Other information measurement such as the so called "direct method" constitutes an interesting avenue of study as a follow up to our investigation. This method is as widely used as the reconstruction technique; it consists in quantifying the transfer of information by computing the explicit entropy of the spike train. As well, the effect of noise over entire networks of encoding units with varying P values are possibly well characterized by the coding fraction and the direct method, and points to an interesting area of future research. It would also be interesting to investigate the encoding of weak AM's in the plateaus of the transfer function in the ML model, as we observed in the LIFDT, since ML is a more realistic model in certain aspects (although this might require to add an adaptation current to the ML model, similar to the dynamic threshold in LIFDT).

Appendix A Fourth order filter

This section presents the derivation of the method used for generation of a bandlimited Gaussian white noise signal for use as the stimulus $s(t)$ in all models. It is done by processing a Gaussian white noise signal through the fourth order filter

$$H(j\omega) = \frac{\alpha^4}{(j\omega - \alpha)^4} \tag{A.1}$$

In the Laplace domain, the filter is written:

$$H(s) = \frac{s^4}{(s - \alpha)^4} \tag{A.2}$$

such that X(s) a general stochastic process obtained by filtering some other process Y(s) with H(s) may be expressed as:

$$X(s) = H(s)Y(s) \tag{A.3}$$

By combining the two last equations and expanding the polynomial term we get:

$$(s^4 - 4\alpha s^3 + 6\alpha^2 s^2 - 4\alpha^3 s + \alpha^4)X = \alpha^4 Y \tag{A.4}$$

which transforms in the time domain to:

$$\frac{d^4x}{dt^4} - 4\alpha\frac{d^3x}{dt^3} + 6\alpha^2\frac{d^2x}{dt^2} - 4\alpha^3\frac{dx}{dt} + \alpha^4 x = \alpha^4 y \tag{A.5}$$

Now letting

$$\begin{aligned} z_1 &= x \\ z_2 &= \frac{dx}{dt} = \frac{dz_1}{dt} \\ z_3 &= \frac{d^2x}{dt^2} = \frac{dz_2}{dt} \\ z_4 &= \frac{d^3x}{dt^3} = \frac{dz_3}{dt} \end{aligned}$$

we find, with very few manipulations on eq. A.5, the equivalent expressions:

$$\dot{z}_1 = z_2 \tag{A.6}$$

$$\dot{z}_2 = z_3 \tag{A.7}$$

$$\dot{z}_3 = z_4 \tag{A.8}$$

$$\dot{z}_4 = 4\alpha z_4 - 6\alpha^2 z_3 + 4\alpha^3 z_2 + \alpha^4(-z_1 + y) \tag{A.9}$$

which are identical to the set of equations 2.13–2.16 in which the input y to the filter is the Gaussian random signal $\xi_2(t)$ and the output x is the stimulus $s(t)$.

The variance of a zero mean process x is given by:

$$\mathrm{Var}(x) = R_{xx}(\tau)|_{\tau=0} \tag{A.10}$$

$$= R_{xx}(0) \tag{A.11}$$

$$= \frac{1}{2\pi}\int_{-\infty}^{\infty} S_{xx}(\omega)d\omega \tag{A.12}$$

where R_{xx} is the autocorrelation function of the filter's output x and its spectrum $S_{xx}(\omega)$ can be written in terms of the white noise spectrum which is a constant function at $2D$ thus:

$$\mathrm{Var}(x) = \frac{2D\alpha^8}{2\pi}\int_{-\infty}^{\infty}\frac{1}{(\omega^2+\alpha^2)^4}d\omega$$

$$= \frac{5}{16}D\alpha$$

Bibliography

[1] A.F. Huxley A.L. Hodgkin. A quantitative description of membrane current and its application to conduction and excitation in nerve. *Journal of Physiology*, 117:500–544, 1952.

[2] J. Bastian. Electrolocation 1. how the electroreceptors of apteronotus leptorynchus code for moving objects and other external stimuli. *J. Comp. Physiol.*, 144:465–479, 1981.

[3] J. Bastian. Electrosensory organisms. *Physics Today*, pages 30–37, February 1994.

[4] M.J. Chacron, A. Longtin, and L. Maler. Negative interspike interval correlations increase the neuronal capacity for encoding time-dependent stimuli. *J Neurosci*, 21(14):5328–5343, 15 July 2001.

[5] M.J. Chacron, A. Longtin, M. St-Hilaire, and L. Maler. Suprathreshold stochastic firing dynamics with memory in p-type electroreceptors. *Physical Review Letters*, 85(7):1576–1579, 14 August 2000.

[6] D.R. Chialvo, A. Longtin, and J. Muller-Gerking. Stochastic resonance in models of neuronal ensembles. *Physical Review E*, 55(2):1798–1808, February 1997.

[7] J.J. Collins, C.C. Chow, and T.T. Imhoff. Aperiodic stochastic resonance in excitable systems. *Physical Review E*, 52(4):R3321–R3324, October 1995.

[8] R. FitzHugh. Thresholds and plateaus in the hodgkin-huxley nerve equation. *J Gen Physiol*, 43:867–896, 1960.

[9] R. FitzHugh. Impulses and physiological states in theoretical models of nerve membrane. *Biophys J*, 1:445–466, 1961.

[10] R.F. Fox. Second order algorithm for the numerical integration of colored-noise problems. *Physical Review A*, 43(6):2649–2654, March 15 1991.

[11] R.F. Fox, I.R. Gatland, R. Roy, and G. Vemuri. Fast, acurate algorithm for numerical simulation or exponentially correlated colored noise. *Physical Review A*, 38(11):5938–5940, December 1 1988.

[12] A.S. French, A.V. Holden, and R.B. Stein. The estimation of the frequency response function of a mechanoreceptor. *Kybernetik*, 11:15–23, 1972.

[13] F. Gabbiani. Coding of time-varying signals in spike trains of linear and half-wave rectifying neurons. *Netw Comp Neural Syst*, 7(1):61–85, February 1996.

[14] F. Gabbiani and C. Koch. http://glab.bcm.tmc.edu/signal_processing_techniques/signal_proc.html.

[15] F. Gabbiani and C. Koch. Coding of time-varying signal in spike trains of integrate-and-fire neurons with random threshold. *Neural Computation*, 8:44–66, June 1996.

[16] F. Gabbiani and C. Koch. *Principles of spike train analysis*, chapter 9, pages 313–360. In Koch and Segev [26], 2nd edition, 2000.

[17] L. Gammaitoni, P. Hänggi, P. Jung, and F. Marchesoni. Stochastic resonance. *Rev Mod Phys*, 70:223–287, 1998.

[18] L. Glass, C. Graves, G.A. Petrillo, and M.C. Mackey. Unstable dynamics of a periodically driven oscillator in the presence of noise. *J Theor Biol*, 86:455–475, 1980.

[19] L. Glass and M.C. Mackey. *From clocks to chaos : the rhythms of life.* Princeton University Press, Princeton, N.J., 1988.

[20] B.S. Gutkin and G.B. Ermentrout. Dynamics of membrane excitability determine inter-spike interval variability: a link between spike generation mechanisms and cortical spike train statistics. *Neural Comp*, 10:1047–1065, 1998.

[21] C. Heneghan, C.C. Chow, J.J. Collins, T.T. Imhoff, S.B. Lowen, and M.C. Teich. Information measures quantifying aperiodic stochastic resonance. *Physical Review E*, 54(3):R2228–R2231, September 1996.

[22] C. Ivey, V. Apkarian, and D. Chialvo. Noise-induced tuning changes in mechanoreceptors. *J Neurophysiol*, 79:1879, 1998.

[23] S.J. Bolanowski Jr, G.A. Gescheider, R.T. Verillo, and C.M. Checkosky. Four channels mediate the mechanical aspect of touch. *J acoust Soc Am*, 84:455–475, 1988.

[24] J. P. Keener, F.C. Hoppensteadt, and J. Rinzel. Integrate and fire models of nerve membrane response to oscillatory input. *SIAM J Appl Math*, 41:127–144, 1981.

[25] B. Knight. Dynamics of encoding in a population of neurons. *J Gen Physiol*, 59:734–766, 1972.

[26] C. Koch and I. Segev, editors. *Methods in Neuronal Modeling.* MIT Press, Cambridge, MA, 2nd edition, 2000.

[27] A. Longtin. Autonomous stochastic resonance in bursting neurons. *Physical Review E*, 55(1):868–876, January 1997.

[28] A. Longtin. Effect of noise on the tuning properties of excitable systems. *Chaos, Solitons and Fractals*, 2000.

[29] A. Longtin and D.M. Racicot. Spike train patterning and forecastability. *Biosystems*, 40(1–2):111–118, 1997.

[30] A. Longtin and M. St-Hilaire. Encoding carrier amplitude modulations via stochastic phase synchronization. *International journal of bifurcation and chaos*, 10(10):2447–2463, 2000.

[31] M.E. Nelson, Z. Xu, and J.R. Payne. Characterization and modeling of p-type electrosensory afferent responses to amplitude modulations in a wave-type electric fish. *Journal of Computational Physiology A*, 181:532–544, 1997.

[32] A. Papoulis. *Probability, Random Variables and Stochastic Processes.* McGraw-Hill International Book Company, 1981.

[33] R. Patuzzi and D. Robertson. Tunning in the mammalian cochlea. *Physiol Rev*, 68:1009–1082, 1988.

[34] W.H. Press, S.A. Teukolski, W.T. Vetterling, and B.P. Flannery. *Numerical Recipes in C: The art of scientific computing.* Cambridge University Press, Cambridge, second edition, 1992.

[35] F. Rieke, D. Warland, R. the Ruyter van Steveninck, and W. Bialek. *Spikes, Exploring the Neural Code.* The MIT Press, Cambridge, Mass., 1996.

[36] J. Rinzel and B. Ermentrout. *Analysis of neural excitability and oscillations*, chapter 7, pages 251–291. In Koch and Segev [26], 2nd edition, 2000.

[37] H. Scheich, T. Bullock, and R.H. HamstraJr. Coding properties of two classes of afferent nerve fibers: high frequency receptors in the electric fish eigenmannia. *J Neurophysiol*, 36:39–60, 1973.

[38] S.H. Strogatz. *Nonlinear dynamics and Chaos : with applications in physics, biology, chemistry, and engineering.* Addison-Wesley, Reading, Mass, 1994.

[39] M.V. Tsodyks and T. Markram. The neural code between neocortical pyramidal neurons depends on neurotransmitter release probability. *Proc. Natl. Acad. Sci. USA*, pages 719–723, January 1997.

[40] R. Wessel, C. Koch, and F. Gabbiani. Coding of time-varying electric field amplitude modulations in a wave-type electric fish. *Journal of Neurophysiology*, 75(6):2280–2293, June 1996.

[41] Z. Xu, J.R. Payne, and M.E. Nelson. Logarithmic time course of sensory adaptation in electrosensory afferent nerve fibers in a weakly electric fish. *Journal of Neurophysiology*, 76(3):13, September 1996.

[42] A. Zador. Impact of synaptic unreliability on the information transmitted by spiking neurons. *Journal of neurophysiology*, 79:1219–1229, 1998.

[43] H.H. Zakon. The electroreceptive periphery. In T.H. Bullock and W. Heilingenberg, editors, *Electroreception*, pages 103–156. John Wiley and Sons, New York, 1986.